

RECLAMATION

Managing Water in the West

**Desalination and Water Purification Research
and Development Program Report No. NMSU003**

**New Mexico Water Resources Research Institute
Technical Completion Report No. 383**

Reducing Treatment Costs of Alternative Waters with Antifouling Ion-Exchange Membranes



**U.S. Department of the Interior
Bureau of Reclamation
Technical Service Center
Denver, Colorado**

May 2020

REPORT DOCUMENTATION PAGE

*Form Approved
OMB No. 0704-0188*

The public reporting burden for this collection of information is estimated to average 1 hour per response, including the time for reviewing instructions, searching existing data sources, gathering and maintaining the data needed, and completing and reviewing the collection of information. Send comments regarding this burden estimate or any other aspect of this collection of information, including suggestions for reducing the burden, to Department of Defense, Washington Headquarters Services, Directorate for Information Operations and Reports (0704-0188), 1215 Jefferson Davis Highway, Suite 1204, Arlington, VA 22202-4302. Respondents should be aware that notwithstanding any other provision of law, no person shall be subject to any penalty for failing to comply with a collection of information if it does not display a currently valid OMB control number.

PLEASE DO NOT RETURN YOUR FORM TO THE ABOVE ADDRESS.

1. REPORT DATE (DD-MM-YYYY) 24-06-2019		2. REPORT TYPE Final Report		3. DATES COVERED (From - To) April 2016 to May 2019	
4. TITLE AND SUBTITLE Reducing Treatment Costs of Alternative Waters with Antifouling Ion-Exchange Membranes				5a. CONTRACT NUMBER Agreement No. R16AC00002	
				5b. GRANT NUMBER	
				5c. PROGRAM ELEMENT NUMBER	
6. AUTHOR(S) Dr. Pei Xu, Dr. Huiyao Wang, Dr. Xuesong Xu, Guanyu Ma, Million Tesfai				5d. PROJECT NUMBER	
				5e. TASK NUMBER	
				5f. WORK UNIT NUMBER	
7. PERFORMING ORGANIZATION NAME(S) AND ADDRESS(ES) Department of Civil Engineering New Mexico State University 3035 S Espina St. Las Cruces, NM 88003-8001				8. PERFORMING ORGANIZATION REPORT NUMBER	
9. SPONSORING/MONITORING AGENCY NAME(S) AND ADDRESS(ES) Bureau of Reclamation U.S. Department of the Interior Denver Federal Center PO Box 25007, Denver, CO 80225-0007				10. SPONSOR/MONITOR'S ACRONYM(S) Reclamation	
				11. SPONSOR/MONITOR'S REPORT NUMBER(S) DWPR Report No. NMSU003	
12. DISTRIBUTION/AVAILABILITY STATEMENT Available from the National Technical Information Service, Operations Division, 5285 Port Royal Road, Springfield VA 22161					
13. SUPPLEMENTARY NOTES Online at https://www.usbr.gov/research/dwpr/DWPR_Reports.html					
14. ABSTRACT Fouling of ion-exchange membranes (IEMs) hinders electrodialysis (ED) for water/wastewater treatment because it affects membrane performance, increases energy consumption, and shortens membrane life. This study aims to modify commercially available IEMs by surface coating polymers in combination with TiO ₂ nanoparticles or graphene oxide (GO) nanosheets to enhance fouling resistance of the IEMs. Membrane modification significantly improved biofouling resistance, enhanced desalting efficiency, permselectivity of monovalent ions over divalent ions, and reduced energy consumption of ED process compared to that using unmodified membranes.					
15. SUBJECT TERMS Electrodialysis, antifouling, ion-exchange membrane, desalination, membrane modification					
16. SECURITY CLASSIFICATION OF:			17. LIMITATION OF ABSTRACT	18. NUMBER OF PAGES	19a. NAME OF RESPONSIBLE PERSON
a. REPORT	b. ABSTRACT	THIS PAGE			Katherine (Katie) Guerra
U	U	U			19b. TELEPHONE NUMBER (Include area code) 303-445-2013

**Desalination and Water Purification Research
and Development Program Report No. NMSU003**

**New Mexico Water Resources Research Institute
Technical Completion Report No. 383**

Reducing Treatment Costs of Alternative Waters with Antifouling Ion-Exchange Membranes

**Prepared for the Bureau of Reclamation Under Agreement No.
R16AC00002**

by

**Dr. Pei Xu, Dr. Huiyao Wang, Dr. Xuesong Xu, Guanyu Ma,
Million Tesfai
NMSU Department of Civil Engineering**



**U.S. Department of the Interior
Bureau of Reclamation
Technical Service Center
Denver, Colorado**

May 2020

Mission Statements

The U.S. Department of the Interior protects America's natural resources and heritage, honors our cultures and tribal communities, and supplies the energy to power our future.

The mission of the Bureau of Reclamation is to manage, develop, and protect water and related resources in an environmentally and economically sound manner in the interest of the American public.

Disclaimer

The views, analysis, recommendations, and conclusions in this report are those of the authors and do not represent official or unofficial policies or opinions of the United States Government, and the United States takes no position with regard to any findings, conclusions, or recommendations made. As such, mention of trade names or commercial products does not constitute their endorsement by the United States Government.

Acknowledgments

Work on this project was made possible by funding from a cooperative agreement between the U.S. Bureau of Reclamation (BOR) and New Mexico State University (#R16AC00002, Center for the Development and Use of Alternative Water Supplies). The research team gratefully acknowledges the following individuals for their valuable contribution to the project:

- Bureau of Reclamation: Drs. Katherine (Katie) Guerra and Julie Korak, for managing the project; and Randy Shaw and Steve Holland for technical support during field testing at the Brackish Groundwater National Desalination Research Facility (BGNDRF), New Mexico
- New Mexico Water Resources Research Institute (NM WRRI): Catherine T. Ortega Klett and Dr. Alexander Fernald for managing the project
- New Mexico State University: Drs. Lu Lin and Wenbin Jiang for electrochemistry impedance spectroscopy (EIS) analysis, and Mark Chidester for water samples analysis

Acronyms and Abbreviations

AC	Alternating Current
AEM(s)	Anion-exchange Membrane(s)
BSA	Bovine Serum Albumin
CE	Counter Electrode
CEM(s)	Cation-exchange Membrane(s)
CLSM	Confocal Laser Scanning Electron Microscopy
DC	Direct Current
<i>E. coli</i>	<i>Escherichia coli</i>
ED	Electrodialysis
EDR	Electrodialysis Reversal
EIS	Electrochemical Impedance Spectroscopy
Em	Emission Wavelength
EPS	Extracellular Polymeric Substance
FEEM	Fluorescence Excitation-Emission Microscope
GO	Graphene Oxide
HA	Humic Acid
I	Current through the Electrodialysis Stack
IC	Ion Chromatography
IEC	Ion Exchange Capacity
IEM(s)	Ion-exchange Membrane(s)
LB	Luria-Bertani
NF	Nanofiltration
OCP	Open Circuit Potential
PDA	Polydopamine
PEI	Polyethyleneimine
PLC	Programmable Logic Controller
PTFE	Polytetrafluoroethylene
PVDF	Polyvinylidene Fluoride
PVDF	Polyethylene Difluoride
RE	Reference Electrode
Reclamation	Bureau of Reclamation
RO	Reverse Osmosis
RTN	Relative Transport Number
SDBS	Sodium Dodecyl Benzene Sulfonate
SDS	Sodium Dodecyl Sulfate
SEM	Scanning Electron Microscopy
TDS	Total Dissolved Solids
TiO ₂	Titanium Oxide
TOC	Total Organic Carbon
WE	Working Electrode

Measurements

°F	degree Fahrenheit
cm	centimeter
µg/L	micrograms per liter
mg/L	milligrams per liter
ml/min	milliliters per minute
cm/s	centimeters per second
psi	pounds per square inch
g/L	grams per liter
mA/cm ²	milliamps per square centimeter
µm	micro-meter
Ω	ohm
meq	milli-equivalent

Contents

	Page
Mission Statements	i
Disclaimer	i
Acknowledgments.....	i
Acronyms and Abbreviations	ii
Measurements	iii
Executive Summary	1
1. Introduction.....	3
1.1. Project Background.....	3
1.1.1. Membrane Desalination Technologies	3
1.1.2. Membrane Fouling & Permselectivity.....	4
1.1.3. Membrane Surface Modification	5
1.2. Project Objectives	7
1.3. Personnel.....	7
2. Approach and Methods.....	9
2.1. Materials and Experimental Setup	9
2.1.1. Membrane & Chemical Agencies for Surface Modification	9
2.1.2. Experimental Setup.....	10
2.1.2.1. Bench-scale ED stack	10
2.1.2.2. Coupon Fouling Testing	13
2.2. Methodology	14
2.2.1. Hydrophobicity	14
2.2.2. Ion Exchange Capacity (IEC)	15
2.2.3. Electrochemical Impedance Spectroscopy (EIS).....	16
2.2.4. Biofouling Propensity Analysis	17
2.2.5. Fluorescence Excitation-Emission (FEEM) Spectrum	18
2.2.6. Chemical Extraction of foulants	19
2.2.7. Scanning Electron Microscopy (SEM)	19
2.2.8. Desalination Performance.....	20
2.3. Calculations.....	20
3. Results and Discussions.....	22
3.1. Development of Antifouling AEMs.....	22
3.1.1. Ion Exchange Capacity (IEC)	22
3.1.2. Hydrophilicity	23
3.1.3. Membrane Resistance Measurements	25
3.1.4. Confocal Laser Scanning Microscope and COMSTAT Analysis ..	26
3.1.5. Overall Desalination Efficiency.....	31
3.1.5.1. Conductivity Reduction	31
3.1.5.2. Permselectivity.....	32
3.1.5.3. Energy Consumption	33
3.2. Development of Antifouling CEMs.....	36
3.2.1. Ion Exchange Capacity	36
3.2.2. Hydrophilicity	36
3.2.3. Membrane Resistance Measurements	37
3.2.4. Confocal Laser Scanning Microscope and COMSTAT Analysis ..	38

Antifouling Ion-Exchange Membranes

3.2.5. Overall Desalination Efficiency.....	40
3.3. Investigation of Organic-Induced Fouling Using Modified and Unmodified Membranes.....	42
3.3.1. Hydrophilicity.....	43
3.3.2. Membrane Imaging.....	45
3.3.3. FEEM.....	46
3.3.4. Overall Desalination Performance and Energy Consumption	52
4. Conclusions.....	56
References.....	57
Metric Conversions.....	66

Figures

	Page
Figure 1. PDA Solution 15 Minutes after Preparation.....	10
Figure 2. Bench Scale ED at NMSU Environmental Lab	11
Figure 3. Bench Experimental Setup for <i>E. coli</i> Membrane Fouling. (a) Full Circulation Setup; (b) Circulation Model; and (c) Single Cell Setup.....	13
Figure 4. Contact angle for (a) Captive bubble method, (b) Sessile drop method	15
Figure 5. Schematic diagram of the experimental setup used for electrochemical impedance spectroscopy (EIS) measurements (WE: working electrode, CE: counter electrode, SE: sensitive electrode, RE: reference electrode, AEM: anion exchange membrane).	16
Figure 6. A Prepared Membrane Sample for CLSM	17
Figure 7. TCS SP5 II confocal microscope at NMSU Electron Microscopy Lab	18
Figure 8. Ion Exchange Capacity for Unmodified and Modified Membranes. (a) Raw AR204, PDA and PDA + different dosage of GO modified AR204, (b) Raw AR204, PDA and PDA + different dosage of TiO ₂ modified AR204.....	23
Figure 9. Contact Angle Measurements of Fouled and Unfouled Membranes	24
Figure 10. Electrochemical impedance spectroscopy (EIS) of raw AR204 and AR204 coated with PDA.	25
Figure 11. Electrochemical impedance spectroscopy (EIS) of AR204 coated with PDA and different concentration of TiO ₂ after membrane biofouling experiments.....	26
Figure 12. CLSM images of biofilm formed on AR204 coated with PDA and different concentration of TiO ₂ after membrane biofouling experiments	29
Figure 13. COMSTAT Analysis on CLSM Images of Fouled Membranes. (a) and (b) biomass by live and dead cells and EPS coverage of membrane respectively for Raw AR204, PDA and PDA + GO modified membranes, (c) and (d) biomass by live and dead cells and EPS coverage of membrane respectively for Raw AR204, PDA and PDA + TiO ₂ modified membranes.....	30
Figure 14. Conductivity Cut Comparison of (a) Unmodified AR204, AR204 coated with PDA and AR204 coated with PDA + different dosage of TiO ₂ , (b) Unmodified AR204, AR204 coated with PDA and AR204 coated with PDA + different dosage of GO.	32
Figure 15. Permselectivity of SO ₄ /Cl for Raw AR204 and Modified Membranes. (a) Raw, PDA and PDA+different dosage of TiO ₂ ; (b) Raw, PDA and PDA+different dosage of GO.....	33
Figure 16. Energy Consumption Comparison in kWh/ kgal Product Water. (a) Unmodified AR204, AR204 coated with PDA and AR204 coated with PDA + different dosage of TiO ₂ ; (b) Unmodified AR204, AR204 coated with PDA and AR204 coated with PDA+different dosage of GO.	35
Figure 17. Normalized energy consumption. (a) Unmodified AR204, AR204 coated with PDA and AR204 coated with PDA + different dosage of TiO ₂ ; (b) Unmodified AR204, AR204 coated with PDA and AR204 coated with PDA+different dosage of GO	35
Figure 18. Contact angles of fresh and <i>E. coli</i> fouled. (a) TiO ₂ modified CEMs and (b) GO modified CEMs	37
Figure 19. Biomass coverage comparison of TiO ₂ coated membranes. (a) <i>E. coli</i> cells, (b) EPS.....	40

Antifouling Ion-Exchange Membranes

Figure 20. Biomass coverage comparison of GO coated membranes. (a) <i>E. coli</i> cells, (b) EPS.....	40
Figure 21. Conductivity removal comparison among different membrane coatings.....	41
Figure 22. Energy consumption comparison among different membrane coatings.	41
Figure 23. Normalized salt removal comparison among different membrane coatings...	42
Figure 24. Comparison of contact angles among different membrane coatings fouled by (a)control set, (b) HA, and (c) BSA.....	45
Figure 25. SEM Images of Organic Fouled Cation Exchange Membranes.....	46
Figure 26. FEEM plot of (a) BSA solution and (b) HA solution at 100 mg/L equivalent TOC.....	47
Figure 27. Illustration of FRI Zoning for a FEEM Contour Plot.....	47
Figure 28. FEEM Plot of 500 mg/L PEI Solution	48
Figure 29. FEEM Results of CEMs with Different Coatings and Foulants.....	50
Figure 30. FRI Volume Comparison of HA and BSA Accumulation on Different Types of Cation Exchange Membranes.	51
Figure 31. FRI Volume Percentage of BSA and HA for Different Types of Cation Exchange Membranes	51
Figure 32. Conductivity removal comparison of different membranes. (a) control set; (b) with HA added; and (c) with BSA added.	54
Figure 33. Normalized salt removal comparison between different membrane coatings with (a) no added foulant; (b) humic acid; and (c) BSA.....	55

Tables

	Page
Table 1. Ion-Exchange Membranes Properties	9
Table 2. ED Stack Specifications and Experimental Operational Parameters.....	12
Table 3. IEC Results of Selected Membranes	36
Table 4. Membrane Resistance of Unfouled and Fouled TiO ₂ Coated Membranes.....	38
Table 5. Membrane Resistance of Unfouled and Fouled GO Coated Membranes.....	38

Executive Summary

Fouling of ion-exchange membranes (IEMs) is a main drawback in using electrodialysis (ED) technology for water and wastewater treatment because it affects the performance of the desalination system, increases energy consumption, and shortens membrane lifetime. In this study, we aimed to enhance the fouling resistance of IEMs by surface modification of Ionics membranes manufactured by Suez Water. The modification was conducted by dipping membranes in freshly prepared polymer solutions in combination with TiO₂ nanoparticles or graphene oxide (GO) nanosheets. The antifouling propensities of the modified membranes were evaluated by circulating *E. coli* solution in coupon cells for 48-hour duration. Biofouling characterization was done by staining sample membranes with SYTO 9 and Texas Red, and then analyzing samples using a confocal laser scanning electron microscopy (CLSM). Contact angle measurements were taken to determine the impact of the modification on the hydrophilicity of membrane surface, and was measured after foulant circulation in the coupon cells. Ion-exchange capacity (IEC) and electrochemical impedance spectroscopy (EIS) were used to analyze membranes' ion exchange capacity after modification and their stability, and resistance of the fouled membranes to determine the impact of the fouling layer on membrane resistance, respectively.

For anion-exchange membranes (AEMs), the polydopamine (PDA) modified membrane AR204 attained higher hydrophilicity, IEC, salt removal, and reduced energy consumption. At the same current density, the AR204 coated with PDA showed higher overall desalting efficiency compared to the unmodified AR204; that is, for the same conductivity reduction, the coated membranes consumed less energy than the pristine membranes. Coating a thin layer of PDA incorporated with GO or TiO₂ improved the Cl⁻ selectivity in terms of the relative transport number by selectively transporting Cl⁻ and hindering the transport of SO₄²⁻ ions. This is due to the electrostatic repulsive force exerted by the PDA coating and the improved sieving effect resulting from the compact cross-linked coating layer. PDA coating reduced the electrical resistance of the membranes as indicated by the EIS analysis. The study also demonstrated that modifying AEMs with PDA+TiO₂ and GO significantly improved membranes biofouling resistance, while PDA+10 wt% TiO₂ and PDA+7.5 wt% GO exhibited higher tolerance against *E. coli* biofouling. PDA+TiO₂/GO modified membranes showed at least about 95% attachment reduction of live cells and 88% reduction in extracellular polymeric substance (EPS) coverage of the membrane surface ($\mu\text{m}^3/\mu\text{m}^2$).

For cation-exchange membranes (CEMs), the CR67 membrane modified under the optimal GO dosage (7.5 wt%) exhibited high normalized salt removal efficiency. Minor changes in ion-exchange capacity and membrane resistance were found among different coating materials and dosages. Thus, the surface modification with polyethyleneimine (PEI) and nanoparticles was effective in improving membrane anti-biofouling properties. For anti-organic properties, GO coating increased the energy efficiency of the ED system under all experimental conditions, while TiO₂ coated CEMs showed equal or slightly lower energy efficiency. The energy efficiency of PEI coated membranes was consistent even under relatively severe humic acids (HA) fouling, but

Antifouling Ion-Exchange Membranes

showed a significant decrease with Bovine Serum Albumin (BSA) fouling. The antifouling potential against HA and BSA was evaluated quantitatively for foulant accumulation on the membrane surface through fluorescence spectroscopy. Visualization of fouled membrane surfaces obtained by scanning electron microscopy (SEM) agreed with the results, in that: 1) PEI coating attracted more HA on membrane surfaces by the binding of functional groups; 2) polymers and nanomaterials inhibited BSA fouling by increasing the hydrophilicity of the membrane surface; and 3) PEI coating showed high stability, as well as increased chemical stability of CEM against strong bases.

Overall, the modified membranes exhibited improved fouling resistance, and demonstrated significant reduction of live cell attachment and extracellular polymeric substance (EPS) coverage of membrane surfaces. Surface modification enhanced desalting efficiency, permselectivity of monovalent ions over divalent ions, and reduced energy consumption of the ED system compared to the results using pristine membranes.

1. Introduction

1.1. Project Background

1.1.1. Membrane Desalination Technologies

Water availability and water quality have become increasingly important with the continuous depletion of available freshwater resources. Currently, many regions in the world are in the midst of water crises that have been identified as a grand challenge, especially in the arid and semi-arid southwestern United States. Some of the alarming causes are non-uniform distribution of precipitation and frequent droughts, depletion of groundwater sources due to excessive usage, and insufficient recharge. The water shortage will be further aggravated due to the continuously growing urbanization and improving life standards [1]. The insufficiency of traditional water supplies necessary to meet growing demand and concerns about water scarcity have fueled the development of alternative water resources using advanced treatment technologies. Desalination of alternative water sources such as brackish groundwater, municipal and industrial wastewater, and oil- and gas-produced water has been implemented to improve water security. Pressure-driven membrane treatment technologies such as reverse osmosis (RO) and nanofiltration (NF) are the primary methods for water reuse and desalination to fill the gap in water scarcity [2]. However, membrane fouling and scaling, high energy consumption, and limited desalination concentrate disposal options have been challenges for the broad application of desalination technologies, and in particular for pressure-driven membrane processes such as RO [3].

Electrodialysis and electrodialysis reversal (ED/EDR) are membrane desalination technologies that separate salts from water using ion-exchange membranes (IEMs) under an electric potential. ED/EDR have been used for desalination of wastewater, brackish water, and food industries [4, 5]. In an ED stack, the anion- and cation-exchange membranes are placed alternately between two electrodes. Under an electrical potential provided by a direct current (DC) power to the stack, cations move toward the negatively charged electrode (cathode) and anions move toward the positively charged electrode (anode). Hence, the concentration of ions in the concentrate chambers increase with a simultaneous decrease in the diluate chambers [6]. Ion-exchange membranes have relatively high tolerance to silica, suspended solids, hardness, free chlorine residual, and organic matter as compared to RO membranes [7-9]. These advantages of IEMs allow ED to treat alternative waters with less stringent pretreatments, lower costs, and to achieve higher water recovery with less scaling and fouling potential than is the case for RO [3, 9]. Unlike RO, which produces high-purity product water at high cost, one of the unique advantages of ED is its flexibility of varying the product water quality, achieved by adjusting applied voltage, installing different types of membranes, and using a varying number of hydraulic stages. These flexible operational conditions allow ED to control the product water salt concentration and composition tailored for fit-for-purpose end use.

Antifouling Ion-Exchange Membranes

ED has several advantages over other membrane desalination technologies. It requires less pretreatment, has higher water recovery (typically up to 90%), and is more tolerant to the presence of suspended particles and sparingly soluble salts (e.g., CaSO_4 , SiO_2 , and CaCO_3) [10]. ED is also preferable over other technologies because it allows the alteration of the product water quality by controlling the operating parameters like applied voltage and/or the feed flow rate. The direct relationship between the adjustable operating conditions and the product water quality makes it possible to explore the effect of operating parameters and to optimize the ED performance [11]. The selective separation of divalent and monovalent ions is another unique feature of ED, which allows the selective removal of certain harmful ions from water such as F^- , NO_3^- , Cl^- or Na^+ for drinking or agricultural uses [12-14].

1.1.2. Membrane Fouling & Permselectivity

Despite ion-exchange membranes demonstrating higher tolerance to fouling and scaling than RO membranes, it is still considered as a significant challenge for ED to treat impaired waters, and no complete solution that can avoid membrane fouling has emerged. There are different types of fouling, namely, colloidal fouling (particulate based), inorganic fouling/scaling, organic fouling, and biofouling. Solute adhesion and biofouling is a large impediment for membrane technologies [15, 16]. Approximately 45% of membrane fouling is due to microbial growth on the membrane surface, that is, biofouling [17]. Some of the adverse effects of fouling are: 1) reduced quality and quantity of product water due to the less permeable biofilm formed on the membrane surface, and to the increased concentration of ions in the biofilm; 2) due to the increased pressure in both feed and concentrate streams of the system, more energy is required to maintain a constant flow through the system; and 3) membranes may undergo biodegradation due to the acidic byproducts, produced by the living microorganisms, accumulated on the membrane surface.

Impaired water that contains rich organic matter, nutrients, and microorganisms can cause organic fouling by adhering onto membrane surfaces, and thereby create advantageous conditions for biofouling. Microorganisms embed on membrane surfaces, generate polysaccharides during growth, and consequently leads to inorganic scaling due to uneven membrane surfaces and concentration polarization [18]. The natural organic matter and microbial cells are negatively charged and driven toward the anode under the electric field, which cause organic and biofouling on IEMs, in particular on anion-exchange membranes [19]. The biofilm that consists of organic fouling and microbial biofouling is a poor electrical conductor, thereby increasing the electrical resistance of the system and reducing energy efficiency. In addition, the accumulation of organics and microorganisms on the membrane surfaces induces pressure loss in the ED stack and reduces the ion flux across ion-exchange membranes. Thus, fouling and scaling degrades membrane performance, shortens membrane lifetime, increases cleaning frequency, and thereby increases overall cost.

Fouling control for RO membranes has been extensively investigated including membrane performance optimization and membrane surface modification [20-22].

Limited research, however, has been conducted to reduce fouling on ion exchange membranes. Among a variety of membrane fouling control methods, surface modification through coating materials that are biocidal, have a low bacterial affinity and high self-cleaning ability, is the most cost-effective and adaptable method for current manufacturing processes [23]. There are several types of surface modification, of which the most reported is surface coating with hydrophilic polymer incorporated with inorganic antimicrobial nanoparticles [24].

The modification of IEMs with polymers bearing different charges can also alter the permselectivity of monovalent ions, which is a unique and desirable property of IEMs. It allows the selective removal of certain undesired monovalent ions and increases the flexibility of producing specified product water quality based on the intended use and/or to mitigate scale formation in concentrate streams caused by accumulation of sparingly soluble divalent ions [10]. Surface modification of commercially available membranes to improve monovalent permselectivity by coating a thin layer of the same charge as the permeable ions has been widely researched [10, 25, 26]. Membrane surface modification with polyethyleneimine (PEI) on IEMs was shown to improve the monovalent cation permselectivity while maintaining comparable overall desalination performance [26, 27]. The thin polymer coating with polydopamine (PDA) or PEI was reported to have improved permselectivity for the ions with the same charge based on their hydrated radius and hydration energy. TiO₂ and GO might be added to improve the stability, mechanical stiffness and hydrophilicity of the coating with a lower wt% (weight percent) dose, as aggregation tends to happen when they are added in abundance [22, 24]. It has been reported that modification of AEM surfaces with PDA increases the monovalent permselectivity and improves hydrophilicity of NEOSEPTA AMX [10]. Normal grade CEM (CR67) coated with PEI improved the sieving of multivalent cations due to the negatively charged thin layer of PEI [26]. Selectivity is also more likely to be affected by the salt composition, system flow rate and the applied electric potential to the ED system [6, 28].

1.1.3. Membrane Surface Modification

Surface modification of membranes with a polymer incorporated with nanoparticles has recently gained substantive interest because it enhances anti-adhesion, self-cleaning, hydrophilicity, and mechanical stability of the membranes [24]. Vasselbehagh and others [29] used polydopamine (PDA) to improve the anti-organic fouling property against sodium dodecyl benzene sulfonate (SDBS) by coating PDA on an anion-exchange membrane. Polydopamine is a strong adhesive polymer (i.e., bio-glue) that bonds non-selectively to any type of inorganic and organic solid surface [30]. Recent studies reported that the hydrophilicity and water flux through polyethersulfone (PES), polyethylene difluoride (PVDF), and polytetrafluoroethylene (PTFE) porous membranes were significantly improved by surface modification with PDA [31, 32]. PDA is amphoteric with a reported isoelectric point of pH 4 [33, 34]. Polymer layers containing hydroxyl and amino groups are attached to membranes by strong interactions between PDA and membrane surfaces [32]. PDA coating can increase hydrophilicity and negative surface charge density of an AEM, thus improving the antifouling potential against

Antifouling Ion-Exchange Membranes

organic foulants. The PDA layer on the AEM surface is expected to be highly stable since PDA attaches strongly to the membrane surfaces [30]. As a nature-inspired polymer coating, PDA has attracted considerable interest for various types of biomedical applications, such as biosensing and drug delivery [35], which indicates that PDA can be used safely to modify membranes for drinking water production. Modification of a NEOSEPTA AMX membrane with PDA simultaneously improved its antifouling potential against organic fouling, and its permselectivity for monovalent anions [10, 29].

Polyethyleneimine (PEI) was reported to improve anti-organic fouling and anti-biofouling when coated on membrane surfaces for RO membranes, proton exchange membranes, and polyvinylidene difluoride (PVDF) membranes [36-38]. Polyethyleneimine possesses highly branched polyamino groups so that the deposition of a cationic polyethyleneimine layer on a CEM surface may improve the membrane permselectivity of monovalent cations [26]. In addition, high molecular weight polyamino groups could minimize the reaction with the functional groups within the CEM matrix and thus alleviate the decrease in current efficiency as a result of increased electrical resistance [39].

In addition to using PDA/PEI as an antifouling coating for AEM/CEM, commercially available graphene oxide (GO) nanoflakes or TiO₂ nanoparticles could be used to provide additional, anti-adhesive, and anti-microbial surface properties. Nanomaterials, such as titanium dioxide (TiO₂) and graphene oxide (GO), have been studied for their antifouling properties, through either membrane surface modification or fixation in membrane structure. TiO₂ is one of the most practical nanoparticles that offers a promising platform for modification of membrane surface properties [24, 40, 41]. Anti-microbial TiO₂ nanoparticles play an important role in enhancing antifouling, reducing electrical resistance, and in modifying ion-exchange properties. Kwak and Kim [22] reported that adding TiO₂ nanoparticles to thin-film-composite RO membranes improved anti-biofouling properties against *Escherichia coli* (*E. coli*) as a model bacterium. The antifouling property of TiO₂ against organic matter was evaluated together with enhanced salt rejection and membrane hydrophilicity [42-47]. The contribution of the self-cleaning property of TiO₂ nanoparticles to its anti-organic fouling property has been explored [48]. One key mechanism of the cytotoxicity and genotoxicity of TiO₂ nanoparticles is the generation of oxidative stress called intracellular reactive oxygen species, which disturb the homeostasis of the intracellular milieu and cause membrane lipid breakdown and DNA damage [49-53].

The two-dimensional structure and tunable physicochemical properties of GO offer an exciting opportunity to make a fundamentally new class of ion-exchange membranes by increasing the ionic and molecular sieving effect on multivalent ions [41, 54]. GO is extremely hydrophilic, an important property to reduce adhesion of particulates, organics, and microbes on the membrane surface. Incorporating GO nanosheets with the polymer can increase the bonding between a polymer coating with the membrane, thereby preventing the coating from leaching during long-term operation. GO has been reported to effectively reduce organic fouling with sodium dodecyl benzene sulfonate as the model foulant, because of its hydrophilicity and negative charge [54].

Antifouling Ion-Exchange Membranes

Alam and others [55] investigated the antifouling properties of GO against *E. coli* and humic acid. GO nanosheets interact with cell membranes, resulting in cholesterol molecules and phospholipids extraction, which leads to cell membrane deformation, surface pores, void formation, and loss of membrane integrity [56-59]. Long-term antifouling properties against various organic matter such as bovine serum albumin (BSA), sodium dodecyl sulfate (SDS), pepsin, trypsin, and lysozyme have been studied with hollow fiber membranes [60]. Despite the studies focused on the anti-fouling properties of polymers and nanomaterials, the understanding of biofouling impact on electrodialysis process is still very limited, such as desalination performance and energy consumption. The change of membrane properties due to modification with polymer and nanomaterials also requires systematic investigation into complex membrane and electrolyte systems.

1.2. Project Objectives

The overall goals of this study are to reduce the costs of treating alternative waters by developing low-cost, antifouling, and high energy efficient IEMs. The specific objectives are:

- Coat commercial IEMs with non-leaching, anti-adhesive, anti-microbial materials such as TiO₂ nanoparticles and graphene oxide (GO) nanoflakes in polymers. Surface modification of a readily available cation-exchange membrane (CR67) and anion-exchange membrane (AR204) have been conducted for this purpose, with PEI/PDA for CR67/AR204 as the polymer cross-linker and with nanomaterials such as TiO₂ and GO.
- Investigate membrane properties of unmodified, modified, and fouled membranes using advanced characterization methods such as contact angle measurement, confocal scanning microscopy (CLSM), ion exchange capacity (IEC), and electrochemical impedance spectroscopy (EIS).
- Conduct laboratory-scale tests using a bench-scale ED system to evaluate IEM performance, fouling propensity, and desalination efficiency under representative operating conditions.
- Evaluate energy consumption and permselectivity of modified membranes.

1.3. Personnel

PI Dr. Pei Xu is a professor in the Department of Civil Engineering at NMSU. Dr. Xu's multiple funded research areas include water and wastewater engineering, membrane processes, desalination, potable and non-potable water reuse, produced water treatment, oxidation and photocatalysis, biological and bioelectrochemical processes, removal of emerging contaminants, and membrane fouling.

Co-PI Dr. Huiyao Wang is an associate professor in the Department of Civil

Antifouling Ion-Exchange Membranes

Engineering at NMSU. Dr. Wang conducts advanced research on innovative energy and novel materials for fuel cells, solar energy, hydrogen storage, sensors, electronic devices, and water cleaning. He investigates the dynamics and electronic and thermal transport in thin films, nanomaterials, materials, membranes, photocatalysts for manufacturing energy devices and environmental applications. He develops solar energy materials and processes to enhance surface-thermal-fluid interactions, photons-to-electrons energy conversion, and heat conversion for solar-driven water purification and desalination systems.

Dr. Xuesong Xu is a research assistant professor in the Department of Civil Engineering at NMSU. Dr. Xu's research focuses on membrane processes, desalination, and water reuse. Guanyu Ma and Million Tesfai are graduate research assistants working on the project.

2. Approach and Methods

2.1. Materials and Experimental Setup

2.1.1. Membrane & Chemical Agencies for Surface Modification

In this study, the normal grade CEM (CR67), monovalent permselective CEM (CR671) membranes, and normal grade AEM (AR204) manufactured by General Electric Water & Process Technologies (now Suez Water Technologies & Solutions) were modified and tested. Membrane properties are listed in Table 1. CR67 is a homogeneous CEM that consists of crosslinked vinyl compounds and negatively charged sulfonic acid functional groups. The selective CR671 membrane was developed by coating PEI (analytical standard, 50 wt% in H₂O solution, Sigma-Aldrich) on CR67 under controlled reaction conditions such as solution temperature (40 °C) and reaction time (24 hours) that allows amino groups of PEI to react with epoxy groups on the membrane surface. The PEI solution used in this study has branched chemical structures, with the number-averaged molecular weight of ~60,000 determined by the Gel Permeation Chromatography method and the weight-averaged molecular weight of ~750,000 determined by the Light Scattering method. Further membrane surface modifications were conducted by coating nanoparticles such as TiO₂ ($\geq 99.5\%$ trace metals basis, Sigma-Aldrich) and GO (15-20 sheets, 4-10% edge-oxidized, Sigma-Aldrich). Nanomaterials were dispersed separately into 500 mg/L PEI solutions using ultrasonic measurements (Model 08895, Cole-Parmer) at different dosages (3 wt%, 5 wt%, 7.5 wt%, and 10 wt% of PEI mass), then coated on CR671 using the same method.

Table 1. Ion-Exchange Membranes Properties

Membrane	CR67-HMR-412	AR204-SZRA-412
Type	Cation-exchange	Anion-exchange
Thickness (μm)	560–580	500
Water content	46%	46%
Electrical resistance ($\Omega\text{-cm}^2$) ^a	12	8
Ion exchange capacity (meq/g dry resin)	2.1	2.40
Reinforcement	Acrylic ^b	Acrylic ^b

^a: measured in 0.01 M NaCl

^b: acrylic: polyacrylonitrile

For AEMs coating, polydopamine (PDA) was prepared by dissolving dopamine hydrochloride (Sigma-Aldrich) in 15 mM Tris base buffer solution with an adjusted pH in the range of 8.5-8.8 by addition of HCl [61]. Freshly prepared dopamine solution started to change from a clear solution to darkish brown within 15 minutes upon contact with oxygen in the air, showing the formation of PDA (Figure 1). TiO₂ nanoparticles or

Antifouling Ion-Exchange Membranes

GO nanosheets were then added into PDA solution at a different dosage ranging from 1 wt% to 10 wt% of dopamine mass in the solution. The AR204 membrane was immersed vertically in a freshly prepared PDA solution in a beaker and placed in an electronic temperature adjustable shaker at 40 °C and 125 revolutions per minute (rpm) for 24 hours.

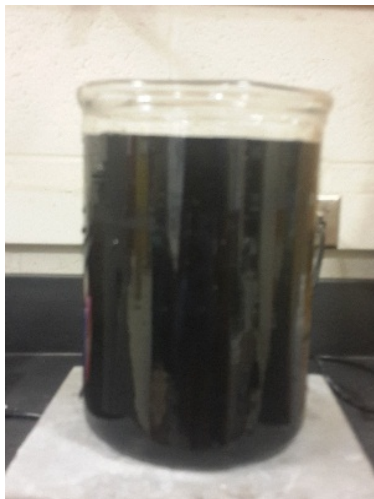


Figure 1. PDA Solution 15 Minutes after Preparation

2.1.2. Experimental Setup

2.1.2.1. Bench-scale ED stack

As shown in Figure 2, a bench-scale electrodialysis stack (PCCell 64 0 02, PCCell GmbH, Germany) was used to study the desalination efficiency and energy consumption of the membranes with different coatings. The ED stack consisted of two pairs of IEMs (three CEMs and two AEMs) with effective membrane area of 64 cm².

For CEM testing, the 20 L feed solution was prepared with total dissolved solids (TDS) 1,050 mg/L, using 750 mg/L of NaCl and 300 mg/L CaCl₂. The feed solution was circulated in the ED system at 6.1 cm/s linear velocity. The electrode solution was 20 L of 1 wt% Na₂SO₄ solution, fed separately to the electrode chambers to prevent the generation of chlorine gas and reduce electrode scaling. A constant current was applied to the stack by DC power to provide 2 mA/cm² current density across the membrane stack. Current and voltage were recorded continuously, and water samples were taken and measured using conductivity and pH meters at one-hour time intervals. All experiments lasted for 48 hours.

Antifouling Ion-Exchange Membranes

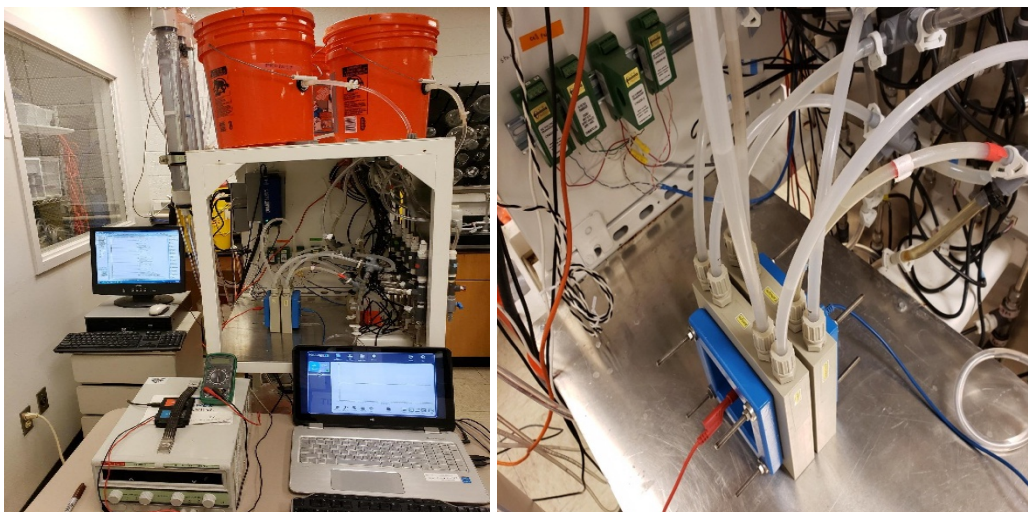


Figure 2. Bench Scale ED at NMSU Environmental Lab

For AEM testing, a 20 L feed solution was prepared by dissolving 750 mg/L NaCl and 300 mg/L CaSO₄. A 10 L electrode rinse solution was prepared by 1% Na₂SO₄ with an adjusted pH 5 by sulfuric acid to reduce scaling on the electrode chambers. Two pairs of membranes were used, that is, three CR67 CEMs and two AEMs (normal grade AR204 membranes or modified AR204). Therefore, a binary Cl⁻/SO₄²⁻ salt solution for AEMs (Na⁺/Ca²⁺ solution for CEMs) was used to compare the unmodified and modified IEMs:

- AR204/CR67 coated with PDA /PEI
- AR204/CR67 coated with PDA/PEI and different dosages of TiO₂ nanoparticles
- AR204/CR67 coated with PDA/PEI and different dosages of GO nanoflakes

The bench-scale ED experiments were operated in once-through (OT) mode, with feed/diluate and concentrate recirculated to a 20 L feedwater tank. Three micro-gear pumps from Langer Instruments (Langer Pump WT3000-1FA) that are designed to communicate with any personal computer and programmable logic controller (PLC) software developed by Automation Direct, were used for the feed, concentrate, and electrode rinse solutions. The solutions were first sent to three solution columns on the upper back side of the ED unit by three miniature gear pumps from Cole-Parmer to keep the downstream pressure head of the micro-gear pumps stable throughout the experiment while the feed water level was changing due to the samples being taken from the outlet, and to eliminate the pressure difference that may accrue due to the water level and position difference between the feed and electrode rinse solution tanks. The solution was then pumped to the ED stack by the micro-gear pumps and passed through feed and concentrate chambers at a flow rate of 300 ml/min. Diluate and concentrate from the stack flowed back to the feed container and recirculated in the ED unit. The mesh spacers between membranes and the end spacers used in the stack had a thickness of 0.4 mm and 0.5 mm, respectively, and a direct flow path. The flow in the system was calculated based on the effective length and thickness of spacers to achieve a linear flow velocity of 6.1 cm/s in each chamber. Direct voltage supply to the stack ranged from 3-8 volts and

Antifouling Ion-Exchange Membranes

pressures were maintained at 4-5 psi for feed-in and 2.3-2.5 psi in the electrode rinse stream. The ED operating conditions and specifications are summarized in Table 2.

To evaluate overall desalination efficiency, the ED testing was repeated five times for each membrane sample, with 30 minutes of membrane stabilization time with tested solutions before power was applied. Water samples were taken when the operating parameters (voltage and current readings) were relatively stable at a specific voltage value. The longer duration stability is one of the most anticipated properties of the modified membrane and could also be an indicator of the secure attachment (bond) between the membrane and modifying reagent [62]. Water flow rates and quality of the feed, permeate, and concentrate streams were monitored throughout the experiments. Conductivity, pH, temperature, water flow rate, and pressure were monitored using online sensors. Common cations and anions including sodium, calcium, chloride, and sulfate were measured using an ion chromatograph (IC, ICS-2100, Dionex, Sunnyvale, CA).

Table 2. ED Stack Specifications and Experimental Operational Parameters

Component	Type	Characteristics
EDR stack (PCCell ED 64 002)	One electrical stage	Two electrodes, Pt/Ir-MMO coated Ti- stretched metal Dimensions: Width 165 mm Depth 150 mm Height 190 mm
IEMs	Homogeneous	AR204/CR67 AR204/CR67 + PDA/PEI AR204/CR67 + PDA/PEI + TiO ₂ AR204/CR67 + PDA/PEI + GO
Effective membrane area		64 cm ²
Spacer	Spacer-gasket	Silicon/polyethylene, thickness 0.4mm,
	End spacer-gasket	Silicone/polyethylene, thickness 0.5mm
Linear flow velocity		6.1 cm/s in all chambers
Volumetric Flow	Concentrate and Diluate chambers	300 ml/min
	Electrode chambers	150 ml/min

Antifouling Ion-Exchange Membranes

2.1.2.2. Coupon Fouling Testing

A micro-scale testing system was set up to simulate the electro dialysis process (Figure 3). The effective membrane surface area is 7.07 cm^2 . Chamber volume on each side of the membrane was approximately 7 ml. Platinum coated titanium plates were used as electrodes to prevent anodic oxidation. A DC power provided constant electric field across the membrane with current density of 2 mA/cm^2 , monitored and recorded by a current sensor (NUL-202, Neulog, US). Feed solutions of 200 ml total volume per membrane sample were circulated in chambers on both sides of the membrane by a peristaltic pump (Masterflex® L/S Variable-Speed Drive, with Masterflex® L/S multichannel pump head, Cole-Parmer, US) at approximately 19 ml/min flow rate at room temperature ($\sim 25 \text{ }^\circ\text{C}$) for 48 hours. Fouling propensity of modified and unmodified IEMs was tested in micro ED cells using *E. coli* as a model microbial foulant.

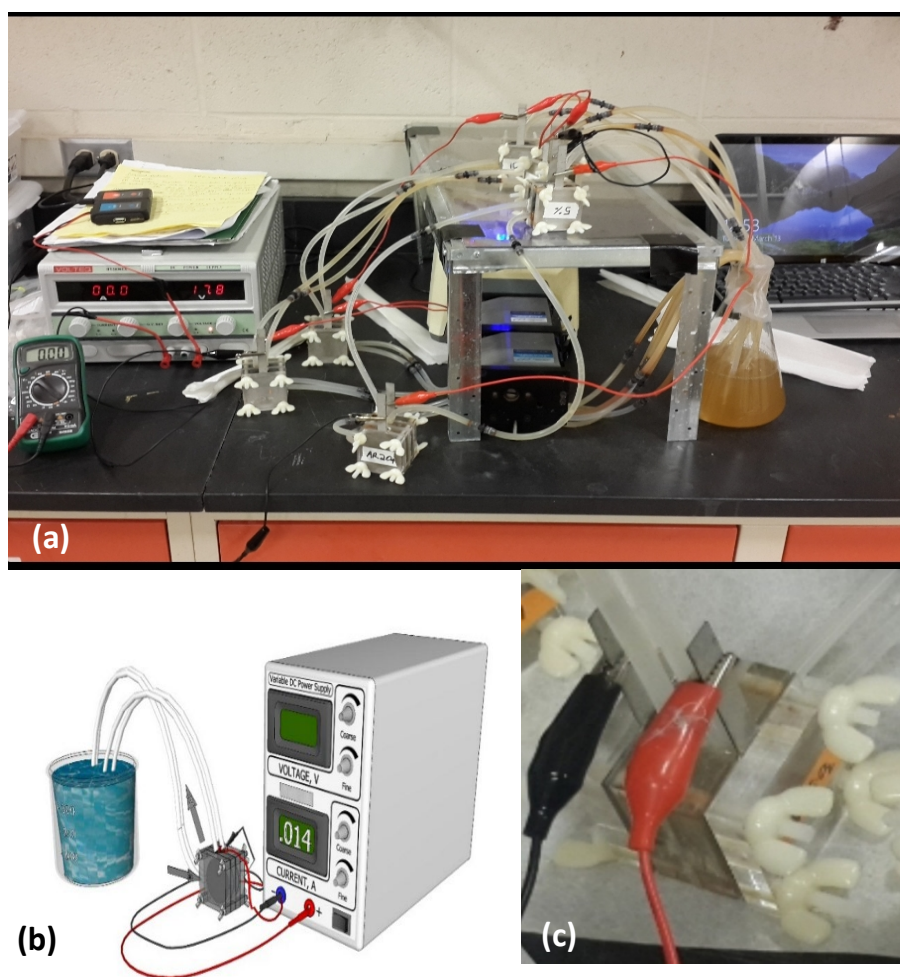


Figure 3. Bench Experimental Setup for *E. coli* Membrane Fouling. (a) Full Circulation Setup; (b) Circulation Model; and (c) Single Cell Setup

Escherichia coli (*E. coli*) was used as the model microbial foulant and was cultivated in a 25 g/L Luria-Bertani (LB) broth (granulated, Fisher Scientific). Before

adding *E. coli*, the solution was placed in an autoclave at 121°C for two hours to sterilize the liquid and glassware. The solution was cooled down to room temperature, and then a 10 ml *E. coli* solution was added into the LB broth and shaken at 37 °C for 24 hours at 225 rpm until the cell dilution reached 1.0×10^7 colony-forming unit (CFU) and the corresponding optical density of 600 nm (OD_{600} , determined by a spectrophotometer), was diluted if it exceeded the desired concentration. The total TDS of the feed solution was approximately 7 g/L NaCl.

2.2. Methodology

2.2.1. Hydrophobicity

Hydrophobicity of the membranes was analyzed by contact angle measurement using an NRL contact angle Goniometer-Model 100-00 (Ramé-hart, Inc. Surface Science Instrument, Landing, NJ). Contact angles of unmodified, modified, and fouled IEMs were examined using two different methods namely, the captive bubble [63] and sessile drop (dry) methods (Figure 4). For the captive bubble method, 2 cm² membrane samples were cut from the membrane specimens, which were kept in 3% NaCl solution. The angle measurement was done by injecting a 5 μL air bubble by a syringe right beneath the submerged membrane and measuring the contact angle made between the bubble and the bottom of the membrane surface. For the sessile drop method, membrane samples were left to dry in open air overnight and measurement was done by dropping 10 μL of DI water on top of the dried membrane surface and measuring the angle made between the dry membrane surface and the water drop. Measurements were taken immediately after a water drop was placed on the membrane surface.

The captive bubble method was adopted, instead of the sessile drop method, as membrane samples were kept moist during the measurement using the captive bubble method. The sessile method requires dry samples, while IEMs lose their surface properties as the functional groups collapse when dried. Smaller contact angle represents a more hydrophilic membrane surface, and vice versa [64]. At least five measurements were taken on each membrane for both methods in order to reduce the inaccuracy due to uneven fouling on membrane surfaces [64].

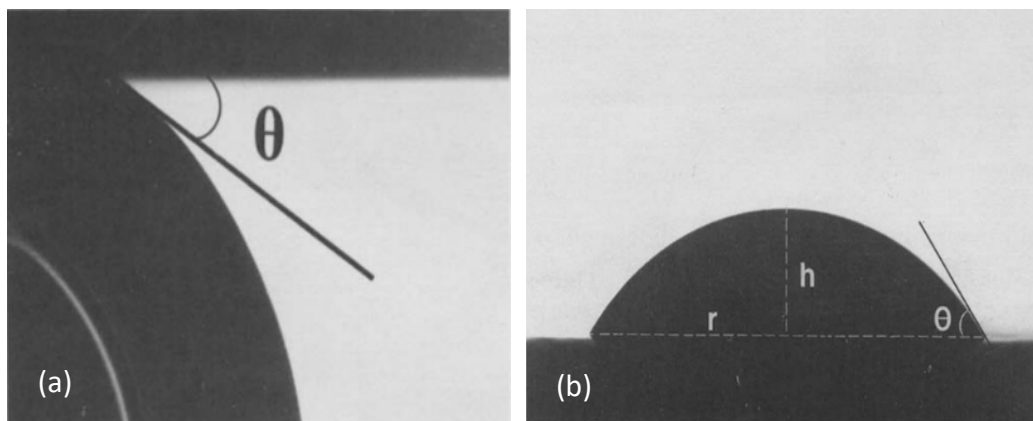


Figure 4. Contact angle for (a) Captive bubble method, (b) Sessile drop method

2.2.2. Ion Exchange Capacity (IEC)

Ion-exchange capacity (IEC) is one of the most fundamental characteristics of ion-exchange membranes, as it determines the capacity of ions transport across the membranes, thus affecting the overall desalination performance [65]. IEC is determined as the number of ion equivalents exchanged per unit dry membrane mass. In this study, IEC was measured to support and further verify the energy consumption and overall desalination efficiency results from the bench-scale ED experiments for the modified and unmodified IEMs.

Pristine (unmodified) and newly modified membrane samples ($4\text{ cm} \times 4\text{ cm}$, 16 cm^2) were first cut into pieces roughly $5\text{ mm} \times 5\text{ mm}$ and soaked in 200 ml of 1 M NaCl solution placed in a shaker at 200 rpm for 24 hours to ensure that the electrostatic bonding of AEM is predominantly to Cl^- , and CEM predominantly being Na^+ form. AEM was then soaked first in 100 ml of 0.1 M NaNO_3 and CEM in 100 ml of 0.1 M KCl for eight hours on a shaker, to exchange the Cl^- and Na^+ to mostly NO_3^- and K^+ on the membranes for AEM and CEM, respectively. After the membranes were soaked for eight hours, the 0.1 M NaNO_3 solution for AEM and KCl solution for CEM were replaced with 100 ml 0.01 M NaNO_3 and KCl solution, respectively, and placed on a shaker for 24 hours. Finally, the 0.01 M solution was replaced a second time with a solution of the same matrix and membranes were soaked for another 24 hours to ensure complete replacement. Each time before the solution was replenished, NaNO_3 solution sample for AEM and KCl solution samples for CEM were collected and analyzed by ion chromatograph (IC, ICS-2000, Dionex, USA). Membrane samples were also collected at the end of the IEC experiment and dried in an oven for eight hours at $105\text{ }^\circ\text{C}$, to get the dry weight of the membrane sample, and to determine the IEC value in meq/g of dry membrane weight, accordingly.

2.2.3. Electrochemical Impedance Spectroscopy (EIS)

Electrochemical Impedance Spectroscopy (EIS) has been widely adopted to characterize electrochemical properties of various membrane materials by quantitatively analyzing the electrical properties, electrochemical phenomena, and membrane structures [66, 67]. In this study, EIS (Figure 5) was employed to measure the electrical resistance of ion-exchange membranes with a Gamry electrochemical workstation (Interface 1000, Warminster, PA), using a four-electrode method that minimizes electrode-solution interface impedance [68].

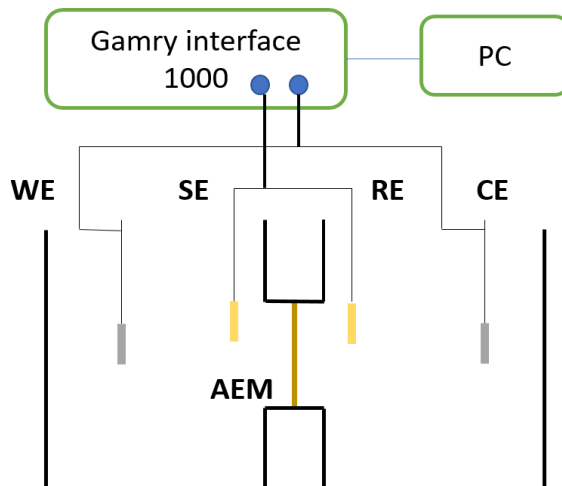


Figure 5. Schematic diagram of the experimental setup used for electrochemical impedance spectroscopy (EIS) measurements (WE: working electrode, CE: counter electrode, SE: sensitive electrode, RE: reference electrode, AEM: anion exchange membrane).

The cell used in this study consisted of two compartments of equal volume (28 ml) separated by a membrane supported with rubber supports having a circular hole of area 0.785 cm^2 . Two platinum wire electrodes were used as the working electrode (WE) and the counter electrode (CE), respectively; and two saturated Ag/AgCl electrodes placed on both sides of IEM were used as the reference electrode (RE) and the sensitive electrode (SE), respectively, to measure the potential difference and impedance across the membrane systems. The impedance from all the electrode-solution interfaces can be minimized by using four-electrode measurements [68].

Alternating current (AC) potential was applied from 1,000 Hz to 0.001 Hz for 0.05 M NaCl electrolyte solution, and 1,000 Hz to 0.01 Hz for 0.5 M NaCl electrolyte solution, at 10 measurements per decade rate and 5 mV amplitude under $25 \pm 1 \text{ }^\circ\text{C}$. The direct current (DC) potential was equal to the open circuit potential (OCP) determined before the EIS measurements. The resistance obtained from the high frequency represents the total resistance of solution and membrane (R_{SM}). The membrane resistances were obtained by subtracting the solution resistance from the total resistance.

2.2.4. Biofouling Propensity Analysis

To examine quantitatively the microbial attachment and growth on biofouled membranes, confocal laser scanning microscopy (CLSM) (TCS SP5 II Confocal, Leica) was used. CLSM is one of the common methods of studying and examining biofilm, where image data acquisition and analysis are performed with a computerized digital online system. CLSM delivers morphological data of the three-dimensional structure of bacteria and biofilm by using specific fluorescent dyes for bacterial nucleic acid (DNA/RNA) or extracellular polymeric substance (EPS) [23]. Therefore, it is possible to identify the live and dead cells using different dyes. Prior to CLSM examination, fouled membrane samples were fluorescently stained with a mixed dye solution of 1) SYTO®9 (5 mM solution, Thermo Fisher Scientific), which is a green-fluorescent nuclear counterstain that stains RNA and DNA of both live and dead *E. coli* cells, as well as in Gram-positive and Gram-negative bacteria; and 2) Concanavalin A, Texas Red™ Conjugate (Texas Red, 10 mg, Invitrogen), which is a bright red-fluorescent dye that stains extracellular polymeric substance (EPS) glycoconjugates [23]. A mixed dye was prepared by mixing the two dyes to achieve the desired concentration together and kept upright at -20 °C in the refrigerator; it was warmed to room temperature before using.

Membrane samples fouled with *E. coli* solution were collected after 48 hours of circulation in mini-coupon ED cells under the constant current density of 2 mA/cm². Membranes were rinsed gently so as not to remove/wash out the fouled layers on the membranes, and a quarter was taken from the 7.07 cm² fouled membrane sample with *E. coli* for CLSM imaging. Both sides of the membrane sample were characterized, and a "+" was marked on the samples to indicate the anode-facing side of the membrane sample during coupon circulation. More biofouling could be formed on the cathode side of the membrane sample because *E. coli* cells have a negative surface charge [69], so that the bacteria cells would flow toward the positive anode in an electric field during the coupon cell circulation and be trapped more on the cathode side as the membrane is opposed to the cell flow. Fouled membrane samples were dyed for 20 minutes using the mixed dye solution and sealed on a microscope slide with a micro cover glass to ensure wet conditions at all times. Three to five drops of mixed dye were applied (SYTO-9 and Texas Red) to fully cover the upper side of the membrane and dyed with 100 scanning layers for each spot to eliminate the inaccuracy caused by uneven bacteria growth, as shown in Figure 6.



Figure 6. A Prepared Membrane Sample for CLSM

Antifouling Ion-Exchange Membranes

CLSM imaging was conducted to measure the biomass of live and dead cells using Sytex Gr and Texas R (PMT 2 and 3) with $\times 64$ lens and Type F immersion liquid as shown in Figure 7. Five spots with each 100 Z-stack size/steps throughout the membrane sample surface were analyzed for better valuation and understanding of the biofilm (live/dead cells and EPS), as bacterial growth may not be evenly distributed or have the same biofilm thickness throughout the membrane surface.

The image stacks from CLSM were further processed using Leica software (LAS X) before loading them to COMSTAT 2 (Figure 7). Based on MATLAB, COMSTAT 2 is a program that quantitatively analyzes image stacks recorded by confocal microscopes (obtained from www.comstat.dk) [70, 71]. Through LAS X, images were analyzed to check if any blank sub volume (pixel) between biomass-filled sub volumes exists, and to eliminate it accordingly in order to simplify images for COMSTAT 2 analysis [72]. COMSTAT 2 performs thresholding of the image stacks acquired from the CLSM, and results in a three-dimensional matrix with threshold values between zero and the set value used in CLSM. The subsequent segmentation process removes pixels that are not connected to the substratum or bonded with another pixel from the bottom. The output provides the volume of biomass per unit area of membrane surface [72]; and the result is displayed in two different channels with one displaying the mass of live and dead *E. coli* cells in green color while the second displays mass of EPS in red color [70, 71].

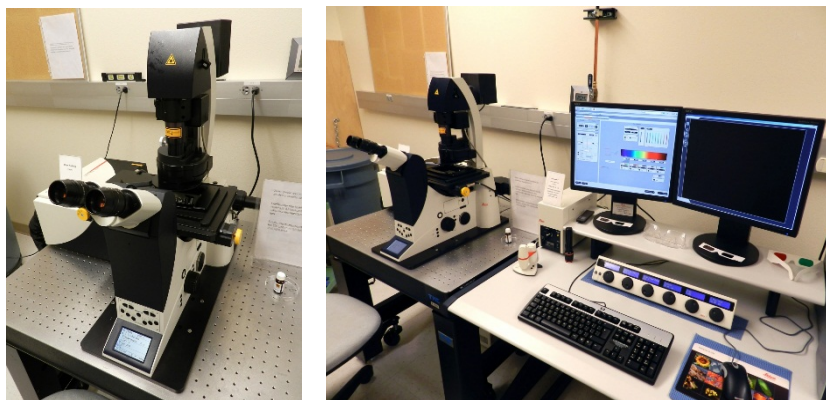


Figure 7. TCS SP5 II confocal microscope at NMSU Electron Microscopy Lab

2.2.5. Fluorescence Excitation-Emission (FEEM) Spectrum

FEEM is a widely used fluorescence spectroscopy that classifies fluorophores based on excitation and emission properties. FEEM generates a 3D scanning contour plot of excitation wavelength [73] vs. emission wavelength (E_m) vs. fluorescence intensity. Fluorescence regional integration [74] is a classification method of dissolved organic matter that divides the FEEM contour plot into different zones [75]. This regional excitation-emission method helps identify and quantify organic compounds in a solution with multiple types of organic matter. The boundary of the FRI method is later defined in the Result and Discussion section by the actual measured peak locations and base areas of the organic compounds of interest.

FEEM was conducted for extracted solutions. Prior to FEEM analysis, all extracted solutions were adjusted to neutral pH with HCl. FEEM measurements were performed at Ex wavelength ranging from 220 to 450 nm and Em wavelength ranging from 240 to 600 nm simultaneously. The slit widths were 5 nm for both Ex and Em. To compare quantitatively the organic fouling on membrane surfaces, the fluorescence volume was calculated using the FRI technique that integrates the area beneath excitation-emission matrix [76] spectra. The volume (Φ_i) beneath region “i” of the EEM can be calculated in:

Equation 1.

$$\Phi_i = \int_{ex} \int_{em} I(\lambda_{ex}, \lambda_{em}) d\lambda_{ex} d\lambda_{em}$$

For discrete data in this takes the form:

Equation 2.

$$\Phi_i = \sum_{ex} \sum_{em} I(\lambda_{ex}, \lambda_{em}) \Delta\lambda_{ex} \Delta\lambda_{em}$$

where $\Delta\lambda_{ex}$ is the excitation wavelength interval (taken as 5 nm), $\Delta\lambda_{em}$ is the emission wavelength interval (taken as 5 nm), and $I(\lambda_{ex}, \lambda_{em})$ is the fluorescence intensity at each excitation-emission wavelength pair. The cumulative volume (Φ_T) is calculated as $\Phi_T = \sum \Phi_i$. The fluorescence intensity was normalized by the Raman area, so that the TOC-normalized FRI volume has units of AU-nm²/[100 mg/L TOC]. The percent fluorescence response [77] is calculated as $P_i = \Phi_i/\Phi_T \times 100\%$, to compare the composition of different organic compounds.

2.2.6. Chemical Extraction of foulants

Chemical extraction was conducted for organic fouled membrane samples in order to further evaluate the fouling conditions quantitatively. A 4 cm × 4 cm membrane sample was measured and cut from the original sample, and cut into small pieces (about 0.5 cm × 0.5 cm) for better extraction results. The cut samples were soaked in 50 ml of 0.1 M NaOH extraction solution, and ultrasonicated for 120 minutes. Solution temperature was controlled below 50 °C. The extracted solution was centrifuged to separate any particles from membrane samples. TOC of the extracted solutions was measured.

2.2.7. Scanning Electron Microscopy (SEM)

SEM is a useful tool to characterize membrane surface properties. In this study, SEM was used to visualize the fouled membrane surfaces to compare qualitatively the antifouling resistance. Prior to SEM imaging, membranes were air-dried overnight. Membrane cracking after drying was expected, as given the nature of ion-exchange membranes. Membrane samples were cut into 1 cm × 0.5 cm pieces, mounted on a

support by carbon tape, and analyzed by SEM (S-3400 N Type II, Hitachi High-Technologies Corp., Pleasanton, CA, USA). Viewing was optimized 100-fold magnification.

2.2.8. Desalination Performance

To study the desalination efficiency and energy consumption of the membranes with different coatings, bench-scale electro dialysis experiments were conducted. Two pairs of IEMs (three CEM and two AEM) with effective membrane area of 64 cm² were installed in a bench-scale electro dialysis stack (PCCell 64 0 02, PCCell GmbH, Germany). Feed solution contained total dissolved solids (TDS) of 1,050 mg/L, including 750 mg/L NaCl and 300 mg/L CaCl₂. 20 L of feed solution was circulated in the system at 6.1 cm/s linear velocity. The electrode solution, 20 L of 1 wt% Na₂SO₄ solution, was fed separately to the electrode chambers to prevent the generation of chlorine gas and to reduce electrode scaling. A constant current was applied to the stack by DC power to provide 2 mA/cm² current density across the membranes. These operating conditions were selected to represent full-scale operation of a brackish water electro dialysis system [26, 27]. Current and voltage were recorded continuously, and water samples were collected and measured with conductivity and pH at one-hour interval. All experiments were conducted for 48 hours.

2.3. Calculations

To evaluate the impact of modification on IEMs, conductivity reduction (i.e., salt removal), ion selectivity, and energy consumption were assessed under the conditions mentioned above. The overall salt removal efficiency is calculated as conductivity reduction as follows:

Equation 3. Conductivity reduction

$$\text{Conductivity reduction (\%)} = \left(1 - \frac{C_d}{C_f}\right) \times 100$$

where C_d and C_f are the conductivity of diluate and feed (mS/cm).

The permselectivity of the membranes is calculated based on the relative transport number (RTN) of divalent ions SO₄²⁻ as opposed to monovalent ions Cl⁻ as follows:

Equation 4. Permselectivity

$$t_{Cl}^{SO_4} = \frac{(\text{Equivalent of } SO_4 \text{ removed}) / (\text{Average equivalent } SO_4 \text{ concentration})}{(\text{Equivalent of Cl removed}) / (\text{Average equivalent Cl concentration})}$$

where the average equivalent concentration was defined as the arithmetic average concentration of the inlet and outlet concentrations in the same stream.

Antifouling Ion-Exchange Membranes

Normalized salt removal allows the comparison of overall ED desalination performance under different operating conditions such as membrane types and feed solution compositions, calculated as the equation below:

Equation 5. Normalized salt removal

$$\text{Normalized salt removal} = \frac{(C_f - C_d) \times Q_d}{S \times I \times V}$$

where I is the current through the ED stack; V is the applied voltage to the ED stack; Q_d is the diluate flow rate.

Equation 6. Energy consumption

$$\text{Energy consumption} = \frac{I \times V}{Q_d}$$

The ion-exchange capacity of IEMs was calculated based on the number of chloride ions replaced by nitrate ions (meq) to the membrane sample dry weight (g) as follows:

Equation 7. Ion exchange capacity

$$IEC = \frac{\text{total amount of exchanged ion (meq)}}{\text{dry weight of membrane (g)}}$$

Average linear velocity in the stack was calculated based on chambers dimension (spacer dimension) and volumetric flow rate as;

Equation 8. Average linear velocity

$$\text{Average linear velocity}(u) = \frac{Q_d}{n \times h \times w}$$

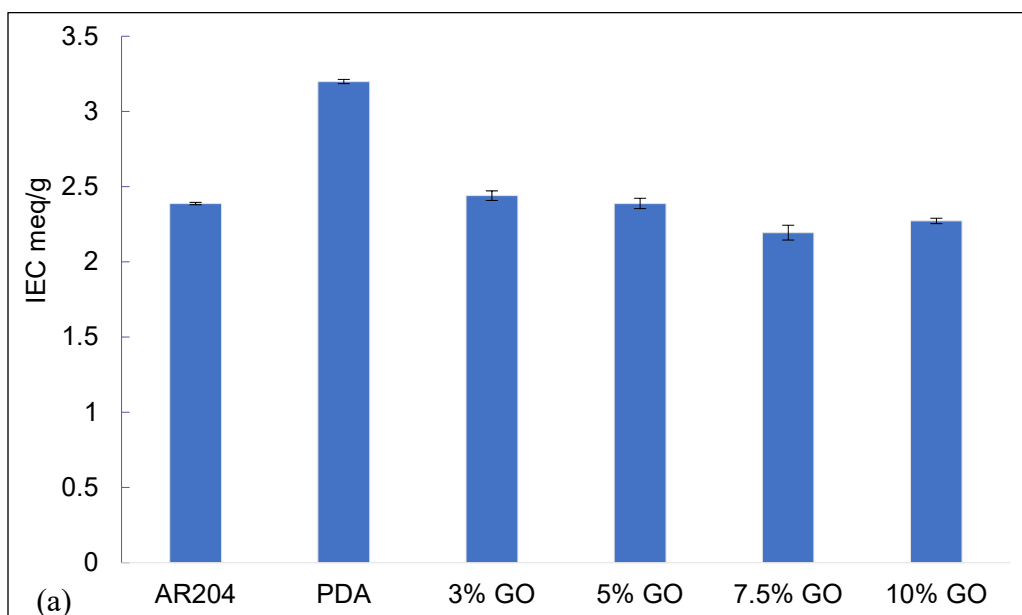
where n is the number of IEM pairs, and h and w are the thickness and width of spacer gasket.

3. Results and Discussions

3.1. Development of Antifouling AEMs

3.1.1. Ion Exchange Capacity (IEC)

The IEC values of pristine and modified membranes with PDA incorporated with different dosage of TiO₂/GO are shown in Figure 8. IEC values of membranes modified with PDA + TiO₂/GO shows marginal difference compared with the unmodified pristine membrane. The modification of AEMs with only PDA showed a 34% increase in IEC, which is very consistent with the conductivity reduction and energy consumption data. The increase in IEC on AEMs modified with PDA was due to the contribution of the amine groups of PDA. The pKa value of the PDA amine group is approximately 10, lower than the neutral pH of the solution for measuring IEC, therefore the amine groups of PDA contributed to the IEC of the coated AEM. With the addition of nano-particles, the accessibility of the ions to the functional groups from PDA decreased as they were partially isolated/surrounded by the increased concentration of nano-particles [78].



Antifouling Ion-Exchange Membranes

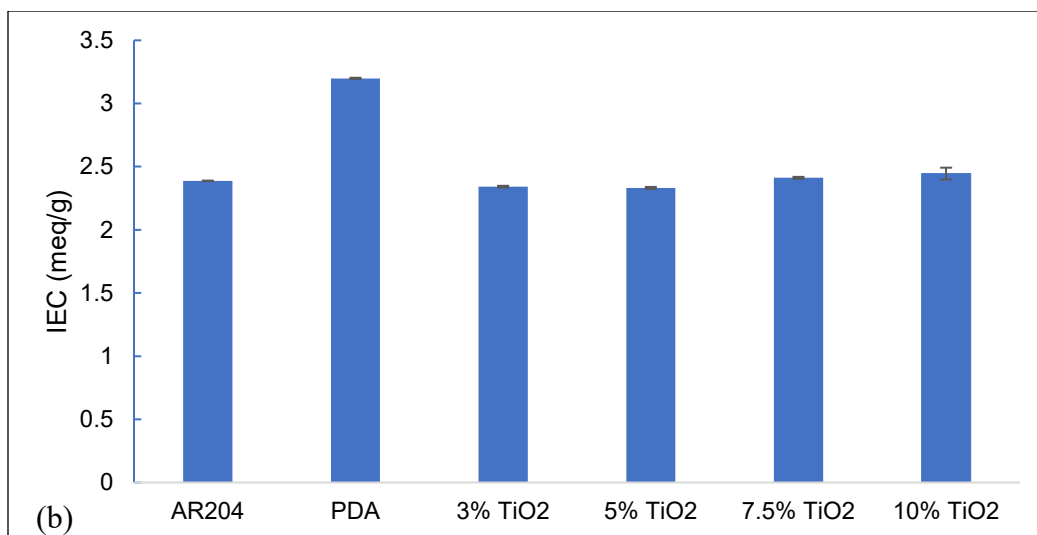


Figure 8. Ion Exchange Capacity for Unmodified and Modified Membranes. (a) Raw AR204, PDA and PDA + different dosage of GO modified AR204, (b) Raw AR204, PDA and PDA + different dosage of TiO₂ modified AR204.

3.1.2. Hydrophilicity

Contact angle is a key parameter in determining the hydrophilicity of a membrane surface. In this study, the determination of the contact angle was performed before and after the membrane fouling tests. Membrane samples obtained from the fouling experiment were rinsed gently with DI and were analyzed using sessile drop and captive bubble methods to evaluate: 1) the effect of foulant on membrane hydrophilicity; 2) the effectiveness of membrane modification on imparting self-cleaning and anti-adhesive properties on membrane surfaces; and 3) to compare the membrane hydrophobicity by the two contact angle measuring methods. In general, smaller contact angle measurement infers more hydrophilic membrane surface and less microbial/organic foulant attachment on the membrane surface [64].

Both fouled GO and TiO₂ incorporated in PDA achieved almost the same enhancement on membrane hydrophilicity as compared to the unmodified membrane, with nearly 20° and about 13.5° less measured angle in the sessile and captive bubble method in an average of five measurements/readings taken on each membrane (Figure 9). For all the modified membranes, there was no significant difference in the measured angles of the captive bubble and sessile drop methods after membrane fouling, with a maximum difference of 1.1° among all the modified membranes and a maximum variability of ±3.2° in the readings taken on the same membrane, which indicates more homogeneous membrane surface and membrane. The fouled uncoated AR204 membranes showed the largest difference in comparing the sessile and captive bubble measuring methods, owing to the wavy nature of the AR204 membrane surface and the uneven distribution of the biofilm formed on the membrane surface. Larger contact angle measurements were obtained using the dry method for uncoated AR204, because when

Antifouling Ion-Exchange Membranes

the membrane dries, the surface contracts and cracks. At the same time, uncoated AR204 exhibited the most substantial variability (± 5.1) from all the captive bubble measurements, due to the irregularity in the alignment of its feathery structure and the uneven distribution of the biofilm on the surface of uncoated AR204. The same phenomenon was not observed on the coated membranes, and this implies that coating decreased the irregularity on the surface of the membrane as well as the resistance toward fouling. The PDA coating covered the membrane surface and made these wavy structures at the surface get partially filled and aligned with a PDA layer, hence yielding less variability in measurements taken on the same membrane. For the dry method of fouled membranes, these partially extruded feather-like structures dry/shrink and sink further into the coating layer and leave a smoother and more hydrophilic coating layer at the membrane surface. For the unfouled membranes dry method, the membranes soaked up the sessile drop (10 ml DI) so that measurements could not be taken.

The results of the contact angle measurement demonstrated that modification of AEMs with just PDA or PDA incorporated with TiO_2/GO enhanced membrane hydrophilicity and self-cleaning ability. This improved hydrophilicity indicated that membranes are becoming more fouling resistant, as has been reported by Safarpour and others [24].

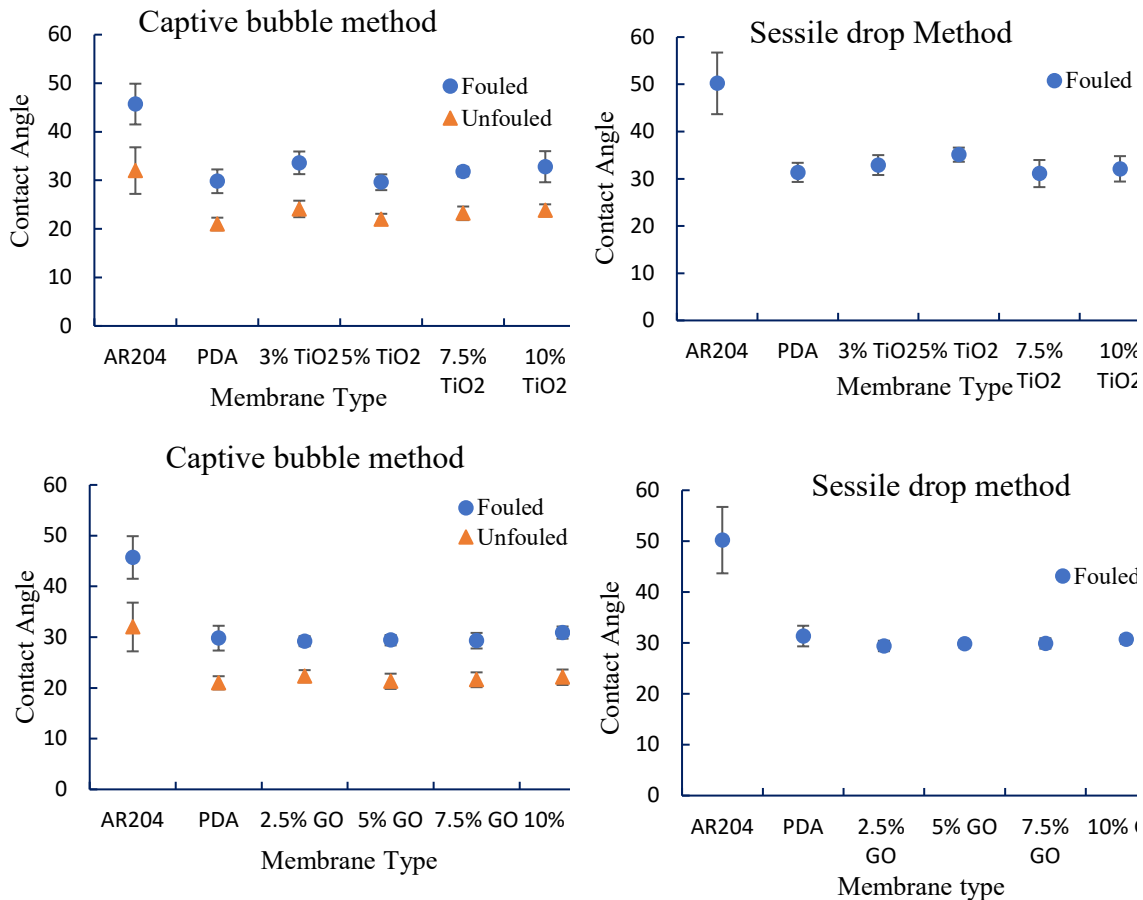


Figure 9. Contact Angle Measurements of Fouled and Unfouled Membranes

3.1.3. Membrane Resistance Measurements

The results for EIS analysis are present in Figures 10 and 11, where the horizontal axis (Z') represents the real membrane resistance, and the vertical axis (Z'') represents the imaginary resistance or the time constant related to ion transport through the membrane which represents the capacitance of the system. After coating PDA, the resistance (R_{SM}) of AR204 membranes at high frequency (100 kHz) decreased to 2.54 Ω in the EIS measurement as shown in Figure 10. After coating 1 wt% TiO_2 onto the surface of AR204 with PDA, R_{SM} increased. However, R_{SM} decreased as the amount of TiO_2 increased. The biofouled AR204 coated with PDA (namely AR204+PDA) shows a higher R_{SM} value compared to the membranes coated with TiO_2 . The resistance difference between unfouled and biofouled AR204+PDA is 4.9 Ω ; however, the resistance difference between unfouled and biofouled AR204+PDA+10 wt% TiO_2 is 2.2 Ω . Furthermore, the shape of the impedance spectra at low frequencies of the biofouled AR204+PDA and biofouled AR204+PDA+1 wt% TiO_2 are different from the rest of the membranes. The reason could be the fouling layers on the membrane surface blocked the transmembrane migration of the ions and the formation of the diffusion layer.

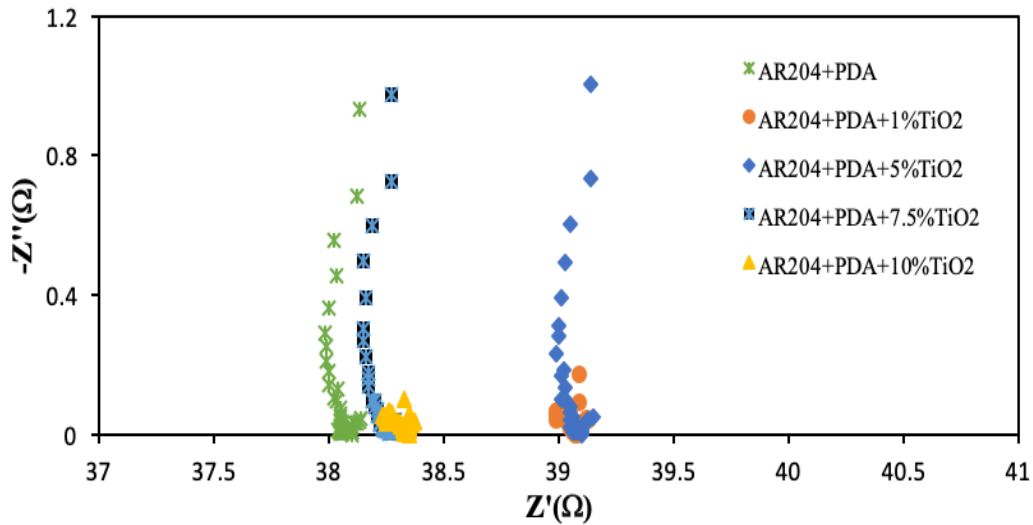


Figure 10. Electrochemical impedance spectroscopy (EIS) of raw AR204 and AR204 coated with PDA.

Antifouling Ion-Exchange Membranes

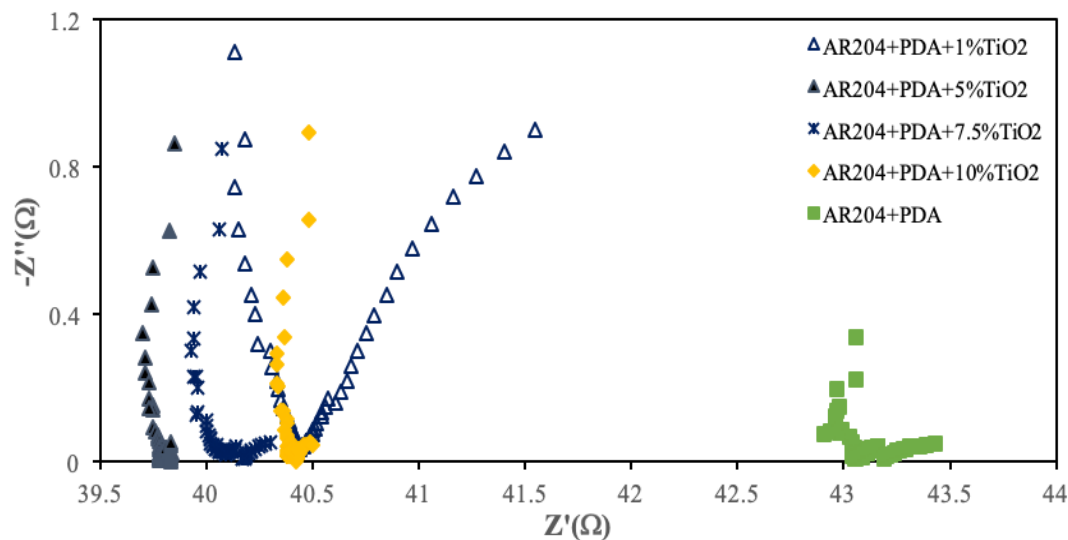


Figure 11. Electrochemical impedance spectroscopy (EIS) of AR204 coated with PDA and different concentration of TiO_2 after membrane biofouling experiments

3.1.4. Confocal Laser Scanning Microscope and COMSTAT Analysis

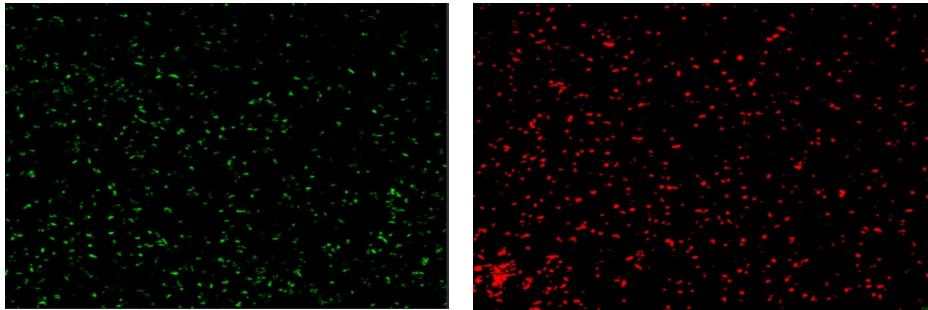
The CLSM images for biofouled membranes including the pristine AR204 and those modified with coatings of PDA as well as TiO_2 and GO are shown in Figure 12. Green bright spots (Channel 1) show both live and dead stained *E. coli* cells, while red bright spots (Channel 2) are related to extracellular polysaccharides in the formed biofilm. The bright spots of Channel 1 and Channel 2 images are highly comparable, given that: 1) extracellular polymeric substance (EPS) is secreted by *E. coli* cells during cell growth, and 2) the cell outer membrane contains lipopolysaccharides and is stained by Texas Red. Bright spots for both channels are not evenly distributed or spread because the period of the fouling experiments (48 hours) was not long enough for *E. coli* to develop throughout the membrane surface and cover the entire surface with biofilm. It is clear from the CLSM images that there was a considerably greater amount of *E. coli* cells attachment on the unmodified membranes versus the PDA modified membranes. Consequently, a more significant amount of EPS was observed on these membranes compared to AEMs modified with PDA+ TiO_2 /GO. Therefore, images were analyzed with COMSTAT 2 to quantify the befouling attachment.

Figure 13 shows the amount of biomass calculated by COMSTAT 2 in terms of volume of biomass accumulated over unit membrane area. Figures 13(a) and (c) describe the volume of biomass by live and dead cells, and (b) and (d) shows EPS coverage of membrane for unmodified AR204, PDA, and PDA+ TiO_2 /GO modified membranes. Both TiO_2 and GO reduced membrane biofouling remarkably, with regard to mitigating cell attachment and biofilm formation on the membranes. For example, AR204+PDA+10 wt% TiO_2 and AR204+PDA+7.5 wt% GO showed 97% and 95% reduction in cell attachment and 92% and 88% reduced biofilm layer formation, respectively, as compared to unmodified normal grade AR204 membranes. As biofouling begins with the

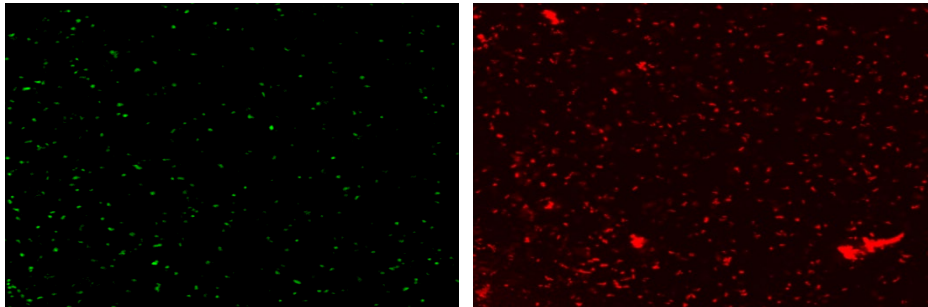
Antifouling Ion-Exchange Membranes

attachment of microorganisms that then develop to biofilm, the EPS with its hydrophobic characteristic and highly porous structure gives microorganisms perfect shelter from the scouring effect of the flowing water. Hence, it leads to further advancement of fouling which is the case in unmodified AR204 fouling. This result is consistent with the contact angle measurements discussed in section 3.1.2, showing that membrane biofouling resistance improved considerably due to improved hydrophilicity, and that this explained the reason behind the biggest biofilm accumulation on the surface of unmodified AR204. Coating TiO_2/GO into polymer membranes was also reported to enhance hydrophilicity and impart self-cleaning and antibacterial property [24]. An additional reason for the reduced fouling on modified membranes is the rejection of negatively charged *E.coli* cells, zeta potential -21.9 ± 3 mV [79], by the thin negatively charged coating layer due to their negatively charged surface [69]. Improved membrane surface hydrophilicity and smoothness reduces the adsorption characteristics, and this also contributes in fouling resistance as well [24]. In the case of TiO_2 coated membranes, the anti-bacterial TiO_2 nanoparticles inactivate the attached bacteria from multiplying and producing more biofilm [22]. Greater resistance against toxicity and mechanical stability of GO makes the membrane surfaces more resistant and stiffer and introduces more mechanical stability to the PDA coating so that it stays smooth longer, thereby reducing fouling accumulation on the surface of PDA+ TiO_2 and GO modified membranes.

AR204

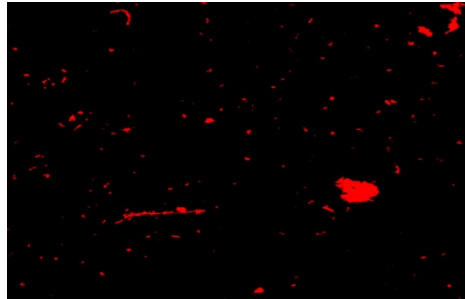
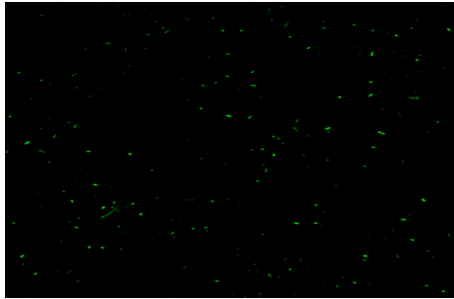


AR204 +PDA

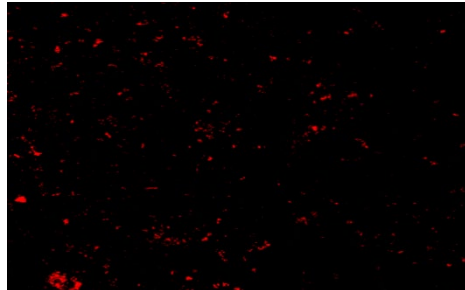
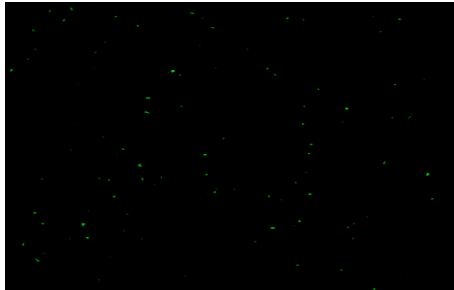


Antifouling Ion-Exchange Membranes

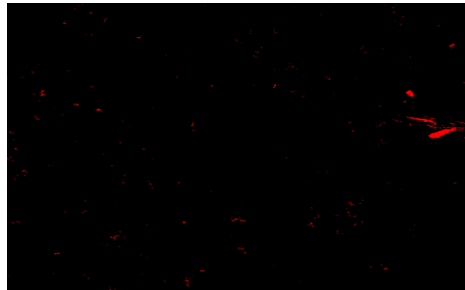
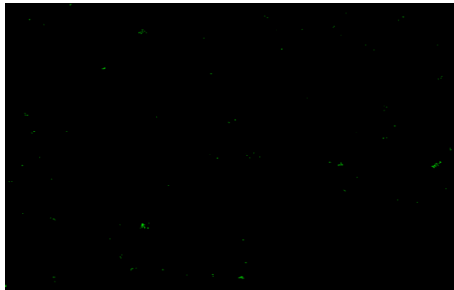
AR204 + PDA + 3 wt% TiO₂



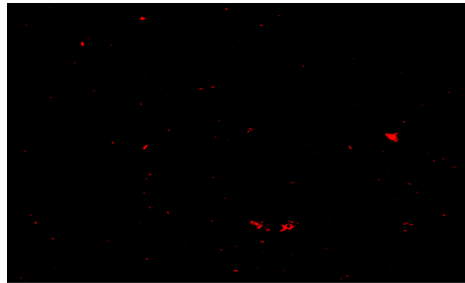
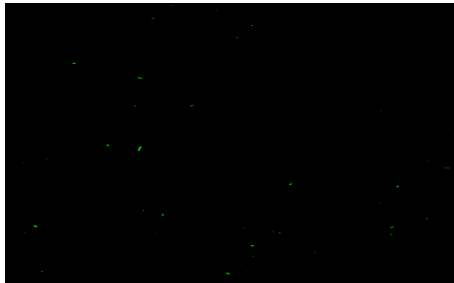
AR204 + PDA + 5 wt% TiO₂



AR204 + PDA + 7.5 wt% TiO₂

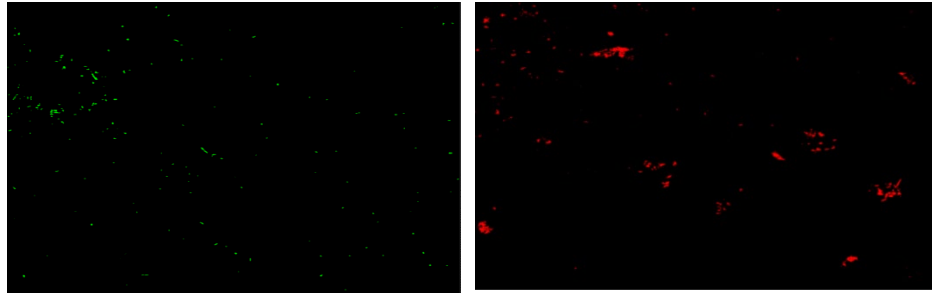


AR204 + PDA + 10 wt% TiO₂

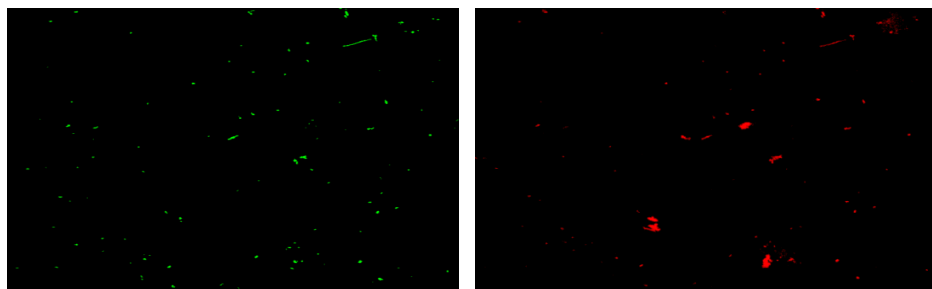


Antifouling Ion-Exchange Membranes

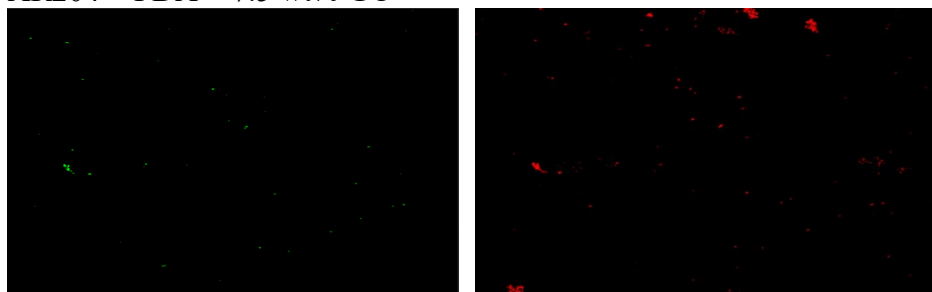
AR204 + PDA + 2.5 wt% GO



AR204 + PDA + 5 wt% GO



AR204 + PDA + 7.5 wt% GO



AR204 + PDA + 10 wt% GO

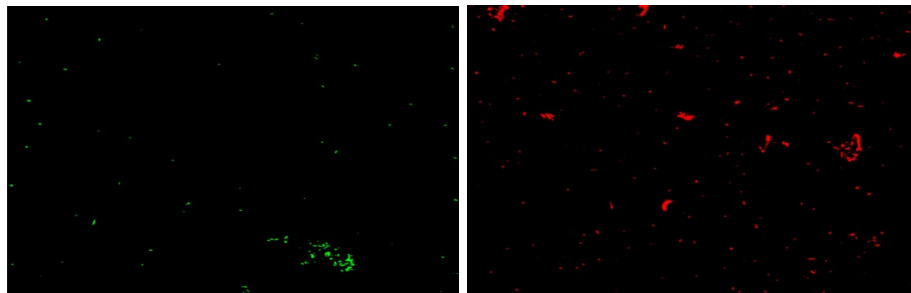


Figure 12. CLSM images of biofilm formed on AR204 coated with PDA and different concentration of TiO_2 after membrane biofouling experiments

Antifouling Ion-Exchange Membranes

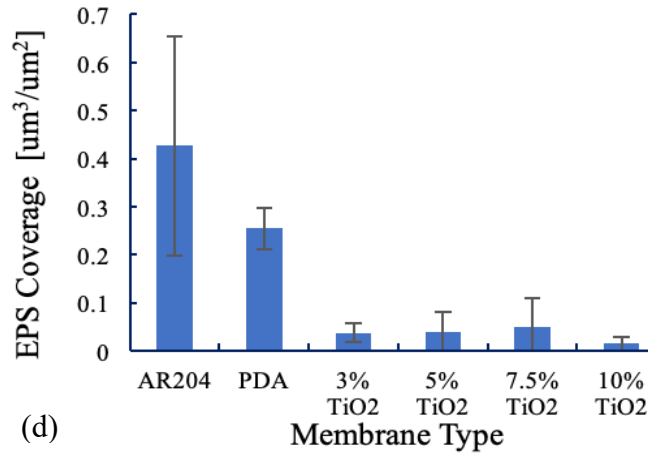
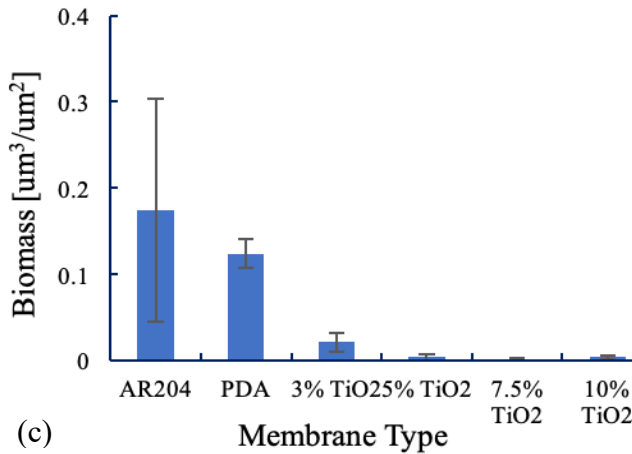
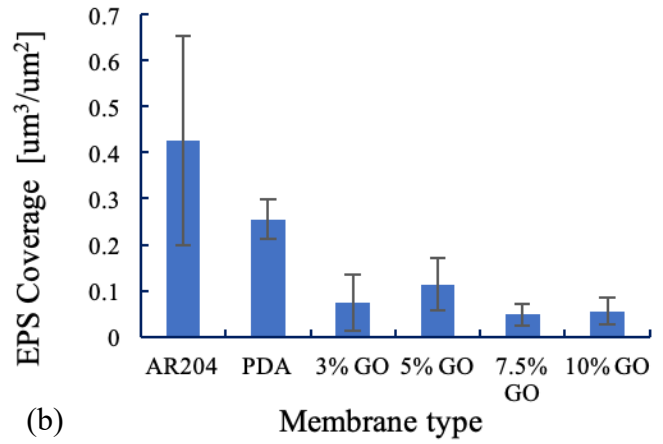
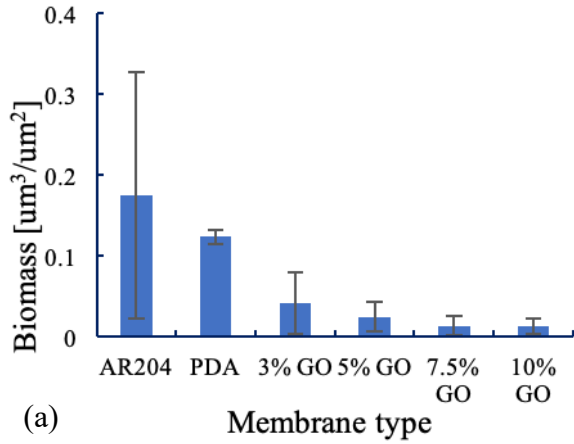
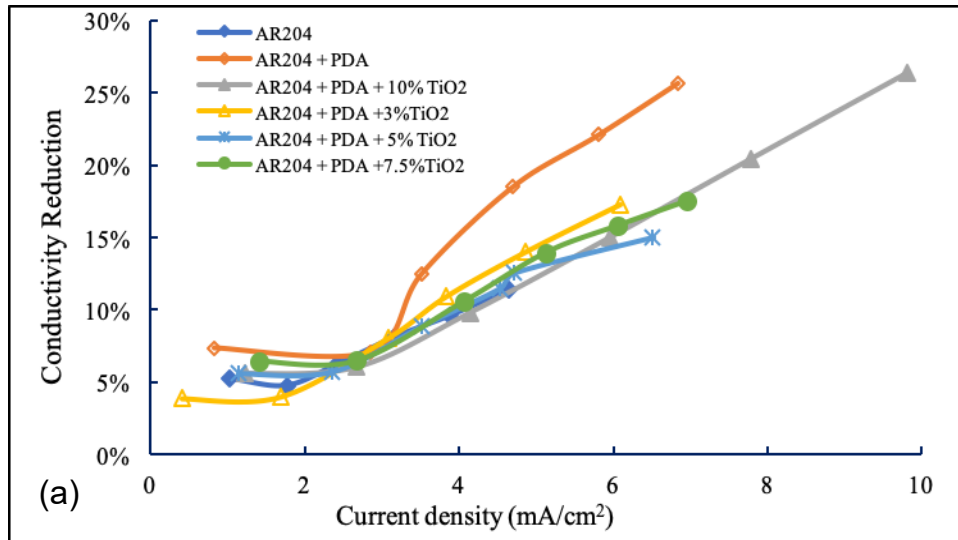


Figure 13. COMSTAT Analysis on CLSM Images of Fouled Membranes. (a) and (b) biomass by live and dead cells and EPS coverage of membrane respectively for Raw AR204, PDA and PDA + GO modified membranes, (c) and (d) biomass by live and dead cells and EPS coverage of membrane respectively for Raw AR204, PDA and PDA + TiO₂ modified membranes.

3.1.5. Overall Desalination Efficiency

3.1.5.1. Conductivity Reduction

Overall desalination efficiency of all membranes was analyzed and compared under the same operating parameters including voltage applied and flow rate. For each testing condition, the experiments were repeated five times for reliable results and reproducibility. For consistency, the fifth run of the rejection test was selected as representative results for comparison because membranes and the ED system need time to stabilize and to examine membrane durability as it runs for longer times. Except for the PDA coated membranes, all the rest of the modified (AR204+PDA+TiO₂/GO) and unmodified (normal grade AR204) membranes achieved almost the same desalination performance. PDA coated membrane achieved the highest removal efficiency under the same current density during the bench-scale testing, which matches perfectly with the IEC data demonstrated in Figure 14. Both 10 wt% and 7.5 wt% of TiO₂ and GO show nearly the same conductivity reduction and both reached the highest current density for the same applied voltage, indicating lower resistance compared to other tested membranes. Unmodified AR204 attained the lowest conductivity reduction compared to all PDA+TiO₂ modified membranes at current density less than 2 mA/cm². Therefore, it can be concluded that modification of the AR204 membrane with PDA had a positive impact on salt removal efficiency compared to the unmodified AR204, while incorporation of nanomaterials demonstrating insignificant change.



Antifouling Ion-Exchange Membranes

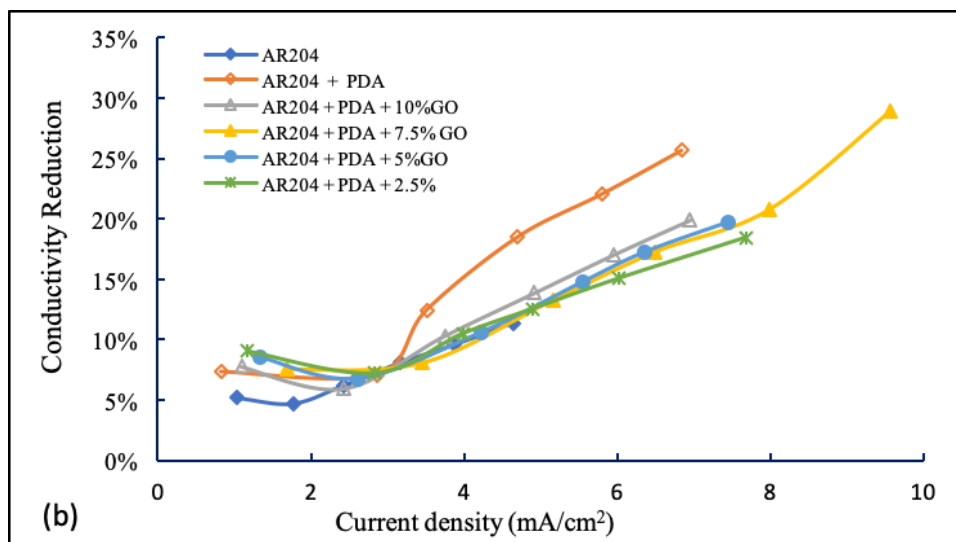


Figure 14. Conductivity Cut Comparison of (a) Unmodified AR204, AR204 coated with PDA and AR204 coated with PDA + different dosage of TiO₂, (b) Unmodified AR204, AR204 coated with PDA and AR204 coated with PDA + different dosage of GO.

3.1.5.2. Permselectivity

Permselectivity of monovalent over multivalent anions was analyzed using relative transport number (RTN) ratio of SO₄²⁻ over Cl⁻ through the modified and unmodified AEMs with Cl⁻ as the standard ion. As is reflected by the RTN number difference, the permselectivity of monovalent ions improved considerably through modification of AEMs with PDA incorporated with TiO₂/GO. The normal grade AR204 selectively removed divalent SO₄²⁻ ions over monovalent Cl⁻ ions, that is, higher RTN number relative to modified AR204 membrane under the same current density (Figure 15). The selectivity of divalent ions decreased with an increase in current density. The selective transport of divalent ions was due to: 1) divalent anions SO₄²⁻ facing higher electrostatic attraction from the positively charged functional groups at the surface of the normal grade AEMs as compared to the monovalent ions Cl⁻ under an electrical field [10]; 2) for coated membranes in general, selectivity of monovalent ions increases with increasing current density, until it reaches a certain value wherein afterward the RTN value remains stable. For example, as the current density increases from 2 mA/cm² to 4 mA/cm², there is a reduction in RTN value by 1.5 times for unmodified AR204 membrane and approximately 0.5 times reductions in RTN for all the modified AR204 membranes (PDA, PDA+TiO₂ and PDA+GO). As current density increases beyond 4 mA/cm², the RTN value remains relatively stable for both modified and unmodified AR204 membranes.

All the modified membranes have RTN values less than one, and both PDA+10 wt% GO and PDA+10 wt% TiO₂ modified membranes have slightly lower monovalent selectivity compared to the other modified membranes. The high dosage of nanomaterials led to aggregation, and possibly blocked ion-exchange functional groups, thus reduced monovalent cation selectivity [24]. Selectivity is also a function of the hydrated radius

Antifouling Ion-Exchange Membranes

where it plays a role in molecular sieving effect. As the coating fills the pore spaces on membranes, it gets tighter and rejects divalent ions more due to their larger hydrated radius, SO_4^{2-} (3.76 Å), as compared to monovalent ions Cl^- (3.32 Å) [80]. Besides, PDA is negatively charged, with zeta potential at approximately -4.6 mV around neutral pH [81]. This negatively charged coating layer provided a greater repulsion force to divalent anions than monovalent anions, thus increased the monovalent anion selectivity.

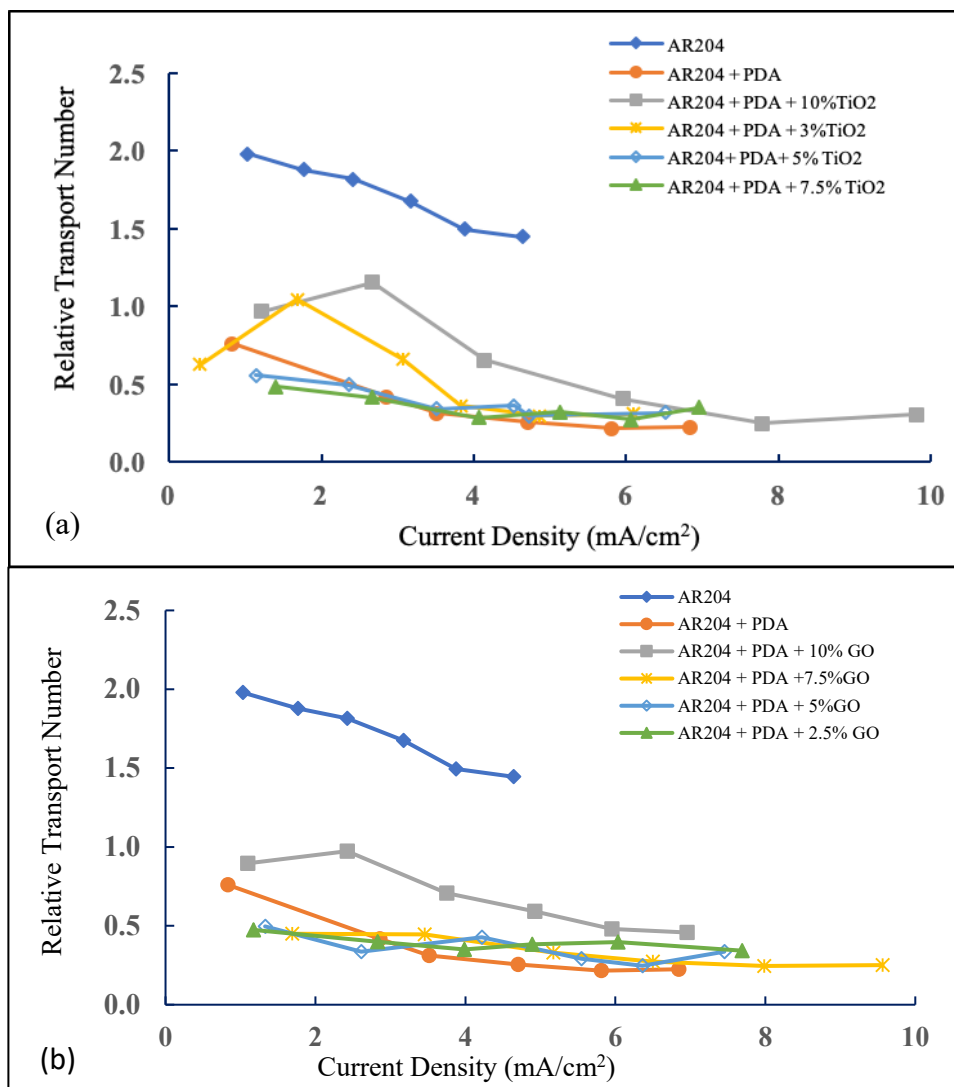


Figure 15. Permselectivity of SO_4/Cl for Raw AR204 and Modified Membranes. (a) Raw, PDA and PDA+different dosage of TiO_2 ; (b) Raw, PDA and PDA+different dosage of GO

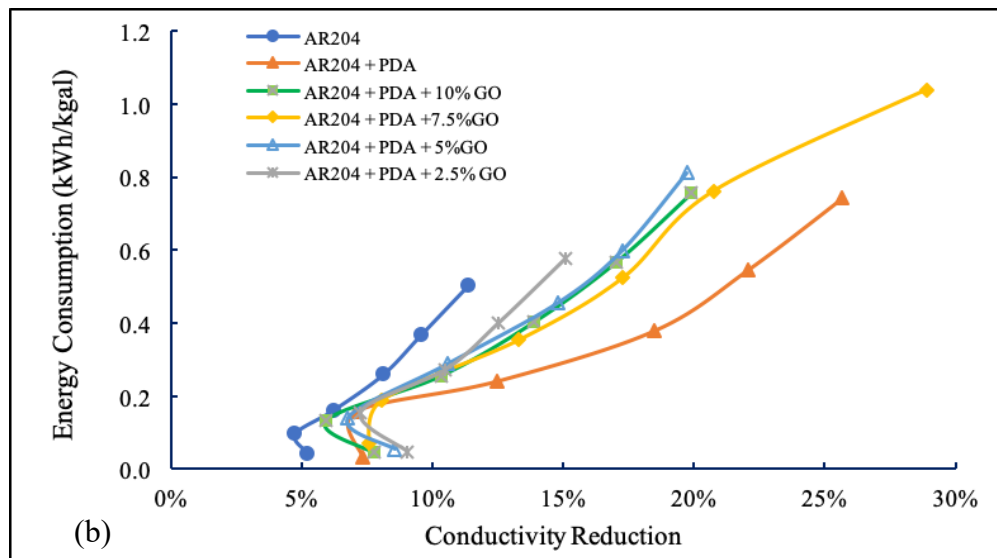
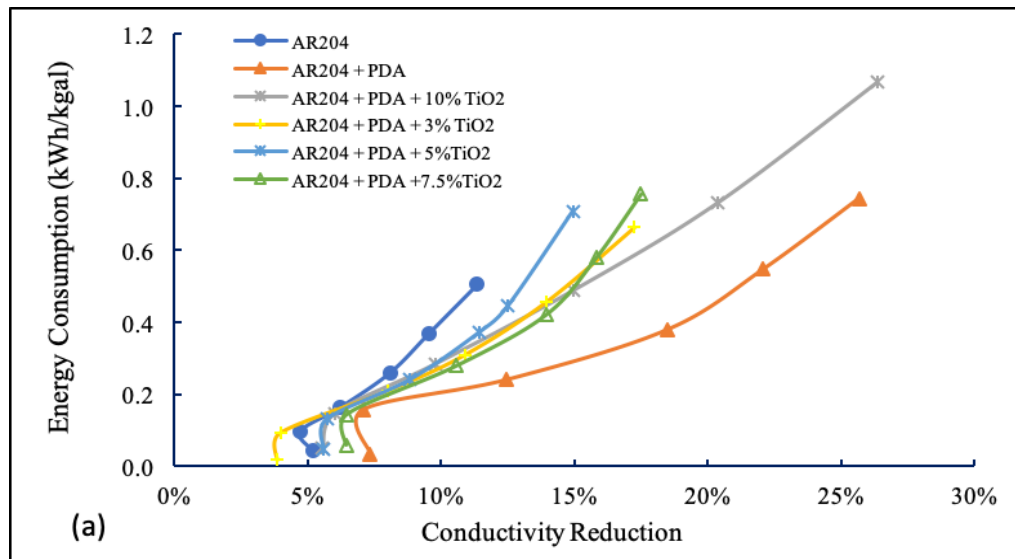
3.1.5.3. Energy Consumption

The energy consumption of the normal grade AR204 and modified membranes was evaluated as kWh/kgal, and as kg/m²/kWh (kg of salt removed per membrane area m² per kWh). The AR204 modified with PDA showed the least energy consumption to

Antifouling Ion-Exchange Membranes

reach a specific conductivity removal. The comparison in energy consumption is analogous to overall salt removal efficiency aforementioned (Figure 16). The normal grade membranes exhibited the highest energy consumption compared to all of the modified AEMs to achieve a specific conductivity removal, and this reflects or matches its higher resistance as measured by the EIS.

The energy consumption in terms of kg salt removed/m²/kWh decreased as current density increased and remained nearly constant beyond 3 mA/cm², signifying that as the current density exceeds the threshold value of 3 mA/cm², the energy efficiency declined and most of the applied energy was wasted on water splitting (Figure 17). Unmodified AR204 demonstrated the lowest normalized salt removal in comparison with all modified membranes. It is analogous to the contact angle measurements, showing both pure water flux and hydrophilicity have the same trend for both PDA+TiO₂ and PDA+GO membranes.



Antifouling Ion-Exchange Membranes

Figure 16. Energy Consumption Comparison in kWh/ kgal Product Water. (a) Unmodified AR204, AR204 coated with PDA and AR204 coated with PDA + different dosage of TiO₂; (b) Unmodified AR204, AR204 coated with PDA and AR204 coated with PDA+different dosage of GO.

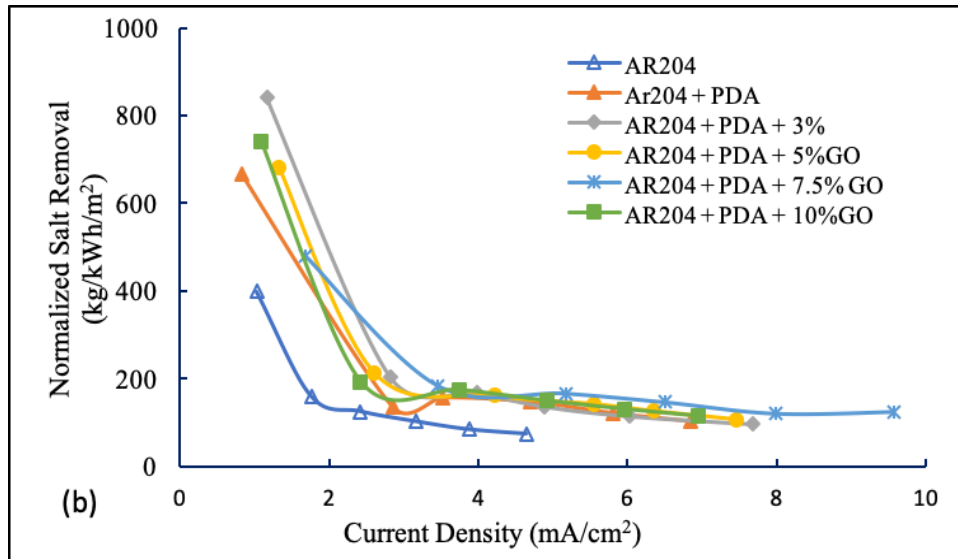
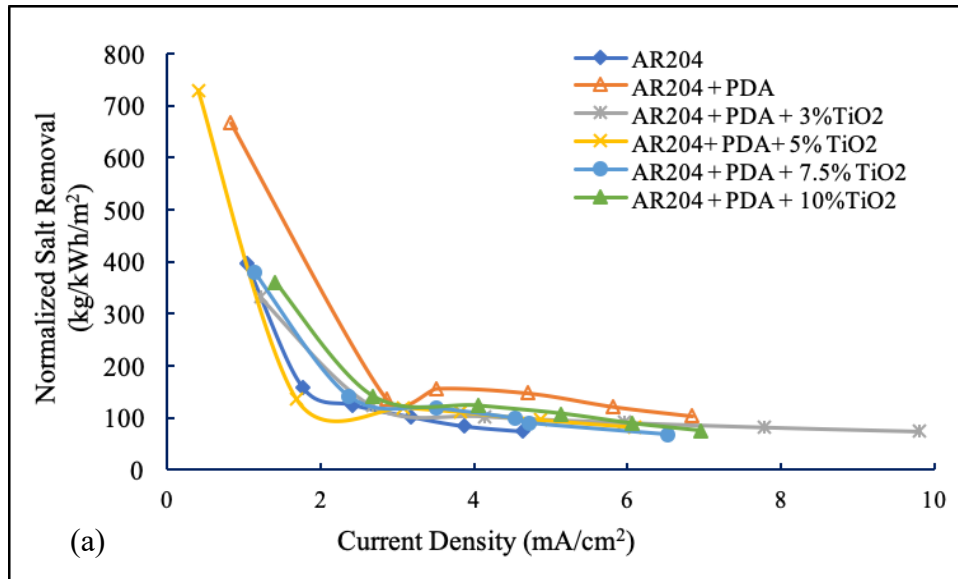


Figure 17. Normalized energy consumption. (a) Unmodified AR204, AR204 coated with PDA and AR204 coated with PDA + different dosage of TiO₂; (b) Unmodified AR204, AR204 coated with PDA and AR204 coated with PDA+different dosage of GO

3.2. Development of Antifouling CEMs

3.2.1. Ion Exchange Capacity

Ion exchange capacity (IEC) represents the number of counter-ions in equivalents exchanged in unit dry mass of membrane, and thereby quantitatively determines the rate of ion flux across the membrane. The results of IEC are exhibited in Table 3, showing that unmodified CEM and PEI coated CEM had very close IEC values at 2.04 ± 0.16 meq/g and 1.99 ± 0.02 meq/g, respectively. TiO₂ and GO coated membranes showed lower IEC values at 1.70 ± 0.20 and 1.62 ± 0.02 meq/g, respectively. This reduced IEC could be explained by increased membrane dry weight of coated nanoparticles and reduced accessibility of ion-exchange functional groups in the membrane matrix [82, 83].

Table 3. IEC Results of Selected Membranes

Membrane Type	Ion Exchange Capacity (meq/g)
Unmodified CR67	2.04 ± 0.16
PEI	1.99 ± 0.02
PEI + TiO ₂	1.70 ± 0.20
PEI + GO	1.62 ± 0.02

3.2.2. Hydrophilicity

Contact angle quantifies membrane hydrophilicity based on the different surface energy of different membrane coatings and fouling conditions [64, 84]. The results from captive bubble measurement are presented in Figure 18, which shows the comparison of contact angles before and after the biofouling experiments. Contact angle increased from $35.75^\circ \pm 3.9^\circ$ to $40.02^\circ \pm 5.04^\circ$ after coating the CEMs with PEI, due to the hydrophobic nature of the branched PEI used [27]. Contact angles of PEI coated membranes increased slightly from $40.02^\circ \pm 5.04^\circ$ to $40.16^\circ \pm 3.41^\circ$ after the biofouling experiment. Fouled PEI coated membranes showed lower contact angles and lower contact angle increase than unmodified membranes, as the branched PEI used in this study has high toxic impacts on bacteria cells that inactivated *E. Coli* and reduced biofouling on the CEMs [85]. Decreasing contact angle trends can be found with increased dose of TiO₂ for both unfouled and fouled membranes, indicating the hydrophilicity increased with higher dosage of TiO₂. The unfouled and fouled membranes both showed lowest contact angles with 7.5 wt% TiO₂ at $29.92^\circ \pm 2.42^\circ$ and $32.98^\circ \pm 1.74^\circ$, respectively, which was determined to be the optimum TiO₂ dose for subsequent experiments. Contact angles of 10 wt% TiO₂ coated membranes are higher than that of 7.5 wt%, because a high TiO₂ dose forms big clusters by

Antifouling Ion-Exchange Membranes

self-assembly on the membrane surface. The uneven surface captures more microbes and thus leads to more fouling [86].

Contact angles of GO coated membranes showed similar trends as TiO₂ coated membranes. Graphene oxide is a strong hydrophilic nanosheet material that can impede biofouling as its functional groups would ensure a large negative zeta potential [87]. The nanosheet GO also contributes to lower roughness of the membrane surfaces [24]. Unfouled GO coated CEMs demonstrated smaller contact angles than TiO₂ coated CEMs in all conditions. The contact angle of fouled membranes had a sharp decrease or “breakthrough”, from 35.93°±2.88° to 30.26°±1.55° when the GO dose increased from 5 wt% to 7.5 wt%, which accordingly was determined as the optimum dose of GO.

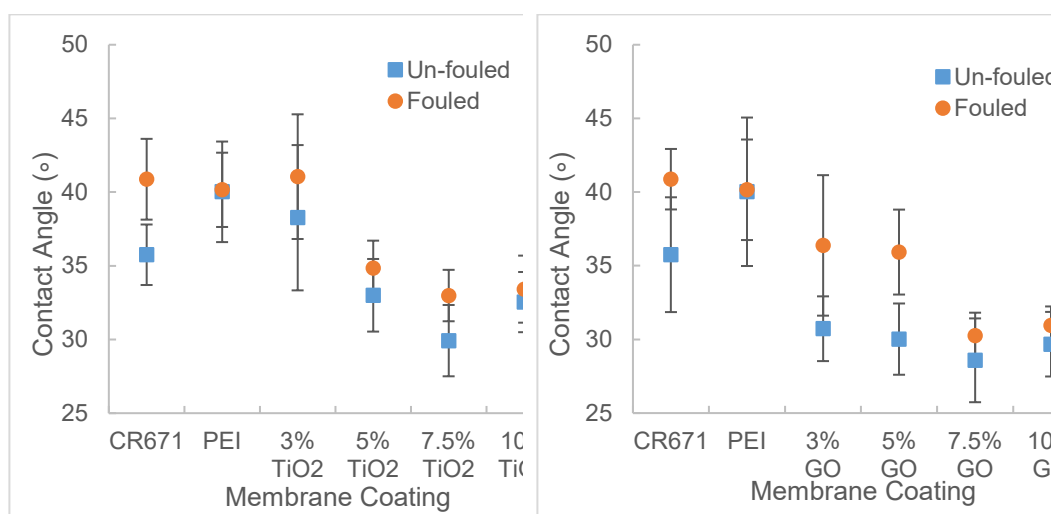


Figure 18. Contact angles of fresh and *E. coli* fouled. (a) TiO₂ modified CEMs and (b) GO modified CEMs

3.2.3. Membrane Resistance Measurements

The obtained EIS impedance was fitted to the Maxwell-Wagner model using Gamry Echem Analyst (version 6.23), which reduces the fitting error between modeling results and measured data [88]. By coating a layer of PEI, the unfouled membrane resistances increased from 9.87 Ω to 14.4 Ω, while fouled membrane resistances were 19.75 Ω and 23.05 Ω, respectively. The resistance increases of unmodified and PEI coated membranes were 9.88 Ω and 8.65 Ω, respectively, indicating the antifouling properties of PEI reduced the generation of biofilm. Unfouled and fouled membrane resistance of TiO₂ and GO coated membranes are shown in Tables 4 and 5. There are no significant differences among unfouled membrane resistances, except for a slight increase of 10 wt% TiO₂ coated membrane, which potentially is caused by the poor conductivity of TiO₂ nanoparticle.

Antifouling Ion-Exchange Membranes

Table 4. Membrane Resistance of Unfouled and Fouled TiO₂ Coated Membranes

Unit: Ω	3% TiO ₂	5% TiO ₂	7.5% TiO ₂	10% TiO ₂
Unfouled	14.29	14.88	14.32	15.63
Fouled	21.8	20.3	26.5	29.6
Increase (%)	52.6	36.4	85.1	89.4

Table 5. Membrane Resistance of Unfouled and Fouled GO Coated Membranes

Unit: Ω	3% GO	5% GO	7.5% GO	10% GO
Unfouled	14.22	14.16	14.05	13.87
Fouled	23.7	23.9	20.25	21.25
Increase (%)	66.7	68.8	44.1	53.2

3.2.4. Confocal Laser Scanning Microscope and COMSTAT Analysis

Biomass coverage, or biofilm, on membrane surfaces was used as direct evidence of membrane biofouling. The biofilm consists of two types of constituents: 1) microbial cells, which in this study are *E. coli* cells; and 2) extracellular polymeric substances (EPS) generated during microorganism growth [89]. EPS are mostly composed of polysaccharides and proteins. The formation of EPS creates a matrix for bacterial settlement, promotes more cell attachment, and may secrete into its growth medium [90-92]. The attachment of *E. coli* cells and coverage of EPS were examined by staining fouled membrane samples with different fluorescent dyes and calculating the volume of fluorescence spots per membrane area. The results of CLSM and COMSTAT 2 of cell and EPS biomass coverage on membrane surfaces are shown in Figures 19 and 20.

Cell attachment on unmodified membranes and PEI coated membranes was very similar at 0.0186 and 0.0180 $\mu\text{m}^3/\mu\text{m}^2$. EPS coverage on the two membranes, however, differs significantly, with 0.032 $\mu\text{m}^3/\mu\text{m}^2$ for unmodified membrane and 0.011 $\mu\text{m}^3/\mu\text{m}^2$ for PEI coated membrane. Resulting from its slightly hydrophobicity and thus increased contact angle of PEI coated membrane discussed aforementioned, cell attachment is more likely to happen as *E. coli* cells are also hydrophobic. However, the negative charge of PEI provides a repulsive force to *E. coli* cells that are also negatively charged. The result of these contradictory properties of PEI coated membranes is cell attachment that is similar to that of unmodified membranes. The significant difference in EPS coverage, however, is a result of PEI's toxicity against microbes. Branched PEI used in this study has greater cytotoxicity because of greater internalization into cells. The physicochemical properties of amine groups of PEI indicate the capacity for DNA condensation and the formation of polyplexes, thus reducing the fluorescence from dyed DNA [85]. While similar amounts of *E. coli* cells

Antifouling Ion-Exchange Membranes

attached on membrane surfaces, most of the cells on PEI coated membranes were inactivated by the PEI, and thus less EPS was generated during microbial growth.

Three and five percent TiO₂ coated membranes showed similar cell coverages ($0.0093 \mu\text{m}^3/\mu\text{m}^2$ and $0.0085 \mu\text{m}^3/\mu\text{m}^2$, respectively) that were approximately 50% lower than PEI only coated membranes ($0.018 \mu\text{m}^3/\mu\text{m}^2$). This improvement is achieved by the anti-microbial properties of TiO₂ [22]. Moreover, TiO₂ nanoparticles mitigates cell attachment by increasing the hydrophilicity on membrane surfaces [93]. Researchers have also implied that TiO₂ itself, without ultraviolet (UV) light, causes minute photocatalysis on *E. coli*, which also increases the membrane's anti-biofouling properties [22]. TiO₂ dosage of 7.5 wt% showed the lowest cell attachment and EPS coverage, as well as the lowest standard deviation, which indicates a more even coating of TiO₂ nanoparticles. At 10 wt% TiO₂ dosage, however, the cell attachment approximately doubled over that of 7.5 wt% TiO₂ dosage, and EPS coverage increased nearly four times. This inverse trend is very likely caused by the aggregation of TiO₂ nanoparticles on the membrane surface due to high dosage. Uncovered membrane surface led to an unprotected membrane surface and an uneven coating layer led to higher surface roughness, both of which promote cellular attachment and EPS coverage [86]. Thus, the optimal dosage of TiO₂ coating is determined to be 7.5 wt%, the same as given by the contact angle measurement.

GO is considered a promising material for surface modification of membranes regarding its physical and chemical properties [54]. The cell attachment trend of GO coated membrane is very similar to the trend of bio-fouled GO coated membrane contact angles; 3 wt% and 5 wt% dosage of GO reduced cell attachment by approximately 30 wt% more than PEI coated membranes, while breakthrough occurred at 7.5 wt% GO dosage. Cell attachment on 7.5 wt% GO coated membrane is $0.000774 \mu\text{m}^3/\mu\text{m}^2$, reduced by almost 96% compared with unmodified membranes. The antifouling properties of GO, such as its high hydrophilicity and negative charge density, mitigates cell attachment [54, 94]. At GO dosage of 10 wt%, cell attachment and EPS coverage increased compared with 7.5 wt% GO dosage, but it was still much lower than for other coating conditions. Thus, the optimal GO dosage was determined to be 7.5 wt%.

Antifouling Ion-Exchange Membranes

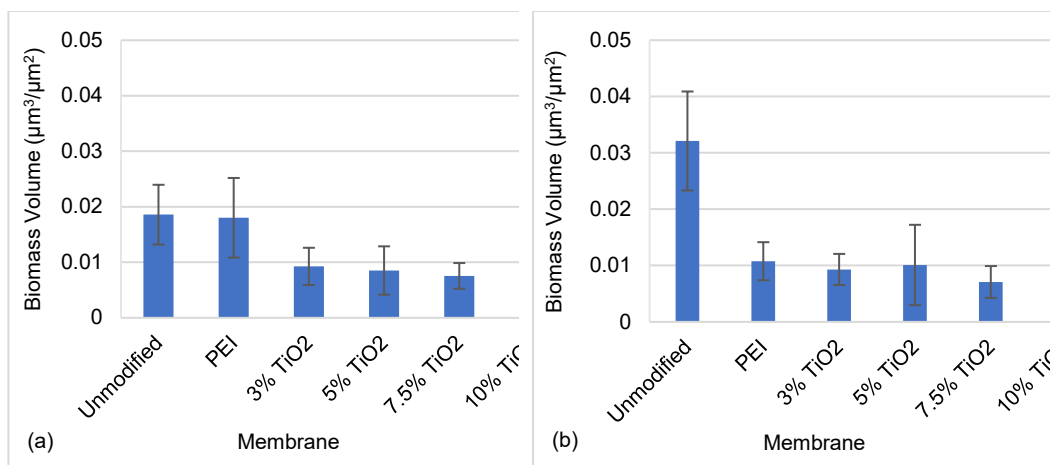


Figure 19. Biomass coverage comparison of TiO₂ coated membranes. (a) *E. coli* cells, (b) EPS.

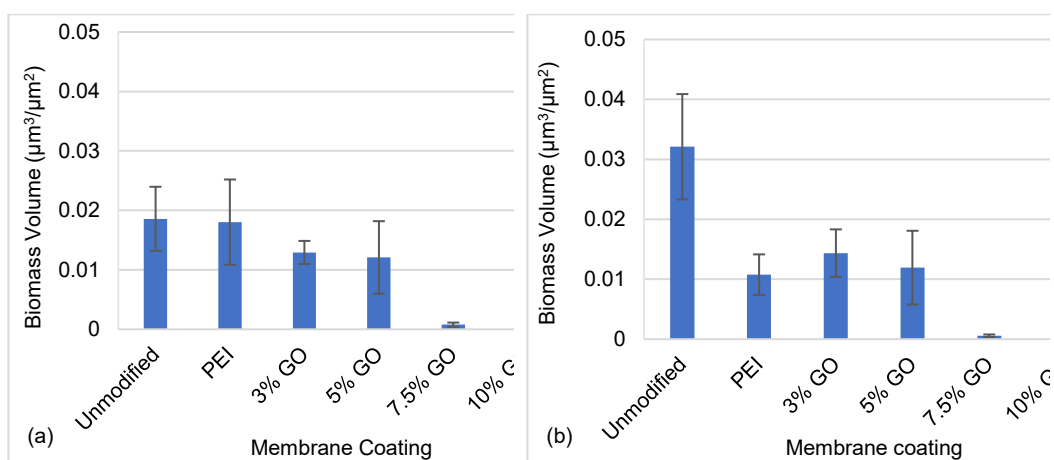


Figure 20. Biomass coverage comparison of GO coated membranes. (a) *E. coli* cells, (b) EPS.

3.2.5. Overall Desalination Efficiency

Overall desalination performance and energy consumption were studied for unmodified membranes, PEI coated membranes, and TiO₂/GO coated membranes at the optimal dosage determined by contact angle tests and anti-biofouling experiments. The experiments were conducted at 2 mA/cm² current density to ensure all experiments are below limiting current density.

All membranes reached stable conductivity removal through a 48-hour duration experiment, as shown in Figure 21. PEI and GO coated membranes showed similar conductivity removal at approximately 9% to 9.5%, while unmodified membranes and TiO₂ coated membranes showed lower conductivity removal at 6%. This difference of conductivity removal is considered minor, but

Antifouling Ion-Exchange Membranes

one possible reason for it would be the formation of a bipolar membrane as the positively charged PEI layer combined with the negatively charged CEM [95].

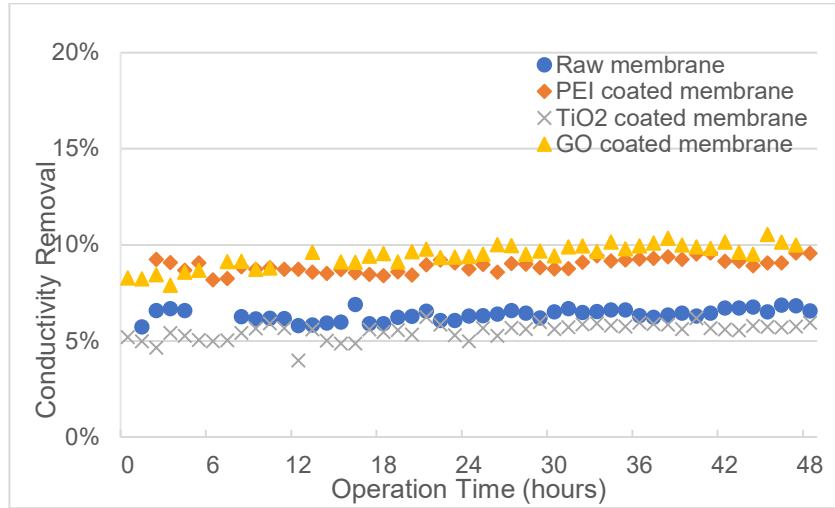


Figure 21. Conductivity removal comparison among different membrane coatings.

Energy consumption comparisons among different membranes is shown in Figure 22. Unmodified membranes showed the lowest energy consumption in kilowatts per thousand gallons of product water, while all other coated membranes had higher energy consumption due to the coated layer of PEI, which is a poor electric conductor. TiO₂ coated membranes showed the highest energy consumption, indicating the highest electric resistance of the modified membranes given by the poor conductivity of TiO₂ nanoparticles [96]. GO, as a good electric conductor, reduced the overall electric resistance of the coating layer, and thus reduced the energy consumption [97].

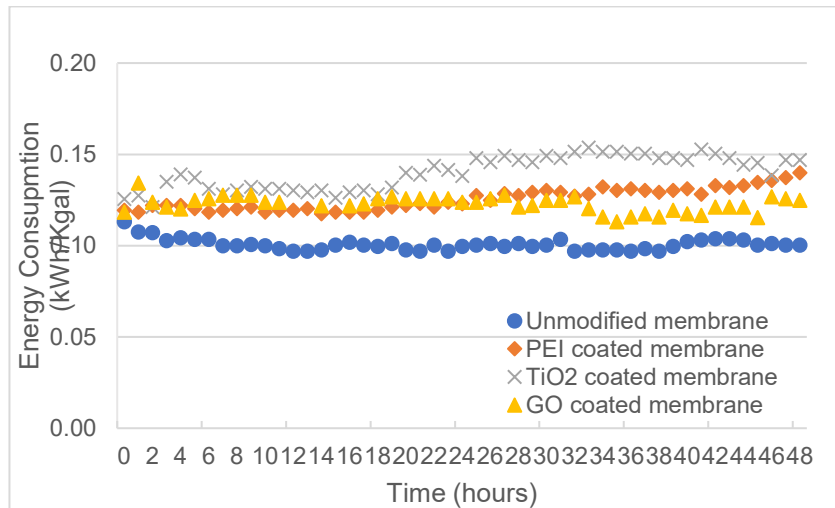


Figure 22. Energy consumption comparison among different membrane coatings.

Antifouling Ion-Exchange Membranes

Normalized salt removal allows the comparison of membrane performance under different operating conditions; thus, the only variable is different membrane coatings. As shown in Figure 23, unmodified membranes and PEI coated membranes reached very similar normalized salt removal at approximately 550 kg/kWh·m² after 20-hour operation to reach equilibrium. GO coated membrane showed the highest normalized removal at approximately 620 kg/kWh·m², 45% higher than unmodified/PEI coated membranes, because of its low electric resistance and good conductivity removal. As coated on CEMs with negatively charged functional groups on membrane surfaces, GO promotes the transport of cations by increasing the attraction force due to its negative surface charges [98, 99]. Membranes coated with TiO₂ showed the lowest normalized salt removal at approximately 300 kg/kWh·m², 30% lower than that of unmodified membranes. The pH values of the diluate stream of all energy consumption experiments were equal or below 6, at which TiO₂ was reported to have positive surface charges, resulting in a stronger positively charged coating layer with PEI [100-103]. This stronger positive charge provides a higher repulsion force to cations, making it more difficult for them to transport through CEMs, thus resulting in low energy efficiency.

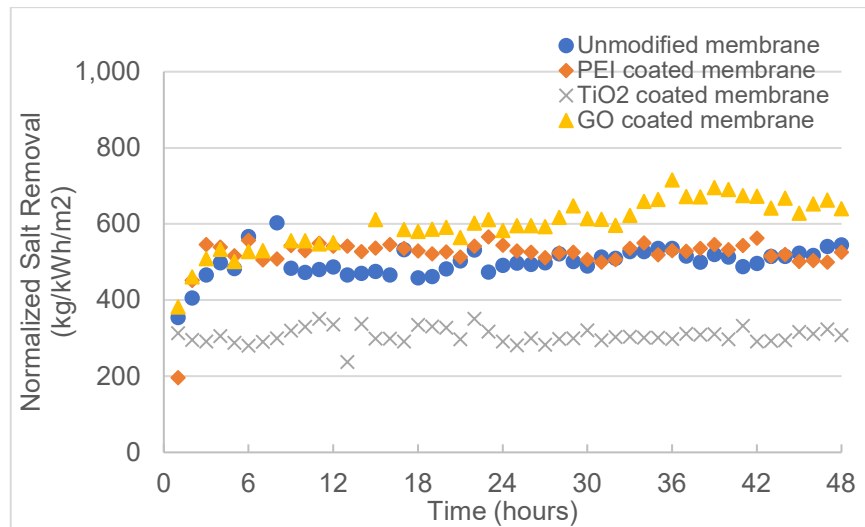


Figure 23. Normalized salt removal comparison among different membrane coatings.

3.3. Investigation of Organic-Induced Fouling Using Modified and Unmodified Membranes

Natural organic matter with large molecular weight fouls IEMs by accumulation, adsorption, and precipitation on membrane surfaces, and also considerably increases the electric resistance of IEMs due to the slow ion transport rate in the fouling layer [18, 104]. The fouling layer also increases the

Antifouling Ion-Exchange Membranes

pressure in ED chambers by blocking flow channels, thereby increasing energy consumption to pump water through ED stacks. The fouling layer, which is rich in organic matter, provides nutrients for microbial growth and leads to consequent biofouling [18]. Among the variety of organic matter, humic acid (HA) and bovine serum albumin (BSA) are two model foulants, used because of their wide occurrence in natural and effluent water systems, and also because of their relatively high chemical stability.

Many efforts have been made to investigate membrane organic fouling and fouling control, especially for anion exchange membranes (AEMs), as AEMs are positively charged and easily attract negatively charged organic matters [10, 29, 54, 105, 106]. In contrast, only a few studies have focused on organic fouling of cation exchange membranes (CEMs). Organic matter transport and deposition onto CEM surfaces, under electric potential during the ED process, shows the potential of forming fouling layers. Moreover, little attention has been paid to the fouling potential change that occurs after membrane modification. Studies have shown the strong binding effect of PEI and HA under a wide range of pH, which may negatively affect the antifouling properties of the modified membranes [107]. The interaction between PEI and BSA was also studied to understand the mechanisms of reaction and adsorption [37, 108]. GO has been widely adopted in the biomedical field and was reported to have an influence on BSA diffusion and conformational dynamics [109, 110]. Many researchers have focused on modifying membranes with hydrophilic GO nanosheets to increase HA rejection and antifouling potential against HA [111, 112]. Anti-organic fouling mechanisms and properties of TiO₂ were also extensively discussed in many studies [109, 113-115]. Two synthetic organic foulants, humic acid (HA, technical grade, Sigma Aldrich) and bovine serum albumin (BSA, lyophilized powder, ≥ 96%, Sigma Aldrich), were chosen as representatives of natural organic matter. Humic acid is the major component of humic substances, which are the major organic components of soil, peat, and coal [116]. BSA is a monomeric protein derived from cows and is widely used for its stability and moderately non-reactive properties. Each of the foulants were added separately at 10 mg/L of equivalent total organic carbon (TOC) in the feed solution, adjusted to neutral pH.

Fluorescence excitation emission spectrum was employed to analyze quantitatively organic fouling on membrane surfaces. Scanning electron microscopy was adopted to visualize the fouled membrane surfaces. Desalination performance of membranes was evaluated by normalized salt removal of bench-scale ED testing.

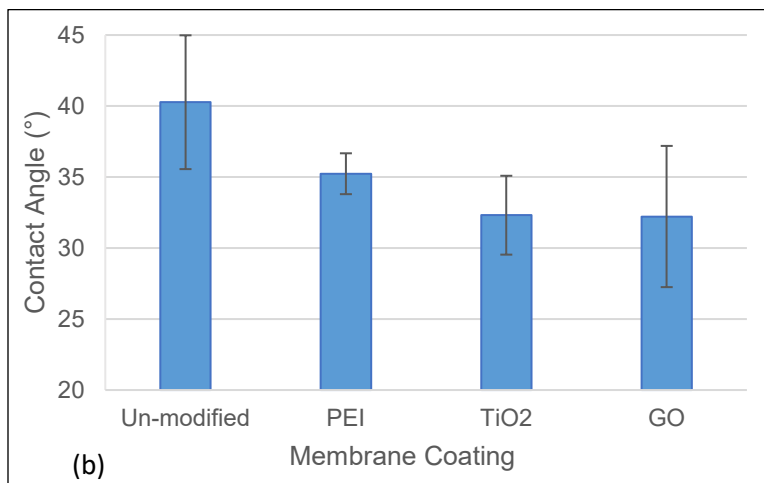
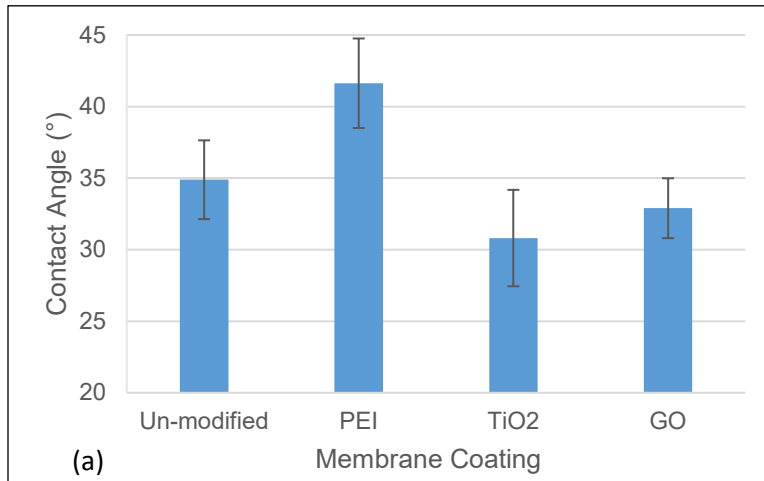
3.3.1. Hydrophilicity

Membrane hydrophilicity was evaluated through contact angle measurements, as shown in Figure 24. PEI coated membranes in the control set had approximately 6° higher contact angle than unmodified membranes, due to the hydrophobic property of PEI [27]. TiO₂ and GO coated membranes showed

Antifouling Ion-Exchange Membranes

lower contact angles, or higher hydrophilicity, than unmodified membranes, as also demonstrated in the previous Biofouling section. The main contribution of this increased hydrophilicity comes from the hydrophilic nature of TiO₂ and GO nanoparticles [42, 87].

With HA added to the feed solution as organic foulant, the contact angle of unmodified membranes increased from 34.89 ± 2.75 in the control experiment to 40.27 ± 4.71 , indicating the formation of HA organic fouling on membrane surface [117]. The contact angles of TiO₂ and GO coated membranes remained similar to the control set, but with higher standard deviation caused by uneven fouling layers. Compared with unmodified membranes, the TiO₂ and GO membranes showed a 9° lower contact angle, indicating the improved antifouling potential against HA. The contact angles of BSA fouled membranes are very similar to each other and to the control experiment, except for the PEI coated membranes that have lower contact angles. TiO₂ and GO coated membranes showed slightly increased contact angles.



Antifouling Ion-Exchange Membranes

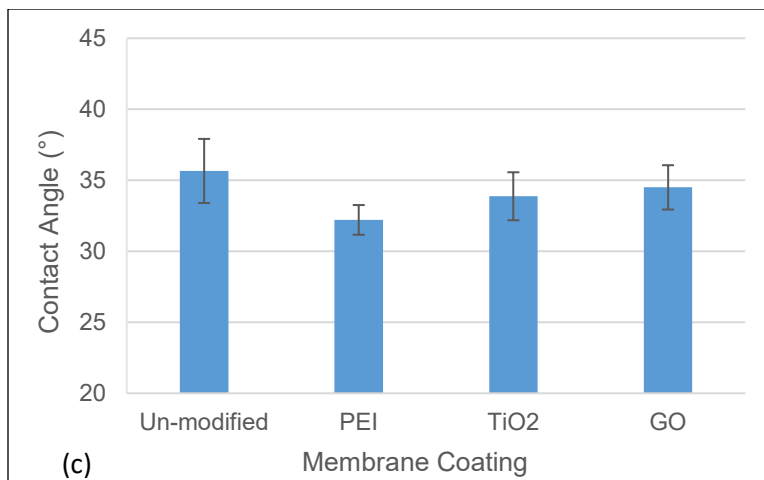
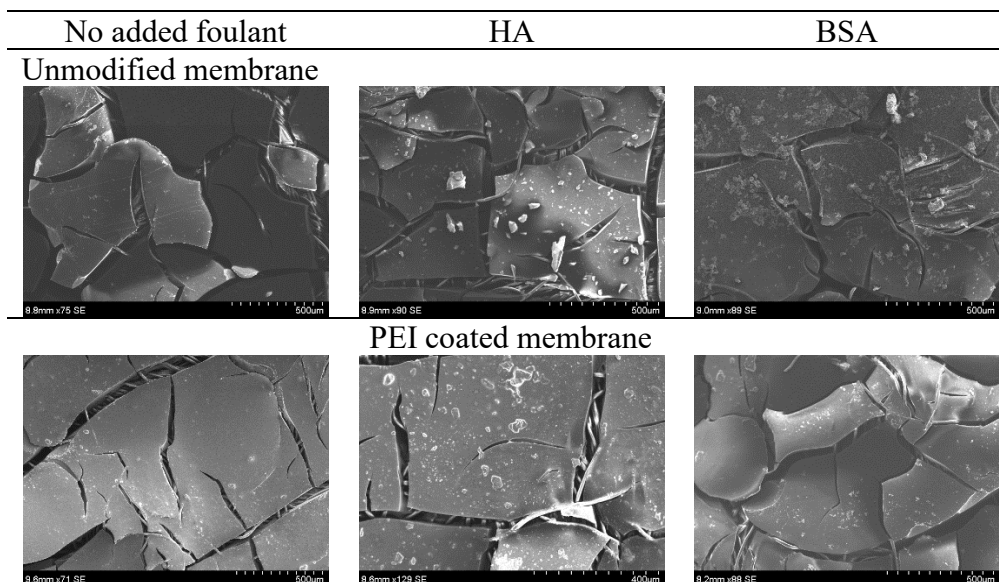


Figure 24. Comparison of contact angles among different membrane coatings fouled by (a) control set, (b) HA, and (c) BSA.

3.3.2. Membrane Imaging

Scanning electron microscopy (SEM) was performed to visualize the membrane surfaces and foulants. As dry samples were required, all membranes were air-dried prior to SEM analysis. Cracks occurred on membrane surfaces due to dryness of IEMs. Clustered HA fouling was observed on unmodified CEM, while more even and spread HA fouling was observed on modified membranes, especially on PEI coated CEM surfaces (Figure 25). This agrees with the FEEM analysis, as HA binds with amino groups on the PEI coating layers and forms an even fouling layer. BSA fouling was found often on unmodified CEM, while PEI and TiO₂ coated membranes were much cleaner. Clustered BSA fouling was observed on GO coated membrane.



Antifouling Ion-Exchange Membranes

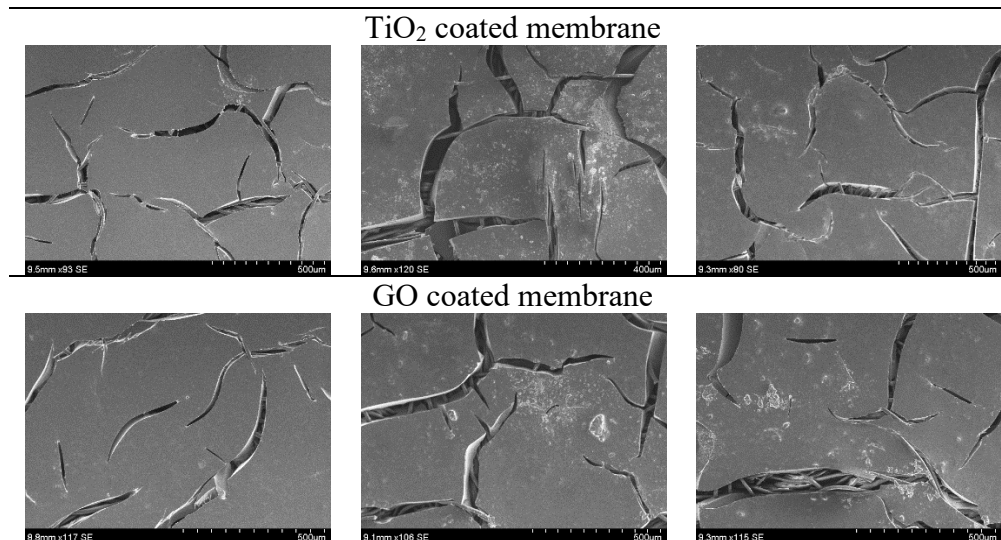


Figure 25. SEM Images of Organic Fouled Cation Exchange Membranes.

3.3.3. FEEM

The zoning boundaries for this study are based on the actual FEEM plot peak locations of the foulant chemicals used. Foulant chemicals were analyzed using the same TOC concentration as added to the experiment feed water at 100 mg/L equivalent TOC. Figure 26 illustrates the measured FEEM peak locations of BSA and HA. Based on literature reports on dominant FEEM peak locations and the actual measurement results, the FRI zoning boundary is defined as: Zones I and II correspond to aromatic proteins, such as tryptophan and tyrosine, including BSA in this case; Zone III corresponds to humic acid-like compounds; and Zone IV corresponds to soluble microbial-like proteins [75, 118, 119]. Visualized FRI boundaries are shown in Figure 27. FEEM plots of all membrane extraction solutions showed peaks in Zone IV, which corresponds to the organic matter leached from membranes. Figure 28 shows the FEEM result of PEI solution at 500 mg/L, adjusted to neutral pH. No obvious peaks were observed that overlap the peaks in the FRI zoning method. Furthermore, the possible existence of PEI in the extracted solutions would come from the leaching of coated membranes under ultrasonication, which is considered very minor compared with other organic matter.

Antifouling Ion-Exchange Membranes

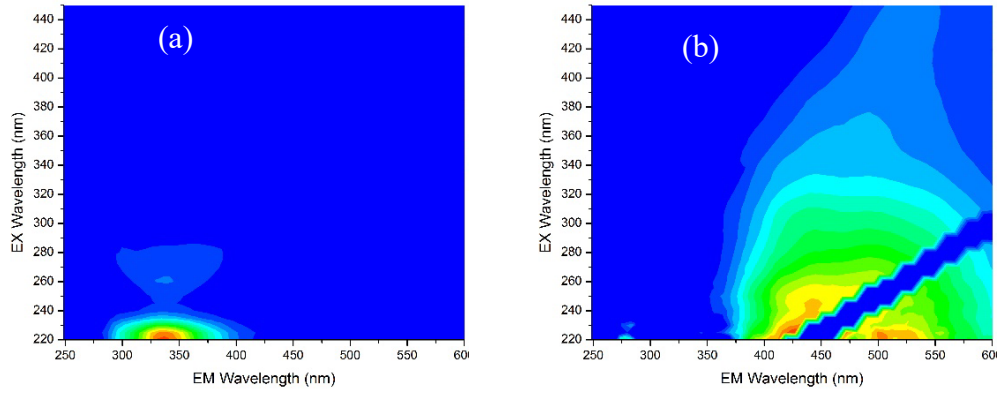


Figure 26. FEEM plot of (a) BSA solution and (b) HA solution at 100 mg/L equivalent TOC

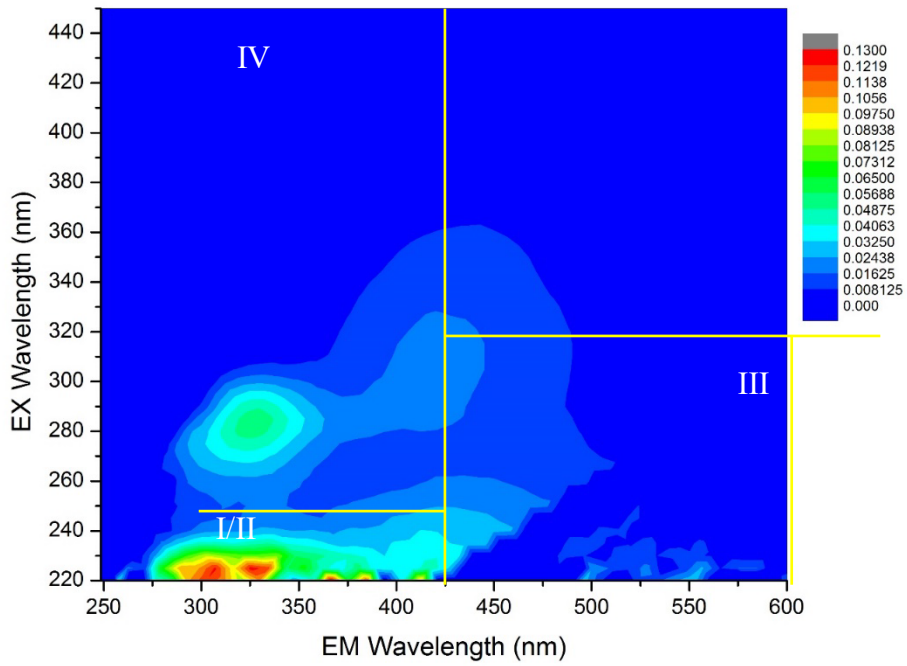


Figure 27. Illustration of FRI Zoning for a FEEM Contour Plot

Antifouling Ion-Exchange Membranes

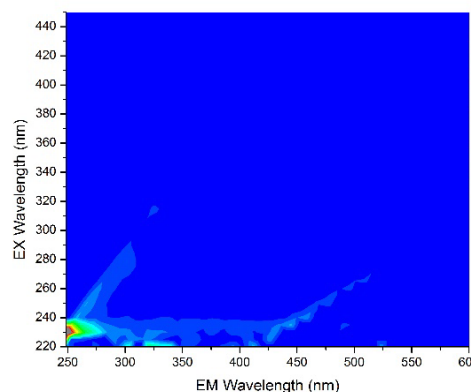


Figure 28. FEEM Plot of 500 mg/L PEI Solution

The FEEM spectra provides a qualitative assessment of organic matter adhesion on membrane surfaces, as shown in Figure 29. Higher peak values and greater base areas can be found in Zone III in Figure 29 middle column, of which HA was added in feed solutions as the foulant. The peak locations and shapes in these graphs accurately overlap with the HA peak measured in Figure 26. PEI coated CEM showed a significantly higher peak values with greater base areas, while TiO₂ coated CEM showed lower peaks compared with unmodified membranes. There are no obvious differences of BSA peaks and base areas when comparing blank sets with BSA fouled membranes. One reason could be the overlapping of BSA peaks with the organic matter leached from membrane resin. PEI and TiO₂ coated membranes showed lower peak values of BSA concentration, while GO-coated membranes showed slightly higher values.

The organic matter composition was further evaluated by comparing the FRI volumes in each zone, as shown in Figure 30. All FRI volumes were normalized to 100 mg/L TOC of extracted solution. HA extracted from unmodified CEM was 11.53 AU-nm²/ [100 mg/L TOC], while PEI coated CEM had a much higher HA attachment of 34.73 AU-nm²/ [100 mg/L TOC]. The presence of amine groups in the PEI layer provided strong mechanical strength between HA and the modified membrane surfaces, thereby increasing the HA attachment on the membrane surfaces. Humic acids were reported to undergo covalent binding with amine groups through nucleophilic addition reactions of quinone groups and carbonyl groups with amine groups [107, 120, 121]. This bonding was affected by the electrostatic interaction, while the strength was highest at pH 5, and decreased with higher pH [107]. Providing the consistent diluate stream with pH at 6 in the fouling experiments, it explains the higher HA attachment of all modified membranes than to unmodified membranes. However, the nano-material added with PEI coatings reduced HA deposition on membrane surfaces by 64% and 27% of TiO₂ and GO, respectively, of which the TiO₂ coating achieved nearly the same HA attachment as the unmodified membranes, indicating that nanomaterial coatings mitigated the negative effect of the increased HA fouling potential of PEI, while at the same time it increased

Antifouling Ion-Exchange Membranes

membrane hydrophilicity; and the GO coating achieved even higher energy efficiency.

The amounts of HA and BSA deposition on membrane surfaces were similar in terms of FRI volumes. Unlike the antifouling potential against HA, all coated membranes showed higher resistance to BSA. PEI, TiO₂, and GO coatings reduced BSA attachment to the membrane surfaces by 73%, 45%, and 27% compared with the unmodified membranes, respectively. The higher BSA attachment of nanomaterial coated membranes was caused by their higher hydrophilicity. BSA was reported to be hydrophilic in its native state, with surface tension 70.0 erg/cm² [122, 123]. With hydrophobic surfaces, BSA interacts through its CH₃ groups, whereas with hydrophilic groups, polar-COOH groups play a more important role. This phenomena leads to higher BSA surface coverage and stronger adsorption and interaction between BSA and hydrophilic surfaces [124]. The higher BSA attachment on GO coated membranes than TiO₂ coated membranes also agrees with the more hydrophilic membrane surface of the GO coating.

The percent fluorescence responses of BSA had the same trend with FRI volumes for each membrane coatings, showing that the BSA deposition on the PEI-coated membrane surfaces was 14%, approximately 46% less than for other coatings. The percent fluorescence responses of HA, however, are similar for all membrane types at approximately 50% (Figure 31). Considering the significant high HA deposition on the PEI-coated membranes, this indicates that the total amount of organic matter deposition on PEI coated membranes is much higher than for other membranes, as both more hydrophobic surface and positively charged polymer layers promote organic membrane adhesion.

Moreover, PEI coated membranes showed 14.3% to 59.1% lower FRI volume in Zone IV than uncoated membranes under all fouling conditions, indicating that PEI inhibited the leaching of ion-exchange resin from the membrane structure, thereby increasing the chemical stability of ion-exchange membranes against strong base. No peaks of PEI were observed in all FEEM images, indicating extreme low PEI concentrations in extracted solutions from membranes, which further revealed the strong chemical stability of PEI against a strong base.

Antifouling Ion-Exchange Membranes

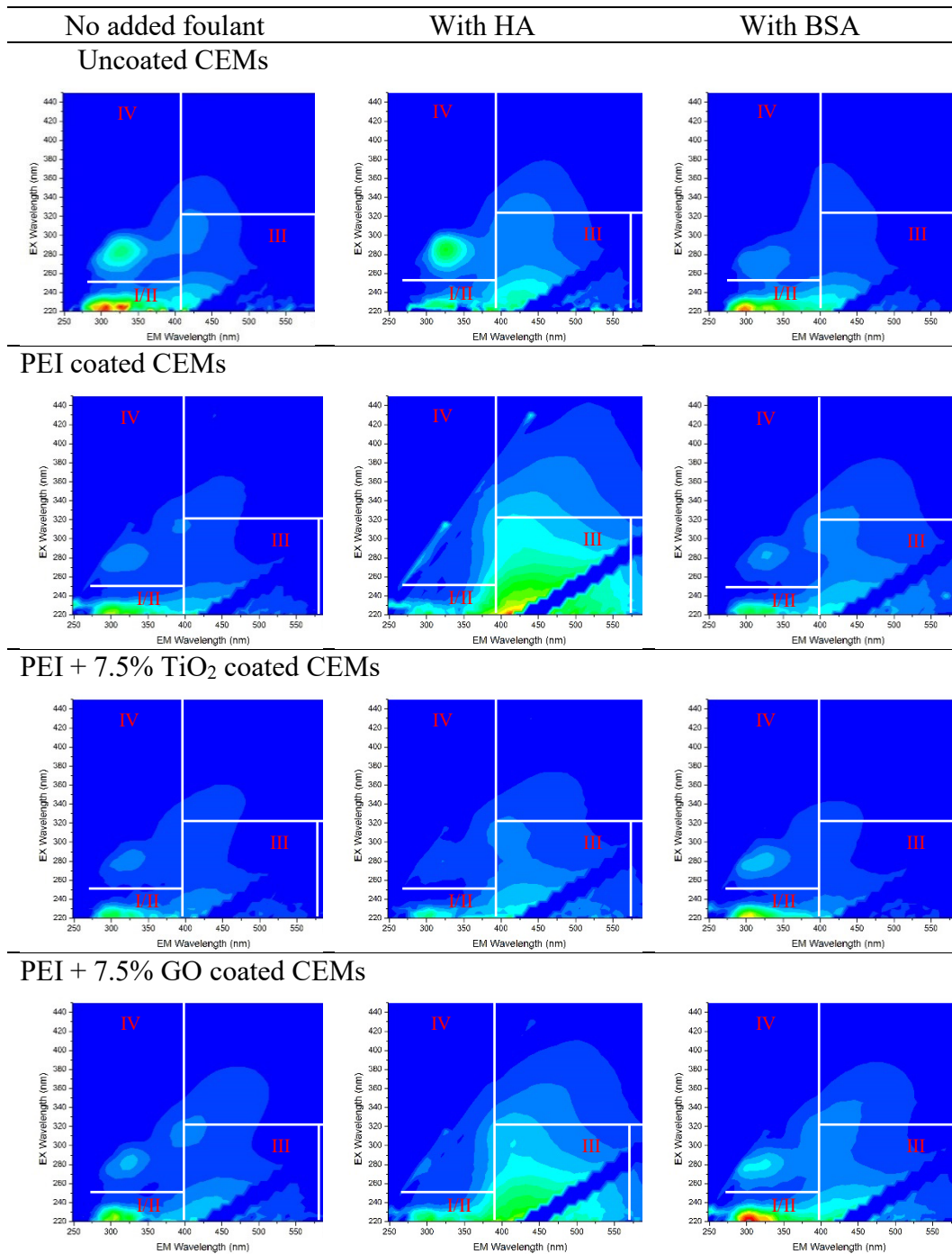


Figure 29. FEEM Results of CEMs with Different Coatings and Foulants

Antifouling Ion-Exchange Membranes

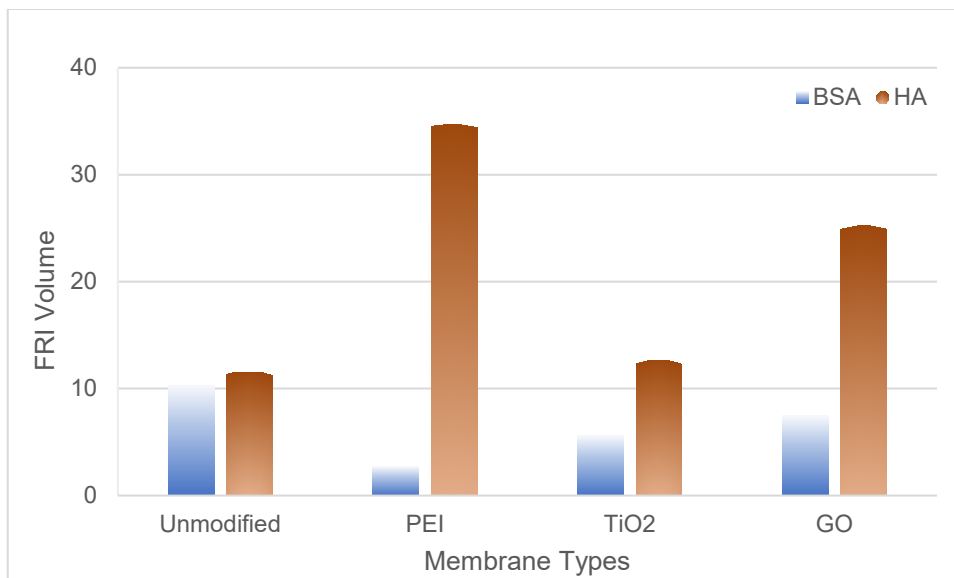


Figure 30. FRI Volume Comparison of HA and BSA Accumulation on Different Types of Cation Exchange Membranes.

(Note: unit of FRI volume is $AU - nm^2 / [100 \text{ mg/L TOC}]$).

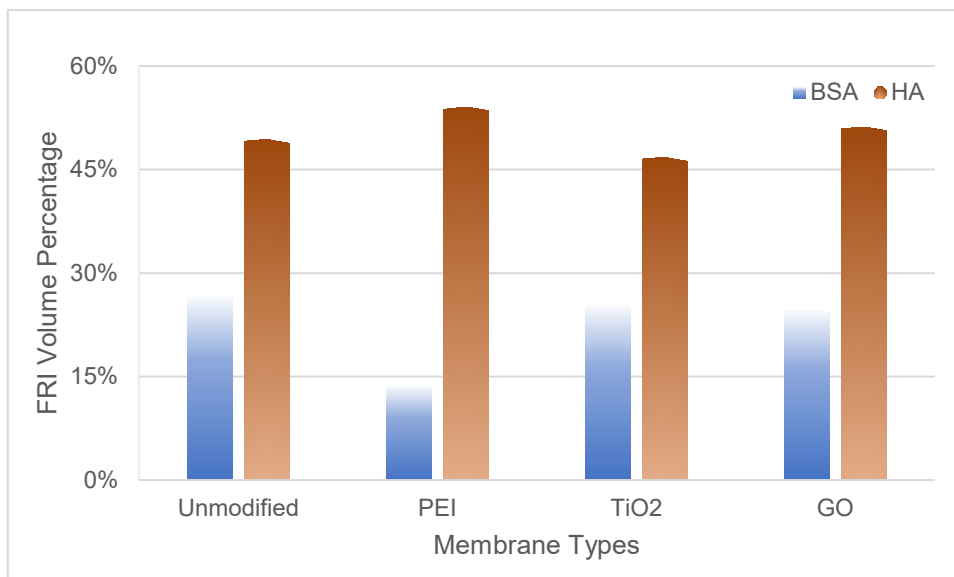


Figure 31. FRI Volume Percentage of BSA and HA for Different Types of Cation Exchange Membranes

3.3.4. Overall Desalination Performance and Energy Consumption

Overall desalination performance and energy consumption were compared among unmodified membranes, PEI coated membranes, and TiO₂/GO coated membranes at the optimal dosage determined by previous sections.

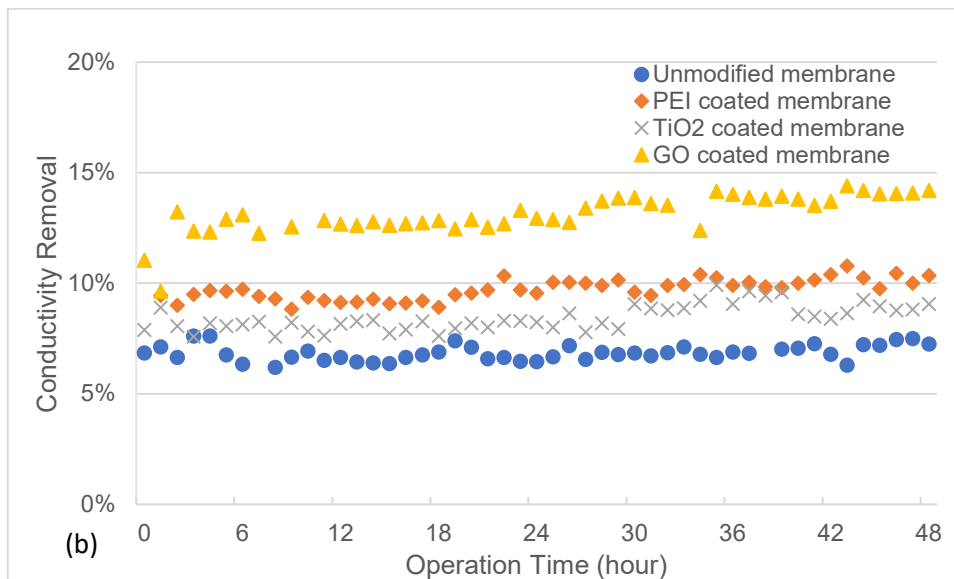
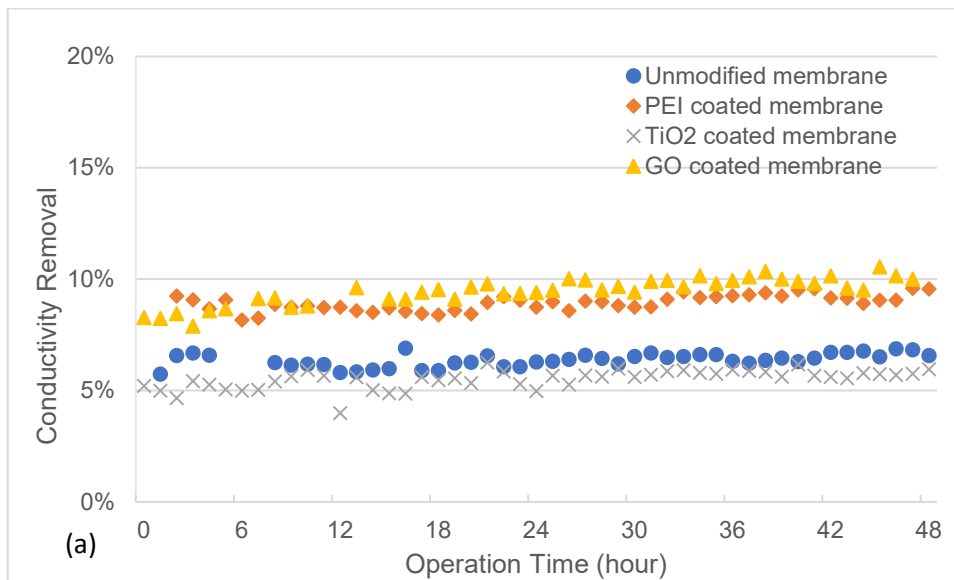
All membranes showed consistent conductivity removal through the 48-hour experiment, as shown in Figure 32. The difference of conductivity removal among different types of membranes in the control set is considered very small. Unmodified membrane and TiO₂ coated membranes had around 6% conductivity removal, while PEI and GO coated membranes showed 9% to 9.5% removal. With HA added as organic foulant, GO coated membranes showed higher conductivity removal at approximately 14% after three-hour equilibrium. Other membranes had similar conductivity removal compared with the control set. With BSA added as foulant, conductivity removal of unmodified membranes reduced to approximately 5%, while TiO₂ and GO coated membranes showed similar conductivity removal as the HA set. PEI coated membranes, however, exhibited a slight decrease from 8% to 3% conductivity removal after 15 hours of operation.

The results of normalized salt removal comparison are shown in Figure 33. Concentrations of feed, diluate, and concentrate were converted from real-time conductivity measurement by a conversion factor of 0.67. All membrane types showed stable normalized salt removal during the experiment without added foulant (control set). Unmodified membranes and PEI coated membranes showed similar normalized salt removal at approximately 520 kg/kWh/m². TiO₂ coated membranes showed relatively lower but consistent normalized salt removal at approximately 300 kg/kWh/m². GO coated membranes showed the highest normalized salt removal, with the average value close to 650 kg/kWh/m².

The normalized salt removal had the same trend with humic acid added in the feed solution. Unmodified membranes and PEI/PDA coated membranes maintained similar normalized salt removal compared with the control set and remained consistent during the experiment period. Normalized salt removal of TiO₂ coated membranes was consistent in the first 15 hours of the experiment, then reduced approximately 20% to 350 kg/kWh/m² after circulation for 40 hours. Considering the stable conductivity removal of TiO₂ coated membranes, the increased normalized salt removal is due to the increased energy consumption, which is potentially caused by organic fouling of humic acid on membrane surfaces. GO coated membranes revealed the same pattern as the control set, but with higher normalized salt removal, that increased from approximately 750 kg/kWh/m² to 850 kg/kWh/m² during the experiment. With negative charge, GO provides an attraction force to cations that promotes cation transport toward and through CEM. In addition, GO is a good electric conductor that reduces the overall electrical resistance of modified membrane, thus improved energy efficiency.

Antifouling Ion-Exchange Membranes

With BSA added in the feed solution, the normalized salt removal of unmodified membranes was reduced by 20%, to approximately 400 kg/kWh/m². PEI coated membranes started with similar normalized salt removal as the control set in the first 15 hours of circulation, then reduced by 80% to approximately 120 kg/kWh/m² and stabilized after 30 hours of circulation. This significant decrease of normalized salt removal is consistent with the trend of conductivity removal, potentially caused by organic fouling of BSA on the membrane surfaces. TiO₂ coated membranes showed similar normalized salt removal as the humic acid experiment at approximately 500 kg/kWh/m² in the first 37 hours, followed by a reduction to 400 kg/kWh/m². GO coated membranes started with similar normalized salt removal as the control experiment, and then increased from 600 kg/kWh/m² to 800 kg/kWh/m² after 25 hours of circulation.



Antifouling Ion-Exchange Membranes

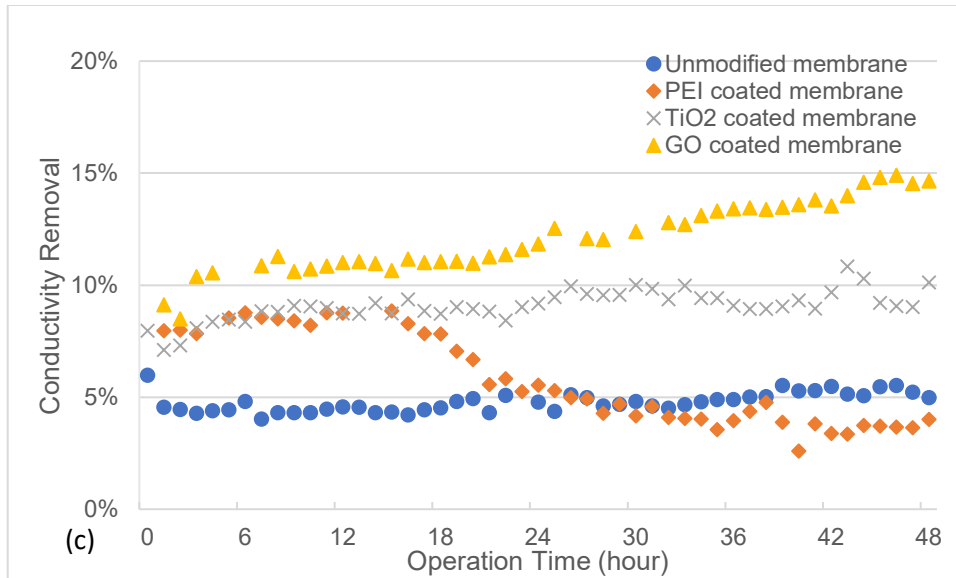
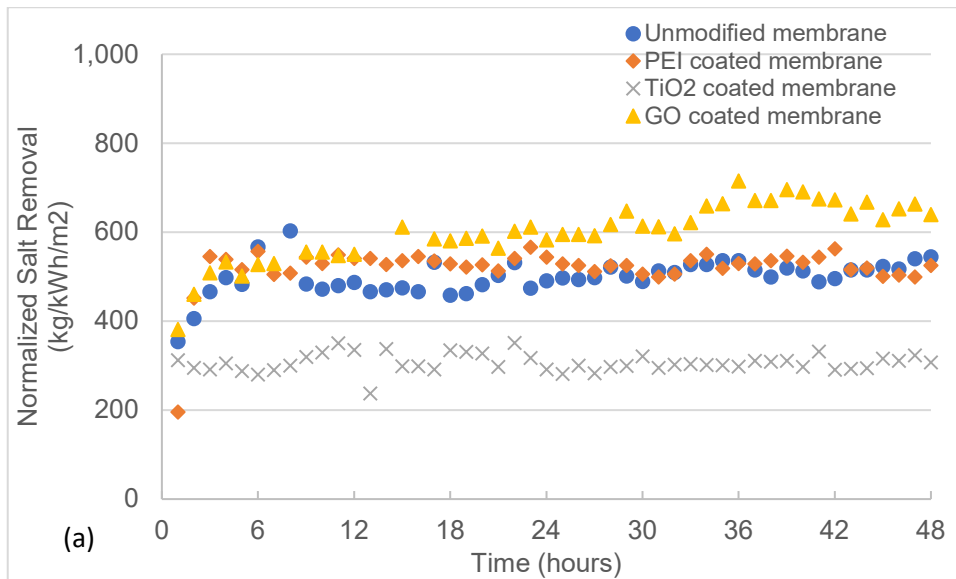


Figure 32. Conductivity removal comparison of different membranes. (a) control set; (b) with HA added; and (c) with BSA added.



Antifouling Ion-Exchange Membranes

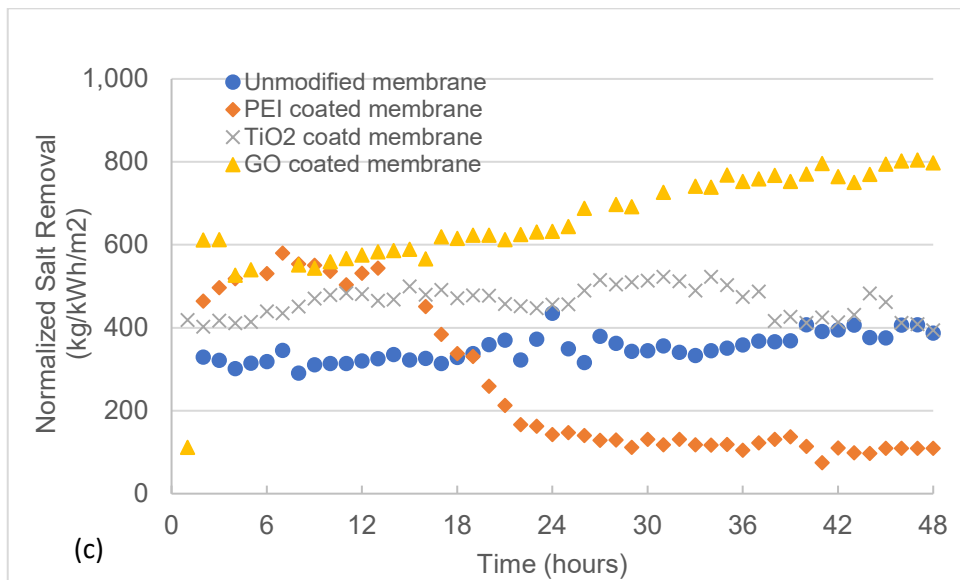
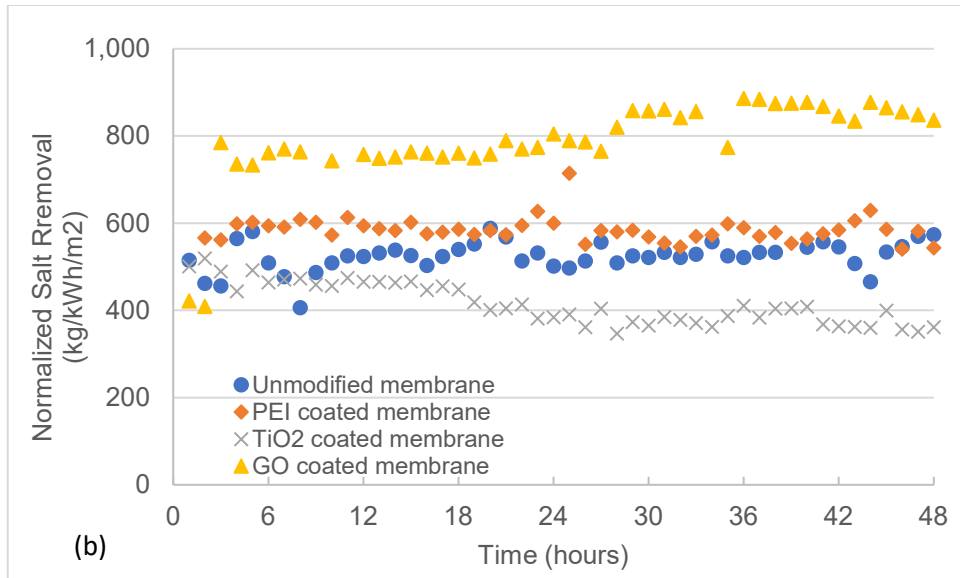


Figure 33. Normalized salt removal comparison between different membrane coatings with (a) no added foulant; (b) humic acid; and (c) BSA

4. Conclusions

The study aims to develop antifouling, anti-adhesive, permselective, and energy efficient ion-exchange membranes to improve electro dialysis performance, in order to contribute to expanding traditional water resources and the treatment of alternative waters.

For AEM, the study demonstrated that modifying AEMs with PDA+TiO₂ and GO significantly improved membranes biofouling resistance, while PDA+10 wt% TiO₂ and PDA+7.5 wt% GO exhibited higher tolerance against *E. coli* biofouling. PDA modified AR204 attained higher hydrophilicity, IEC, salt removal, and reduced energy consumption. At the same current density, AR204 coated with PDA showed higher overall desalting efficiency compared to the unmodified AR204, that is, for the same conductivity reduction, the coated membranes consumed less energy as compared to the pristine membranes. Coating a thin layer of PDA incorporated with GO or TiO₂ improved the Cl⁻ selectivity in terms of the relative transport number by selectively transporting Cl⁻ and hindering the transport of SO₄²⁻ ions. This is due to the electrostatic repulsive force exerted by the PDA coating and the improved sieving effect resulting from the compact cross-linked coating layer. PDA coating reduced the electrical resistance of the membranes as measured by the EIS analysis.

For CEM, membrane surface modification using PEI and nanoparticles TiO₂ and GO was conducted for cation exchange membrane CR67. The antifouling potential of membranes was evaluated by comparing biomass accumulation of cells and EPS, separately. The hydrophilicity of both unfouled and fouled membranes was measured through contact angle measurement. The optimal nanoparticle dosages were determined to be 7.5 wt% TiO₂ and 7.5 wt% GO. Cation exchange membranes modified under the optimal GO dosage exhibited high normalized salt removal efficiency. Minor changes in ion-exchange capacity and membrane resistance were found among different coating materials and dosages. Thus, the surface modification with PEI and nanoparticles was effective in improving membrane anti-biofouling properties. During anti-organic fouling experiments, GO coating increased the energy efficiency of ED under all experimental conditions, while TiO₂ coated CEM showed equal or slightly lower energy efficiency. Energy efficiency of PEI coated membranes was consistent even with relatively severe HA fouling but showed a significant decrease with BSA fouling. The antifouling potential against HA and BSA was quantitatively evaluated by foulant accumulation on the membrane surface through fluorescence spectroscopy. Visualization of the fouled membrane surface obtained by SEM further confirmed that 1) PEI coating attracted more HA on the membrane surface by the binding of functional groups; 2) polymer and nanomaterials inhibited BSA fouling by increasing the hydrophilicity of the membrane surface.

References

- [1] A.E. Ercin, A.Y. Hoekstra, Water footprint scenarios for 2050: A global analysis, *Environment International*, 64 (2014) 71-82.
- [2] A. Al-Karaghoul, L.L. Kazmerski, Energy consumption and water production cost of conventional and renewable-energy-powered desalination processes, *Renewable and Sustainable Energy Reviews*, 24 (2013) 343-356.
- [3] P. Xu, T.Y. Cath, A.P. Robertson, M. Reinhard, J.O. Leckie, J.E. Drewes, Critical review of desalination concentrate management, treatment and beneficial use, *Environmental Engineering Science*, 30 (2013) 502-514.
- [4] Y. Tanaka, R. Ehara, S. Itoi, T. Goto, Ion-exchange membrane electro-dialytic salt production using brine discharged from a reverse osmosis seawater desalination plant, *Journal of Membrane Science*, 222 (2003) 71-86.
- [5] E.R. Reahl, Half a century of desalination with electro-dialysis. Ionics Technical Report, Available at: General Electric Company (GE) <https://pdfs.semanticscholar.org/5391/c71537ced99f87e457413e9fb38776dc4abc.pdf>. (2006), Accessed date: March 20, 2019.
- [6] N. Kabay, M. Arda, I. Kurucaovali, E. Ersoz, H. Kahveci, M. Can, S. Dal, S. Kopuzlu, M. Haner, M. Demircioglu, Effect of feed characteristics on the separation performances of monovalent and divalent salts by electro-dialysis, *Desalination*, 158 (2003) 95-100.
- [7] P. Xu, M. Capito, T.Y. Cath, Selective removal of arsenic and monovalent ions from brackish water reverse osmosis concentrate, *Journal of Hazardous Materials*, 260 (2013) 885-891.
- [8] W. Foundation, R.S. Trussell, G.J. Williams, Reclaimed Water Desalination Technologies: A Full-scale Performance and Cost Comparison Between Electro-dialysis Reversal and Microfiltration, *Water Reuse Research*, 2012.
- [9] M. Turek, J. Was, P. Dydo, Brackish water desalination in RO–single pass EDR system, *Desalination and Water Treatment*, 7 (2009) 263-266.
- [10] M. Vasselbehagh, H. Karkhanechi, R. Takagi, H. Matsuyama, Surface modification of an anion exchange membrane to improve the selectivity for monovalent anions in electro-dialysis—experimental verification of theoretical predictions, *Journal of Membrane Science*, 490 (2015) 301-310.
- [11] L. Karimi, A. Ghassemi, H.Z. Sabzi, Quantitative studies of electro-dialysis performance, *Desalination*, 445 (2018) 159-169.
- [12] M. Galizia, F.M. Benedetti, D.R. Paul, B.D. Freeman, Monovalent and divalent ion sorption in a cation exchange membrane based on cross-linked poly (p-styrene sulfonate-co-divinylbenzene), *Journal of Membrane Science*, 535 (2017) 132-142.
- [13] G.M. Geise, C.L. Willis, C.M. Doherty, A.J. Hill, T.J. Bastow, J. Ford, K.I. Winey, B.D. Freeman, D.R. Paul, Characterization of aluminum-neutralized sulfonated styrenic pentablock copolymer films, *Industrial & Engineering Chemistry Research*, 52 (2013) 1056-1068.
- [14] J. Pan, J. Ding, R. Tan, G. Chen, Y. Zhao, C. Gao, B. Van der Bruggen, J. Shen, Preparation of a monovalent selective anion exchange membrane through

- constructing a covalently crosslinked interface by electro-deposition of polyethyleneimine, *Journal of Membrane Science*, 539 (2017) 263-272.
- [15] S. Anand, D. Singh, M. Avadhanula, S. Marka, Development and control of bacterial biofilms on dairy processing membranes, *Comprehensive Reviews in Food Science and Food Safety*, 13 (2014) 18-33.
- [16] L. Katebian, E. Gomez, L. Skillman, D. Li, G. Ho, S.C. Jiang, Inhibiting quorum sensing pathways to mitigate seawater desalination RO membrane biofouling, *Desalination*, 393 (2016) 135-143.
- [17] R. Komlenic, Rethinking the causes of membrane biofouling, *Filtration & Separation*, 47 (2010) 26-28.
- [18] P. Xu, C. Bellona, J.E. Drewes, Fouling of nanofiltration and reverse osmosis membranes during municipal wastewater reclamation: membrane autopsy results from pilot-scale investigations, *Journal of Membrane Science*, 353 (2010) 111-121.
- [19] I. Levchuk, J.J.R. Márquez, M. Sillanpää, Removal of natural organic matter (NOM) from water by ion exchange—A review, *Chemosphere*, 192 (2018) 90-104.
- [20] Q. Yang, B. Mi, Nanomaterials for membrane fouling control: accomplishments and challenges, *Advances in chronic kidney disease*, 20 (2013) 536-555.
- [21] R.A. Al-Juboori, T. Yusaf, Biofouling in RO system: mechanisms, monitoring and controlling, *Desalination*, 302 (2012) 1-23.
- [22] S.Y. Kwak, S.H. Kim, S.S. Kim, Hybrid organic/inorganic reverse osmosis (RO) membrane for bactericidal anti-fouling. 1. Preparation and characterization of TiO₂ nanoparticle self-assembled aromatic polyamide thin-film-composite (TFC) membrane, *Environmental science & technology*, 35 (2001) 2388-2394.
- [23] T. Nguyen, F.A. Roddick, L. Fan, Biofouling of water treatment membranes: a review of the underlying causes, monitoring techniques and control measures, *Membranes*, 2 (2012) 804-840.
- [24] M. Safarpour, V. Vatanpour, A. Khataee, Preparation and characterization of graphene oxide/TiO₂ blended PES nanofiltration membrane with improved antifouling and separation performance, *Desalination*, 393 (2016) 65-78.
- [25] K. Takata, Y. Yamamoto, T. Sata, Modification of transport properties of ion exchange membranes: XIV. Effect of molecular weight of polyethyleneimine bonded to the surface of cation exchange membranes by acid–amide bonding on electrochemical properties of the membranes, *Journal of Membrane Science*, 179 (2000) 101-107.
- [26] X. Xu, Q. He, G. Ma, H. Wang, N. Nirmalakhandan, P. Xu, Selective separation of mono-and di-valent cations in electro dialysis during brackish water desalination: Bench and pilot-scale studies, *Desalination*, 428 (2018) 146-160.
- [27] X. Xu, L. Lin, G. Ma, H. Wang, W. Jiang, Q. He, N. Nirmalakhandan, P. Xu, Study of polyethyleneimine coating on membrane permselectivity and desalination performance during pilot-scale electro dialysis of reverse osmosis concentrate, *Separation and Purification Technology*, 207 (2018) 396-405.
- [28] N. Kabay, Ö. İpek, H. Kahveci, M. Yüksel, Effect of salt combination on separation of monovalent and divalent salts by electro dialysis, *Desalination*, 198 (2006) 84-91.

Antifouling Ion-Exchange Membranes

- [29] M. Vasselbehagh, H. Karkhanechi, S. Mulyati, R. Takagi, H. Matsuyama, Improved antifouling of anion-exchange membrane by polydopamine coating in electro dialysis process, *Desalination*, 332 (2014) 126-133.
- [30] H. Lee, S.M. Dellatore, W.M. Miller, P.B. Messersmith, Mussel-inspired surface chemistry for multifunctional coatings, *Science*, 318 (2007) 426-430.
- [31] C. Cheng, S. Li, W. Zhao, Q. Wei, S. Nie, S. Sun, C. Zhao, The hydrodynamic permeability and surface property of polyethersulfone ultrafiltration membranes with mussel-inspired polydopamine coatings, *Journal of Membrane Science*, 417 (2012) 228-236.
- [32] Z.Y. Xi, Y.Y. Xu, L.P. Zhu, Y. Wang, B.K. Zhu, A facile method of surface modification for hydrophobic polymer membranes based on the adhesive behavior of poly (DOPA) and poly (dopamine), *Journal of Membrane Science*, 327 (2009) 244-253.
- [33] V. Ball, Impedance spectroscopy and zeta potential titration of dopa-melanin films produced by oxidation of dopamine, *Colloids and Surfaces A: Physicochemical and Engineering Aspects*, 363 (2010) 92-97.
- [34] Q. Liu, B. Yu, W. Ye, F. Zhou, Highly selective uptake and release of charged molecules by pH - responsive polydopamine microcapsules, *Macromolecular bioscience*, 11 (2011) 1227-1234.
- [35] M.E. Lynge, R. van der Westen, A. Postma, B. Städler, Polydopamine—a nature-inspired polymer coating for biomedical science, *Nanoscale*, 3 (2011) 4916-4928.
- [36] L.Y. Chen, X.H. Lin, J.G. Gai, Polyethylenimine linked glycidol surface antifouling reverse osmosis membrane, *Industrial & Engineering Chemistry Research*, 57 (2018) 2322-2328.
- [37] X. Wang, Z. Wang, Z. Wang, Y. Cao, J. Meng, Tethering of hyperbranched polyols using PEI as a building block to synthesize antifouling PVDF membranes, *Applied Surface Science*, 419 (2017) 546-556.
- [38] Y. Liu, Y. Su, J. Cao, J. Guan, L. Xu, R. Zhang, M. He, Q. Zhang, L. Fan, Z. Jiang, Synergy of the mechanical, antifouling and permeation properties of a carbon nanotube nanohybrid membrane for efficient oil/water separation, *Nanoscale*, 9 (2017) 7508-7518.
- [39] T. Sata, R. Izuo, Modification of transport properties of ion exchange membrane. XI. Electrodialytic properties of cation exchange membranes having polyethyleneimine layer fixed by acid–amide bonding, *Journal of Applied Polymer Science*, 41 (1990) 2349-2362.
- [40] P. Goh, T. Matsuura, A. Ismail, N. Hilal, Recent trends in membranes and membrane processes for desalination, *Desalination*, 391 (2016) 43-60.
- [41] J.H. Jhaveri, Z. Murthy, A comprehensive review on anti-fouling nanocomposite membranes for pressure driven membrane separation processes, *Desalination*, 379 (2016) 137-154.
- [42] E. Bet-Moushoul, Y. Mansourpanah, K. Farhadi, M. Tabatabaei, TiO₂ nanocomposite based polymeric membranes: a review on performance improvement for various applications in chemical engineering processes, *Chemical Engineering Journal*, 283 (2016) 29-46.

- [43] J. Zhang, Z. Wang, X. Zhang, X. Zheng, Z. Wu, Enhanced antifouling behaviours of polyvinylidene fluoride membrane modified through blending with nano-TiO₂/polyethylene glycol mixture, *Applied Surface Science*, 345 (2015) 418-427.
- [44] A. Rahimpour, M. Jahanshahi, A. Mollahosseini, B. Rajaeian, Structural and performance properties of UV-assisted TiO₂ deposited nano-composite PVDF/SPES membranes, *Desalination*, 285 (2012) 31-38.
- [45] Y. Mansourpanah, S. Madaeni, A. Rahimpour, A. Farhadian, A. Taheri, Formation of appropriate sites on nanofiltration membrane surface for binding TiO₂ photo-catalyst: performance, characterization and fouling-resistant capability, *Journal of Membrane Science*, 330 (2009) 297-306.
- [46] J.F. Li, Z.L. Xu, H. Yang, L.Y. Yu, M. Liu, Effect of TiO₂ nanoparticles on the surface morphology and performance of microporous PES membrane, *Applied Surface Science*, 255 (2009) 4725-4732.
- [47] M.L. Luo, W. Tang, J.Q. Zhao, C.S. Pu, Hydrophilic modification of poly (ether sulfone) used TiO₂ nanoparticles by a sol-gel process, *Journal of Materials Processing Technology*, 172 (2006) 431-436.
- [48] S. Madaeni, N. Ghaemi, Characterization of self-cleaning RO membranes coated with TiO₂ particles under UV irradiation, *Journal of Membrane Science*, 303 (2007) 221-233.
- [49] M. Hamzeh, G.I. Sunahara, In vitro cytotoxicity and genotoxicity studies of titanium dioxide (TiO₂) nanoparticles in Chinese hamster lung fibroblast cells, *Toxicology in Vitro*, 27 (2013) 864-873.
- [50] S. Barillet, M.L. Jugan, M. Laye, Y. Leconte, N. Herlin-Boime, C. Reynaud, M. Carrière, In vitro evaluation of SiC nanoparticles impact on A549 pulmonary cells: cyto-, genotoxicity and oxidative stress, *Toxicology letters*, 198 (2010) 324-330.
- [51] G. Oberdörster, V. Stone, K. Donaldson, Toxicology of nanoparticles: a historical perspective, *Nanotoxicology*, 1 (2007) 2-25.
- [52] I. Papageorgiou, C. Brown, R. Schins, S. Singh, R. Newson, S. Davis, J. Fisher, E. Ingham, C. Case, The effect of nano- and micron-sized particles of cobalt-chromium alloy on human fibroblasts in vitro, *Biomaterials*, 28 (2007) 2946-2958.
- [53] G. Oberdörster, E. Oberdörster, J. Oberdörster, Nanotoxicology: an emerging discipline evolving from studies of ultrafine particles. *Environ Health Perspect* 113: 823-839, (2005).
- [54] Y. Li, S. Shi, H. Cao, Z. Zhao, C. Su, H. Wen, Improvement of the antifouling performance and stability of an anion exchange membrane by surface modification with graphene oxide (GO) and polydopamine (PDA), *Journal of Membrane Science*, 566 (2018) 44-53.
- [55] I. Alam, L.M. Guiney, M.C. Hersam, I. Chowdhury, Antifouling properties of two-dimensional molybdenum disulfide and graphene oxide, *Environmental Science: Nano*, 5 (2018) 1628-1639.
- [56] C. Liao, Y. Li, S.C. Tjong, Graphene nanomaterials: synthesis, biocompatibility, and cytotoxicity, *International Journal of Molecular Sciences*, 19 (2018) 3564.

- [57] N. Bernabo, A. Fontana, M.R. Sanchez, L. Valbonetti, G. Capacchietti, R. Zappacosta, L. Greco, M. Marchisio, P. Lanuti, E. Ercolino, Graphene oxide affects in vitro fertilization outcome by interacting with sperm membrane in an animal model, *Carbon*, 129 (2018) 428-437.
- [58] G. Duan, Y. Zhang, B. Luan, J.K. Weber, R.W. Zhou, Z. Yang, L. Zhao, J. Xu, J. Luo, R. Zhou, Graphene-induced pore formation on cell membranes, *Scientific Reports*, 7 (2017) 42767.
- [59] L. Zhang, B. Xu, X. Wang, Cholesterol extraction from cell membrane by graphene nanosheets: a computational study, *The Journal of Physical Chemistry B*, 120 (2016) 957-964.
- [60] J. Alam, A.K. Shukla, M. Alhoshan, L. Arockiasamy Dass, M.R. Muthumareeswaran, A. Khan, F.A. Ahmed Ali, Graphene oxide, an effective nanoadditive for a development of hollow fiber nanocomposite membrane with antifouling properties, *Advances in Polymer Technology*, 37 (2018) 2597-2608.
- [61] M. Vasselbehagh, H. Karkhanechi, R. Takagi, H. Matsuyama, Effect of polydopamine coating and direct electric current application on anti-biofouling properties of anion exchange membranes in electro dialysis, *Journal of Membrane Science*, 515 (2016) 98-108.
- [62] L. Ge, L. Wu, B. Wu, G. Wang, T. Xu, Preparation of monovalent cation selective membranes through annealing treatment, *Journal of Membrane Science*, 459 (2014) 217-222.
- [63] N. Bracken, J. Macknick, A. Tovar-Hastings, P. Komor, M. Gerritsen, S. Mehta, Concentrating solar power and water issues in the us southwest, in, *National Renewable Energy Lab.(NREL), Golden, CO (United States)*, 2015.
- [64] W. Zhang, M. Wahlgren, B. Sivik, Membrane characterization by the contact angle technique: II. Characterization of UF-membranes and comparison between the captive bubble and sessile drop as methods to obtain water contact angles, *Desalination*, 72 (1989) 263-273.
- [65] M.R. Hibbs, C.H. Fujimoto, C.J. Cornelius, Synthesis and characterization of poly (phenylene)-based anion exchange membranes for alkaline fuel cells, *Macromolecules*, 42 (2009) 8316-8321.
- [66] W. Zhang, J. Ma, P. Wang, Z. Wang, F. Shi, H. Liu, Investigations on the interfacial capacitance and the diffusion boundary layer thickness of ion exchange membrane using electrochemical impedance spectroscopy, *Journal of Membrane Science*, 502 (2016) 37-47.
- [67] J.S. Park, J.-H. Choi, J.-J. Woo, S.-H. Moon, An electrical impedance spectroscopic (EIS) study on transport characteristics of ion-exchange membrane systems, *Journal of Colloid and Interface Science*, 300 (2006) 655-662.
- [68] A. Galama, N. Hoog, D. Yntema, Method for determining ion exchange membrane resistance for electro dialysis systems, *Desalination*, 380 (2016) 1-11.
- [69] I. Sondi, B. Salopek-Sondi, Silver nanoparticles as antimicrobial agent: a case study on E. coli as a model for Gram-negative bacteria, *Journal of Colloid and Interface Science*, 275 (2004) 177-182.
- [70] M. Vorregaard, Comstat2-a modern 3D image analysis environment for biofilms, Citeseer, 2008.

- [71] A. Heydorn, A.T. Nielsen, M. Hentzer, C. Sternberg, M. Givskov, B.K. Ersbøll, S. Molin, Quantification of biofilm structures by the novel computer program COMSTAT, *Microbiology*, 146 (2000) 2395-2407.
- [72] C. Sternberg, COMSTAT 2.1 Manual, 2015.
- [73] D. Hasson, H. Shemer, A. Sher, State of the art of friendly “green” scale control inhibitors: a review article, *Industrial & Engineering Chemistry Research*, 50 (2011) 7601-7607.
- [74] C. Fritzmann, J. Löwenberg, T. Wintgens, T. Melin, State-of-the-art of reverse osmosis desalination, *Desalination*, 216 (2007) 1-76.
- [75] W. Chen, P. Westerhoff, J.A. Leenheer, K. Booksh, Fluorescence excitation–emission matrix regional integration to quantify spectra for dissolved organic matter, *Environmental science & technology*, 37 (2003) 5701-5710.
- [76] H.B. Park, J. Kamcev, L.M. Robeson, M. Elimelech, B.D. Freeman, Maximizing the right stuff: The trade-off between membrane permeability and selectivity, *Science*, 356 (2017) eaab0530.
- [77] Y. Zhang, K. Ghyselbrecht, B. Meesschaert, L. Pinoy, B. Van der Bruggen, Electrodialysis on RO concentrate to improve water recovery in wastewater reclamation, *Journal of Membrane Science*, 378 (2011) 101-110.
- [78] M. Nemati, S. Hosseini, E. Bagheripour, S. Madaeni, Electrodialysis heterogeneous anion exchange membranes filled with TiO₂ nanoparticles: Membranes' fabrication and characterization, *Journal of Membrane Science and Research*, 1 (2015) 135-140.
- [79] C.S. Alves, M.N. Melo, H.G. Franquelim, R. Ferre, M. Planas, L. Feliu, E. Bardají, W. Kowalczyk, D. Andreu, N.C. Santos, Escherichia coli cell surface perturbation and disruption induced by antimicrobial peptides BP100 and pepR, *Journal of Biological Chemistry*, 285 (2010) 27536-27544.
- [80] E. Nightingale Jr, Phenomenological theory of ion solvation. Effective radii of hydrated ions, *The Journal of Physical Chemistry*, 63 (1959) 1381-1387.
- [81] R. Tejido-Rastrilla, S. Ferraris, W.H. Goldmann, A. Grünewald, R. Detsch, G. Baldi, S. Spriano, A.R. Boccaccini, Studies on Cell Compatibility, Antibacterial Behavior, and Zeta Potential of Ag-Containing Polydopamine-Coated Bioactive Glass-Ceramic, *Materials*, 12 (2019) 500.
- [82] S. Hosseini, M. Nemati, F. Jeddi, E. Salehi, A. Khodabakhshi, S. Madaeni, Fabrication of mixed matrix heterogeneous cation exchange membrane modified by titanium dioxide nanoparticles: Mono/bivalent ionic transport property in desalination, *Desalination*, 359 (2015) 167-175.
- [83] P. Daraei, S.S. Madaeni, N. Ghaemi, E. Salehi, M.A. Khadivi, R. Moradian, B. Astinchap, Novel polyethersulfone nanocomposite membrane prepared by PANI/Fe₃O₄ nanoparticles with enhanced performance for Cu (II) removal from water, *Journal of Membrane Science*, 415 (2012) 250-259.
- [84] W. Zhang, B. Hallström, Membrane characterization using the contact angle technique I. Methodology of the captive bubble technique, *Desalination*, 79 (1990) 1-12.
- [85] V. Kafil, Y. Omid, Cytotoxicity impacts of linear and branched polyethylenimine nanostructures in A431 cells, *Research in Pharmaceutical Sciences*, 7 (2012) 198.

- [86] R.X. Zhang, L. Braeken, T.Y. Liu, P. Luis, X.L. Wang, B. Van der Bruggen, Remarkable anti-fouling performance of TiO₂-modified TFC membranes with mussel-inspired polydopamine binding, *Applied Sciences*, 7 (2017) 81.
- [87] C. Liu, D. Zhang, Y. He, X. Zhao, R. Bai, Modification of membrane surface for anti-biofouling performance: Effect of anti-adhesion and anti-bacteria approaches, *Journal of Membrane Science*, 346 (2010) 121-130.
- [88] W. Jiang, L. Lin, X. Xu, H. Wang, P. Xu, Physicochemical and electrochemical characterization of cation-exchange membranes modified with polyethyleneimine for elucidating enhanced monovalent permselectivity of electro dialysis, *Journal of Membrane Science*, 572 (2019) 545-556.
- [89] J. Wingender, T.R. Neu, H.-C. Flemming, What are bacterial extracellular polymeric substances?, in: *Microbial extracellular polymeric substances*, Springer, 1999, pp. 1-19.
- [90] L.V. Evans, *Biofilms: recent advances in their study and control*, CRC press, 2003.
- [91] R.M. Donlan, Biofilms: microbial life on surfaces, *Emerging Infectious Diseases*, 8 (2002) 881.
- [92] R.M. Donlan, J.W. Costerton, Biofilms: survival mechanisms of clinically relevant microorganisms, *Clinical Microbiology Reviews*, 15 (2002) 167-193.
- [93] M. Safarpour, A. Khataee, V. Vatanpour, Preparation of a novel polyvinylidene fluoride (PVDF) ultrafiltration membrane modified with reduced graphene oxide/titanium dioxide (TiO₂) nanocomposite with enhanced hydrophilicity and antifouling properties, *Industrial & Engineering Chemistry Research*, 53 (2014) 13370-13382.
- [94] M. Safarpour, A. Khataee, V. Vatanpour, Thin film nanocomposite reverse osmosis membrane modified by reduced graphene oxide/TiO₂ with improved desalination performance, *Journal of Membrane Science*, 489 (2015) 43-54.
- [95] Y. Tanaka, Bipolar membrane electro dialysis, *Membrane Science and Technology*, 12 (2007) 405-436.
- [96] D.N. Pei, L. Gong, A.Y. Zhang, X. Zhang, J.J. Chen, Y. Mu, H.Q. Yu, Defective titanium dioxide single crystals exposed by high-energy {001} facets for efficient oxygen reduction, *Nature Communications*, 6 (2015) 1-10.
- [97] O. Moradi, V.K. Gupta, S. Agarwal, I. Tyagi, M. Asif, A.S.H. Makhlof, H. Sadegh, R. Shahryari-ghoshekandi, "Characteristics and electrical conductivity of graphene and graphene oxide for adsorption of cationic dyes from liquids: Kinetic and Thermodynamic study" [*J. Ind. Eng. Chem.* 28 (2015) 294.301], *Journal of Industrial and Engineering Chemistry*, 85 (2020) 310-310.
- [98] Q. Tu, L. Pang, Y. Chen, Y. Zhang, R. Zhang, B. Lu, J. Wang, Effects of surface charges of graphene oxide on neuronal outgrowth and branching, *Analyst*, 139 (2014) 105-115.
- [99] M.J. Li, C.M. Liu, Y.B. Xie, H.B. Cao, H. Zhao, Y. Zhang, The evolution of surface charge on graphene oxide during the reduction and its application in electroanalysis, *Carbon*, 66 (2014) 302-311.
- [100] L. Lin, H. Wang, H. Luo, P. Xu, Enhanced photocatalysis using side-glowing optical fibers coated with Fe-doped TiO₂ nanocomposite thin films, *Journal of Photochemistry and Photobiology A: Chemistry*, 307 (2015) 88-98.

- [101] J.P. Holmberg, E. Ahlberg, J. Bergenholtz, M. Hassellöv, Z. Abbas, Surface charge and interfacial potential of titanium dioxide nanoparticles: experimental and theoretical investigations, *Journal of Colloid and Interface Science*, 407 (2013) 168-176.
- [102] C. Xiang, F. Yang, M. Li, M. Jaridi, N. Wu, Experimental and statistical analysis of surface charge, aggregation and adsorption behaviors of surface-functionalized titanium dioxide nanoparticles in aquatic system, *Journal of Nanoparticle Research*, 15 (2013) 1293.
- [103] J. Jiang, G. Oberdörster, P. Biswas, Characterization of size, surface charge, and agglomeration state of nanoparticle dispersions for toxicological studies, *Journal of Nanoparticle Research*, 11 (2009) 77-89.
- [104] S.T. Kelly, A.L. Zydney, Mechanisms for BSA fouling during microfiltration, *Journal of Membrane Science*, 107 (1995) 115-127.
- [105] H. Guo, L. Xiao, S. Yu, H. Yang, J. Hu, G. Liu, Y. Tang, Analysis of anion exchange membrane fouling mechanism caused by anion polyacrylamide in electro dialysis, *Desalination*, 346 (2014) 46-53.
- [106] H.J. Lee, M.K. Hong, S.D. Han, S.H. Cho, S.H. Moon, Fouling of an anion exchange membrane in the electro dialysis desalination process in the presence of organic foulants, *Desalination*, 238 (2009) 60-69.
- [107] S. Deng, G. Yu, Y.P. Ting, Removal of Humic Acid Using PEI - Modified Fungal Biomass, *Separation Science and Technology*, 41 (2006) 2989-3002.
- [108] Z. Guo, Z. Kong, Y. Wei, H. Li, Y. Wang, A. Huang, L. Ma, Effects of gene carrier polyethyleneimines on the structure and binding capability of bovine serum albumin, *Spectrochimica Acta Part A: Molecular and Biomolecular Spectroscopy*, 173 (2017) 783-791.
- [109] Z. Nan, C. Hao, X. Ye, Y. Feng, R. Sun, Interaction of graphene oxide with bovine serum albumin: A fluorescence quenching study, *Spectrochimica Acta Part A: Molecular and Biomolecular Spectroscopy*, 210 (2019) 348-354.
- [110] J. Kuchlyan, N. Kundu, D. Banik, A. Roy, N. Sarkar, Spectroscopy and fluorescence lifetime imaging microscopy to probe the interaction of bovine serum albumin with graphene oxide, *Langmuir*, 31 (2015) 13793-13801.
- [111] J.J. Song, Y. Huang, S.W. Nam, M. Yu, J. Heo, N. Her, J.R. Flora, Y. Yoon, Ultrathin graphene oxide membranes for the removal of humic acid, *Separation and Purification Technology*, 144 (2015) 162-167.
- [112] B.M. Lee, Y.S. Seo, J. Hur, Investigation of adsorptive fractionation of humic acid on graphene oxide using fluorescence EEM-PARAFAC, *Water Research*, 73 (2015) 242-251.
- [113] H. Younas, J. Shao, Y. He, G. Fatima, S.T.A. Jaffar, Z.U.R. Afridi, Fouling-free ultrafiltration for humic acid removal, *RSC Advances*, 8 (2018) 24961-24969.
- [114] T.X. Tung, D. Xu, Y. Zhang, Q. Zhou, Z. Wu, Removing Humic Acid from Aqueous Solution Using Titanium Dioxide: A Review, *Polish Journal of Environmental Studies*, 28 (2019).
- [115] Z. Xu, V.H. Grassian, Bovine serum albumin adsorption on TiO₂ nanoparticle surfaces: Effects of pH and coadsorption of phosphate on protein-

Antifouling Ion-Exchange Membranes

- surface interactions and protein structure, *The Journal of Physical Chemistry C*, 121 (2017) 21763-21771.
- [116] C.A. Reddy, R.S. Saravanan, Polymicrobial multi-functional approach for enhancement of crop productivity, in: *Advances in Applied Microbiology*, Elsevier, 2013, pp. 53-113.
- [117] L. Han, T. Xiao, Y.Z. Tan, A.G. Fane, J.W. Chew, Contaminant rejection in the presence of humic acid by membrane distillation for surface water treatment, *Journal of Membrane Science*, 541 (2017) 291-299.
- [118] Z.A. Stoll, C. Forrestal, Z.J. Ren, P. Xu, Shale gas produced water treatment using innovative microbial capacitive desalination cell, *Journal of Hazardous Materials*, 283 (2015) 847-855.
- [119] W.T. Li, Z.X. Xu, A.M. Li, Comment on “Identifying well contamination through the use of 3-d fluorescence spectroscopy to classify coalbed methane produced water”, *Environmental science & technology*, 47 (2013) 1770-1771.
- [120] K.A. Thorn, P.J. Pettigrew, W.S. Goldenberg, E.J. Weber, Covalent binding of aniline to humic substances. 2. ¹⁵N NMR studies of nucleophilic addition reactions, *Environmental science & technology*, 30 (1996) 2764-2775.
- [121] T.S. Hsu, R. Bartha, Interaction of Pesticide-Derived Chloroaniline Residues with Soil Organic matter, *Soil Science*, 116 (1973) 444-452.
- [122] E. Gök, M. Kiremitçi, I.S. Ateş, Protein adsorption on functional hydrophilic polymer beads: role of structural properties and medium conditions, *Reactive Polymers*, 24 (1994) 41-48.
- [123] D. Absolom, W. Zingg, A. Neumann, Protein adsorption to polymer particles: role of surface properties, *Journal of Biomedical Materials Research*, 21 (1987) 161-171.
- [124] Y. Jeyachandran, E. Mielczarski, B. Rai, J. Mielczarski, Quantitative and qualitative evaluation of adsorption/desorption of bovine serum albumin on hydrophilic and hydrophobic surfaces, *Langmuir*, 25 (2009) 11614-11620.

Metric Conversions

Unit	Metric equivalent
1 gallon	3.785 liters
1 gallon per minute	3.785 liters per minute
1 gallon per square foot of membrane area per day	40.74 liters per square meter per day
1 inch	2.54 centimeters
1 million gallons per day	3,785 cubic meters per day
1 pound per square inch	6.895 kilopascals
1 square foot	0.093 square meters
°F (temperature measurement)	$(^{\circ}\text{F} - 32) \times 0.556 = ^{\circ}\text{C}$
1 °F (temperature change or difference)	0.556 °C
1 psi	6.9848 kPa
1 lb	453.6 gram